Engineering Oxidoreductases: Towards Artificial Hydrogenases

by

Anindya Roy

A Dissertation Presented in Partial Fulfillment
of the Requirements for the Degree
Doctor of Philosophy

Approved April 2014 by the
Graduate Supervisory Committee:

Giovanna Ghirlanda (Chair)
Hao Yan
Devens Gust

ARIZONA STATE UNIVERSITY

May 2014

ABSTRACT

Natural hydrogenases catalyze the reduction of protons to molecular hydrogen reversibly under mild conditions; these enzymes have an unusual active site architecture, in which a diiron site is connected to a cubane type [4Fe-4S] cluster. Due to the relevance of this reaction to energy production, and in particular to sustainable fuel production, there have been substantial amount of research focused on developing biomimetic organometallic models. However, most of these organometallic complexes cannot revisit the structural and functional fine-tuning provided by the protein matrix as seen in the natural enzyme. The goal of this thesis is to build a protein based functional mimic of [Fe-Fe] hydrogenases. I used a 'retrosynthetic' approach that separates out two functional aspects of the natural enzyme. First, I built an artificial electron transfer domain by engineering two [4Fe-4S] cluster binding sites into an existing protein, DSD, which is a de novo designed domain swapped dimer. The resulting protein, DSD-bis[4Fe-4S], contains two clusters at a distance of 36 Å . I then varied distance between two clusters using vertical translation along the axis of the coiled coil; the resulting protein demonstrates efficient electron transfer to/from redox sites. Second, I built simple, functional artificial hydrogenases by using an artificial amino acid comprising a 1,3 dithiol moiety to anchor a biomimetic [Fe-Fe] active site within the protein scaffold Correct incorporation of the cluster into a model helical peptide was verified by UV-Vis, FTIR, ESI-MS and CD spectroscopy. This synthetic strategy is extended to the de novo design of more complex protein architectures, four-helix bundles that host the di-iron cluster within the hydrophobic core. In a separate approach, I developed a generalizable strategy to introduce organometallic catalytic sites into a protein scaffold. I introduced a

biomimetic organometallic complex for proton reduction by covalent conjugation to biotin. The streptavidin-bound complex is significantly more efficient in photocatalytic hydrogen production than the catalyst alone. With these artificial proteins, it will be possible to explore the effect of second sphere interactions on the activity of the diiron center, and to include in the design properties such as compatibility with conductive materials and electrodes.

DEDICATION

To my wonderful parents for their unconditional love and to my advisor for her endless patience and encouragement

ACKNOWLEDGMENTS

Little did I know how it would all turn out in the end, when six years ago I came to this country for my PhD. Nobody will argue that graduate college is an unorthodox experience, often filled with contradictory emotions. It can be overwhelming and satisfying at the same time. The most important part, which made it much more interesting, I think, is the uncertainty. Each morning, for last five years, I woke up and came to a work that did not provide certainty about the outcome of my day; and that I think, made the whole experience so much more adventurous and exciting. I hope I can be in the same business of making or breaking bonds through out the rest of my life. Three most important people in my life: my parents and my advisor had an irrefutable contribution towards completion of my degree. First and foremost, I am eternally indebted to my parents for the sacrifices they made throughout their life: that led to who I am today. All the good qualities that I have and the values that I cherish deeply in my heart are the result of their upbringing. I would also like to admit the fact that I should have called my mom a little more frequently to reduce her anxiety about my lunch/dinner menu.

Of course the person, without whom, this thesis would not be possible, is my advisor Giovanna Ghirlanda. With visceral admiration and gratitude, I acknowledge the fact that all my scientific achievements today, are a direct result of your sustenance over the years. It does not escape me for a moment that all the accomplishments of my academic life are the consequence of your constant nourishment, encouragement and the intellectual freedom that you provided. You have been an amazing advisor, and ego booster (thank you for all your pep talk to raise my declining level of self worth) and a family away

from family. I truly hope that I get a chance to continue our joint venture in future. I would also like to thank my thesis committee member; Dr. Hao Yan and Dr. Devens Gust for their support over the years.

I have met some extra ordinary people over the years at work. I consider myself the incredibly fortunate to meet Iosifina Sarrou. I cannot express my gratitude in words to describe your contribution in my life, both academic and personal. You have taught me how to be happy and made me a better person. Selvakumar Edwardraja and Michael Vaughn, both of you are the reason that I have decided to leave organic chemistry and join the dark side of molecular biology. I appreciate all your patience during my training period for my extreme ignorance. All the molecular biology that I know today is because of you. Michael Vaughn, you are an extremely talented person with a diverse set of skills, and I hope that both of us succeed in our dreams one day and get to work with each other again, in future.

I would also like to thank all the present and past Ghirlanda group members for their help through out my graduate career: Sandip, Luca, Sonia, Mathieu, Brian, Dayn, Marina, Rafael, Sriram, Jason and Annabelle. Dayn, you have been an amazing colleague and I wish you good luck going forward with the venture we started together. I also would like to acknowledge all the undergrads that I have trained over the years for following all my directions, even if they did not want to. Specially, Garret and Jason, I consider you as a success of my training capability and I am so happy that I convinced you to go to Grad school. Stephanie Cope, I do appreciate all the good times we had together along with countless times you helped me with the flurimeter.

Natalie, Thank you so much for inviting to your house and feeding me on countless occasions. I will miss all our extremely vocal political debates and our frequent visits to the movie theater. I very much enjoyed taking care of Jeff and Maggie, when you guys were out of town.

A special acknowledgement goes to Jack and John from the proteomics lab. I have bothered you so many times over the years, especially when the MALDI was down, and you have been extremely helpful.

I would also like to acknowledge all the help that I got over the years from Arnab. I truly appreciate all your assistance during my early days in this country along with all the other times, when we were roommates. A special thank to my current roommate, Dinesh for being as messy as I am (or may be a little less).

Finally, of course I would like to thank some of the wonderful friends I made here: Jesse, Michael, Anteras, John, Chelsea. Thank you so much for all your kindness and increasing my alcohol tolerance. You guys made my life so much more enjoyable when all my reactions failed in a repetitive manner.

I would like to acknowledge Center for Bio-Inspired Solar Fuel Production, an energy frontier research center funded by the U.S. Department of Energy, Office of Science, Office of Basic Energy Sciences under the award number DE-SC0001016 for supporting me and our research over the years. I would also like to thank the Leroy Eyring Fellowship committee for awarding me a graduate student scholarship.

TABLE OF CONTENTS

APPENDIX Page

LIST OF TABLES

LIST OF FIGURES

LIST OF SCHEMES

LIST OF ABBREVIATIONS

Abbreviation	Extended Form
DCM	Dichloromethane
DMF	Dimethylformamide
BME	β-Mercaptoethanol
EDT	Ethanedithiol
TIPS	Triisopropylsilane
CD	Circulardicroism
EPR	Electron paramagnetic resonance
ESI-MS	Electron spray ionization mass spectrometry
Fmoc	9-fluorenylmethoxycarbonyl
FTIR	Fourier transformed Infra-red
HOBt	Hydroxybenzotriazole
HBTU	O-benzotriazole-N,N,N',N'-tetramethyluronium hexafluorophosphate
MALDI-MS	Matrix assisted laser desorption/ ionization mass spectrometry
NMR	Nuclear paramagnetic resonance
TFA	Trifluoroacetic acid
UV-Vis	Ultraviolet-Visible

PREFACE

'It's not that I'm so smart, it's just that I stay with problems longer'

Albert Einstein

CHAPTER 1

DE NOVO DESIGN OF FUNCTIONAL PROTEINS: TOWARDS ARTIFICIAL HYDROGENASES

Marina Faiella, Anindya Roy, Dayn Sommer, Giovanna Ghirlanda

Department of Chemistry and Biochemistry, Arizona State University, Tempe, AZ

Reproduced by permission from Biopolymers: Peptide Science, 100, 6, 558-571, 2013

Abstract:

Over the last 25 years, de novo design has proven to be a valid approach to generate novel, well-folded proteins, and most recently, functional proteins. In response to societal needs, this approach is been used increasingly to design functional proteins developed with an eye toward sustainable fuel production. This review surveys recent examples of bioinspired de novo designed peptide based catalysts, focusing in particular on artificial hydrogenases.

Introduction

One of the most important challenges facing our society is the development of sustainable energy sources. The current reliance on fossil fuels has unsustainable consequences on the environment; further, the unequal distribution of energy sources throughout the world results in conflicts and societal instability.

Nature utilizes solar energy to power biological processes through photosynthesis, storing solar radiation in energy rich molecules that in turn are used to drive cellular metabolism. This process indirectly powers most life on the planet, as it maintains oxygen levels in the atmosphere, generates key organic molecules, and supports the growth of biomass that in turns is used as food. Fossil fuels are also ultimately derived from biomass resulting from photosynthetic solar energy conversion. To address our society's energy needs, research efforts are focusing on developing new renewable based sources of energy to generate storable fuels.[1] Hydrogen in particular has emerged as an attractive, carbon-free candidate for use as fuel. One of the approaches followed for sustainable hydrogen production is inspired by nature, and aims to capture solar energy by reproducing the fundamental steps of photosynthesis through dedicated functional modules interfaced in a device.[2-5] In such a device, the reductive equivalents needed for hydrogen generation are obtained through the same reaction at the basis of photosynthesis, oxidation of water into O_2 and H^+, also known as water splitting, which is driven by photoinduced charge separation in the light harvester. In turn, molecular hydrogen is generated through appropriate catalysts capable of handling multielectron redox chemistry.

In nature, hydrogen metabolism is mediated by specialized enzymes called hydrogenases found in Bacteria, Archea, and Eucarya.[6-8] Based on the composition of their active sites, natural hydrogenases are divided in [Fe-Fe], [Ni-Fe], and [Fe] only, with the latter group involved in methanogenesis.[9-11] The active site of hydrogenases also contains unusual small-molecule lignands as part of the first coordination sphere. [Ni-Fe] and [Fe-Fe] hydrogenases, in particular are of interest in this chapter, as they catalyze the reversible reduction of protons to hydrogen.[1,6,7,11-14]

Despite no phylogenetic relationship, extensive structural and spectroscopic characterization revealed that both contain binuclear active sites that utilize unique, non-proteinogenic CO and CN ligands.[11,15-21]

Hydrogenases can also be classified in terms of function: uptake hydrogenases, generally present in the periplasm or associated with the membrane, utilize molecular hydrogen as a source of electrons. Conversely, hydrogenases localized in the cytoplasm catalyze proton reduction as a way to dispose excess electrons.[6] Both functions are relevant to technological applications, in the sustainable production of hydrogen, and in the efficient utilization of molecular hydrogen in fuel cells.[1,22]

The utilization of hydrogenases in devices is hindered by the complexity of their biosynthesis and structural architecture, which makes heterologous expression technically challenging, and by their high oxygen sensitivity. The complex pathway required for active site assembly and hydrogenase maturation has also prevented the application of well-established methods to optimize natural enzymes, such as directed evolution, which could in principle be used to ameliorate oxygen sensitivity.[23,24] Over the years, several groups have developed models with the dual purpose of elucidating the mechanistic

requirements of the active site and applying them as a robust alternative to the hydrogenases. These complexes follow two broad philosophies: on one hand, structural mimicry of the natural enzymes, utilizing similar ligands and metals to reproduce the enzyme's active site; on the other hand, functional mimics aim to replicate the function using Earth-abundant metals and artificial ligands to form complexes. With a few notable exceptions, [25-30] however, organometallic complexes present challenges that prevent their utilization in technological applications; they utilize non-earth abundant metals, or carry out proton reduction either at rates much slower than the natural enzymes, or with unfavorable energetics (thus requiring high overpotentials for the reaction), and generally in much harsher conditions (strong acids and/or organic solvents) than the natural enzymes. It is generally thought that such differences between the natural enzymes and the organometallic complexes result from the complexity of the second sphere and outer sphere of coordination in the natural enzyme.

For these reasons, artificial model proteins are emerging as bridging ground between organometallic complexes and the natural proteins. Peptide based catalysts present the advantage of being inherently water-soluble. They also allow for the design of second shell coordination sphere and long-range interactions with much ease compared to organometallic complexes. Compared to the natural protein, they can be easily prepared by synthesis or by expression without the need for maturation enzymes.

The following sections briefly describe the natural enzymes and organometallic model systems, towards artificial bio-inspired hydrogenases.

Catalytic site: Hydrogenase mimics

[Fe-Fe] hydrogenases.

[Fe-Fe] hydrogenases are generally very efficient, with turnover numbers as high as

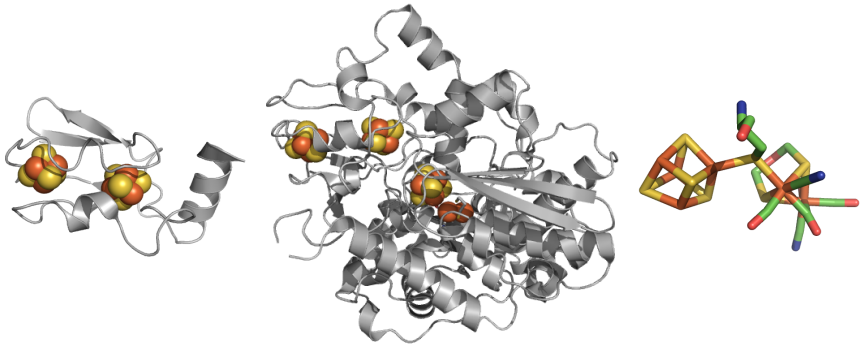

Figure 1.1: Structure of [Fe-Fe] hydrogenase from *Desulfovibrio desulfuricans* (PDB 1HFE). The ferrodoxin-like domain and the H-cluster are highlighted on the left and on the right, respectively. All molecular figures were created with PyMOL (DeLano, W.L. (2002); The PyMOL Molecular Graphics System. (http://www.pymol.org))

10^4 H_2 molecules per second and are usually biased towards hydrogen production.[31] These enzymes function strictly in the absence of oxygen, with exposure resulting in irreversible inhibition.[14] Investigation of the mechanism, maturation, and structure of [Fe-Fe] hydrogenases from different organisms revealed a functional organization into dedicated domains, with some domains, variable in type and number, containing a chain of redox active factors that ferry electrons to/from external donors/acceptors to the catalytic site, and associated with the domain that contains the active site [Figure 1.1].[32,33] The [Fe-Fe] hydrogenase found in *Desulfovibrio desulfuricans* has been characterized by X-ray crystallography, and provides an excellent example of the general architecture of the hydrogenases.[17] Its large subunit comprises a ferredoxin-like domain that contains two [4Fe-4S] clusters and functions as electron conduit to rapidly transfer the two electrons involved in the reaction, and a neighboring domain that contains the catalytic

site, termed the H-cluster. The assembly *in vivo* of the H-cluster requires a number of specific maturation enzymes.[32-34]

The H-cluster is composed by a [4Fe-4S] cluster and by a [Fe-Fe] site coordinated by a non-proteinogenic dithiolate bridging ligand as well as carbon monoxide (CO) and cyanide (CN) ligands, with the [Fe-Fe] site anchored to the protein through a cysteine (Cys) that bridges the iron-sulfur cluster and one iron, designated as proximal (Figure 1.1); depending on the redox states sampled during the catalytic cycle, one of the CO ligands bridges the two metals. [17,35] The central atom in the bridging thiolate ligand has been proposed to be nitrogen, and to be instrumental in assisting proton transfer.[36]Cleavage of the H-H bond has been shown to proceed heterolytically, suggesting that hydrogen production proceeds through an hydride intermediate, postulated to be located on the distal iron.[37-39] The unusual CN and CO ligands play an important role in tuning the electronic properties of the diiron states, and in assisting the transfer of electrons to/from hydrogen. [38,40-42] During the catalytic cycle, the distal iron is thought to undergo a conformational change to assume an inverted square pyramidal conformation, or "rotated" state, which is poised for transfer of electrons through the proximal iron to a coordinated proton.[38,43] The protein matrix is thought to stabilize the catalytically active "rotated" conformation of the distal iron and to facilitate the reaction by rapidly transferring electrons and a proton to the active site.[26,32,43] Phylogenetic analysis of over 800 putative hydrogenase sequences revealed that the cysteines involved in coordinating the cubane-type [4Fe-4S] cluster and more broadly the hydrophobic environment surrounding the active site are highly conserved. [17,39,44,45] An analysis of the high-resolution X-ray structures of two [Fe-Fe] hydrogenases reveals additional

electrostatic interactions with the CO and CN ligands, in particular a hydrogen bond to a conserved lysine, and a proposed bond between conserved cysteine and methionine and the central nitrogen atom in the bridging dithiolate ligand. These latter interactions are thought to modulate the basicity of the central amine and affect its proton-shuffling function during the catalytic cycle.[39] Mutations of these residues have been shown to abolish the catalytic activity.[44] These second sphere interactions participate directly in assisting the catalysis, and thus need to be considered in the design of hydrogenase mimics. The natural hydrogenases, however, necessitate other accessory functions in order to carry out their function in the context of the living organism.[32] Beyond the immediate environment of the H-cluster, other conserved residues are thought to participate in the proton/H_2 transfer pathway or assist electron transfer through stabilization of the accessory clusters.

Organometallic models.

Structural mimics of the [Fe-Fe] hydrogenase were first developed based on a (μ-$S(CH_2)_3$-S)[$Fe_2(CO)_6$] complex, whose similarity to the enzyme's active site was initially recognized by Pickett, Darensbourg, and Rauchfuss (Figure 1.2).[46-48] These mimics revealed features such as the need for a thermodynamically disfavored "rotated" state of the distal iron in the diiron cluster, which frees a position for catalysis, and electron-donating ligands on the same iron atoms; further second-sphere requirements include a pendant base that delivers protons to the active site,

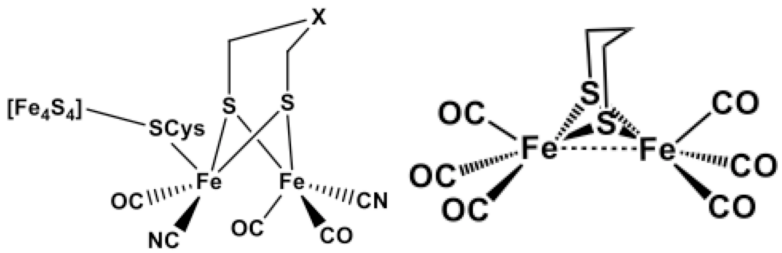

Figure 1.2: Schematic representation of the H-cluster of [Fe-Fe] hydrogenases (left); the X in figure is likely to be NH/NH_2^+; a minimalist structural mimic used as basis for the development of organometallic complexes (right)

and a redox active group to ferry electrons during catalysis.[49-58] A recent, elegant design by the Rauchfuss group utilizes an electron-rich chelating phosphine ligand on the distal iron to lock the complex at the "rotated" state, and a ferrocenyl moiety on the proximal iron as electron relay.[26]

Peptide-based structural models: [Fe-Fe]-hydrogenase.

A typical approach to the de novo design of metalloproteins utilizes the primary coordination sphere of the metal in natural proteins, and builds a peptide scaffold around it.[59] Hydrogenases, however, present a challenge because the catalytic site is formed by non-proteinogenic ligands, and is linked to the protein through a single cysteine shared with the cubane cluster component of the H-cluster. The need for alternative ways of anchoring the active site to the peptide scaffold was recognized early on, and initial work focused on organometallic models of the [Fe-Fe] hydrogenase based on a $(\mu\text{-S-}(CH_2)_3\text{-S})[Fe_2(CO)_6]$ center, which preserves the dithiolate ligation observed in the natural enzyme. Sun and colleagues first observed that cysteinyl ligands could replace the bridging $\mu\text{-S-}(CH_2)_3\text{-S}$ ligands.[60] They reported that Boc-protected L-cysteine methyl ester forms the desired diiron hexacarbonyl complex (Figure 1.3) upon treatment with an

inorganic precursor, $[Fe_3(CO)_{12}]$. Upon refluxing in various solvents, though, the initial complex undergoes an intramolecular cyclization to generate a chiral two-carbon-bridged dithiolate diiron complex, with structural parameters similar to $(\mu\text{-S-}(CH_2)_3\text{-S})[Fe_2(CO)_6]$. This work highlighted the need for structural preorganization of the cysteinyl ligands in a rigid scaffold. A clever solution to the problem utilizes a ferrocene moiety (dicyclopentadienyl iron, Cp_2Fe) tethered to two Cys molecules via peptide bonds to present thiolates at the appropriate distance to form a diiron hexacarbonyl complex. [61-63] In this design the ferrocene group serves as structural scaffold to the thiolates, and also provides a nearby redox-active center: however, no electronic interactions were observed between the iron–carbonyl and the ferrocene cores.

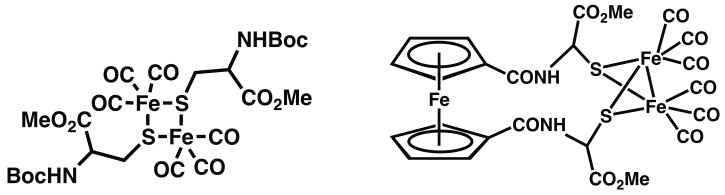

Figure 1.3: Schematic representation of structural models of [Fe-Fe] hydrogenases: (a) Boc-protected L-cysteine methyl ester forming the diiron hexacarbonyl complex developed by Sun and coworkers (adapted from ref. 60); (b) $Fe(C_5H_4CO\text{–Cys–OMe})_2$ di-peptide employed by Metzler-Nolte and coworkers as a chelate for an iron–carbonyl complex (adapted from ref. 61)

The design of cysteinyl ligands within secondary structure motifs of peptide and protein scaffolds is also conductive to preorganization of the thiolate ligands at distances compatible with the formation of a diiron active site. Initial work utilized CXXC motifs within a helical model peptide, so that the cysteinyl ligands are presented at *i, i+3*

positions on the same face of the helix.[64] The design of the hydrogenase maquette, SynHyd1, is based on Baldwin's alanine-rich helical peptides. Reaction with an inorganic precursor resulted in the formation of a structurally intact diiron hexacarbonyl cluster, as shown by UV-vis and FTIR spectroscopies, albeit no activity was reported for Fe_2SynHyd1. Incorporation of the cluster was well tolerated by the peptide, which conserved a high helical content. The peptide component serves the dual function of preorganizing the cysteinyl ligands as well as providing water solubility to the complex.

The approach was successfully extended to functional models in which the diiron hexacarbonyl cluster is tethered within natural proteins by exploiting existing CXXC motifs. Hayashi and colleagues used apo cytochrome c, which contains unique Cys at position 14 and 17.[65] Remarkably, the diiron hexacarbonyl-functionalized apo Cyt *c* catalyzes efficiently the reduction of protons to hydrogen in aqueous solutions at mild pH (4.7), in the presence of $Ru(bpy)_3$ as photosensitizer, and ascorbate as sacrificial electron donor; turnover numbers of approximately 80 are observed over 2 h. Similarly to apo Cyt *c*, though, the reconstituted H cluster-apo Cyt *c* appears only partially folded. In a helical protein, formation of the diiron hexacarbonyl center through a CXXC motif imposes a strain on the structure. The energetically favored rotamers of Cys in an a-helix place the sulfur atoms at a distance of 6 Å, considerably larger than the distance of 3.2 Å measured between the thiols in the hydrogenase bridging dithiolate ligand. Relaxing the requirement for structure at the backbone level opens up new avenues: in a follow-up work, the Hayashi group used the C-terminal sequence of cytochrome c_{556}, which contains both a CXXC motif and a His moiety in close proximity, to preorganize a diiron hexacarbonyl moiety close to a coordinatively attached ruthenium photosensitizer (Figure

1.4).[66] The 18-residue peptide is unfolded both in the apo state and in the functionalized state. Even though the reported turnover numbers for photocatalytic hydrogen production are low compared with other models, this design elegantly demonstrates intramolecular electron transfer between the photosensitizer and the catalytic site: a control in which the photosensitizer is not attached to the peptide, but added externally, is inactive in the conditions tested.

Conversely, the inorganic cluster can impart desired structural constrains to a peptide. For example, coordination to diiron hexacarbonyl was shown to replace a disulfide bond in the cyclic peptide octreotide, (Sandostatin), preserving structural integrity and retaining much of the binding affinity for the somastotin receptors.[67] Preliminary studies show that the octeotride construct retains the active site's ability to catalyze electrochemical proton reduction, albeit in DMF and with efficiency lower than other inorganic analogues.

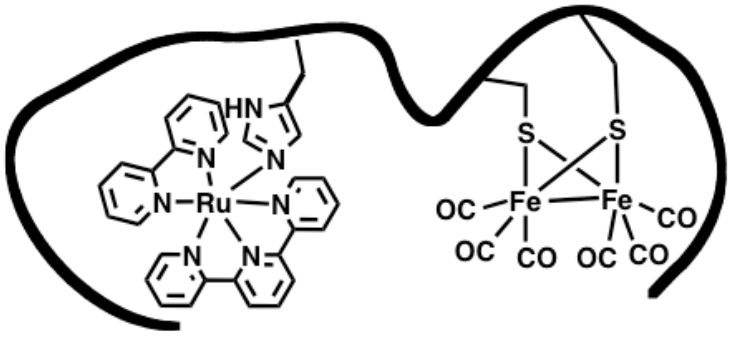

Figure 1.4: Schematic representation of the intramolecular photochemical system developed by Hayashi and coworkers: a $Fe_2(CO)_6$ cluster and a photoactive Ru(bpy)(tpy) complex (bpy = 2,2′-bipyridine, tpy = 2,2′:6′,2″-terpyridine) are attached to a peptide fragment of cyt c_{556} containing the native CXXCH sequence (adapted from ref. 66).

One possible approach to overcome negative constraints on peptide backbone structure utilizes unnatural amino acids to anchor the cluster to a peptide scaffold. Roy *et al.* used an on-resin protocol to derivatize a Lys with a propanedithiol unit, and demonstrated incorporation of the cluster in a simple model heptapeptide; no activity was reported.[68] The synthetic strategy used, however, poses restrictions in the use of the amino acid: the side chain of the lysine-propanedithiolate adduct is polar, long, and flexible, properties that preclude its incorporation within a structured scaffold and leave the cluster fully exposed to the solvent.

Functional models of hydrogenase.

A complementary approach to the design of hydrogenase mimics builds on so-called functional mimics of the enzymes, defined as organometallic complexes capable to carry out hydrogen production reversibly via a different catalytic site. Notable in this area are the Ni-phosphine complexes developed by DuBois, [69-74] the Fe-phosphine complex recently presented by Bullock and DuBois,[25] and the Ni-thiolate, the Co-dithiolene and the cobaloxime complexes developed by Artero, Eisenberg and Holland. [75-82] Recent reviews summarize these achievement.[83] Although the existing literature on these complexes is extensive, very little work has been done to integrate them into peptide scaffolds.

Most notably, DuBois and Shaw explored the use of the DuBois catalysts, consisting of mononuclear organometallic complexes based on nickel that contain chelating phosphine ligands and a bridging pendant tertiary amine that serves as proton donor with the general

formula $[Ni(P^{Ph}_2N^R_2)_2]^{2+}$; an overview of this work can be found in recent reviews.[70,84-86]

Aiming to introduce second coordination and outer coordination sphere interactions, the investigators functionalized the four pendant amines in the complex with amino acids and peptides. The synthetic protocol was modified by forming the cyclic phosphine ligands starting with functionalized precursor amines, and results in identical amino acids displayed onto each of the four amines in the final complex. The prototype glycylglycine adduct shows turnover frequencies (TOF) in the 200 to 1400 s^{-1} range, depending on substitution, in the presence of water; for comparison the unsubstituted $[Ni(P^{Ph}_2N^{Ph}_2)_2]^{2+}$ displays turnover frequencies of 700 s^{-1} in similar conditions. Systematic analysis of the results showed that, surprisingly, polar amino acids had little or no effect on catalytic activity. The presence of charged side chains, however, modulates the activity of the complex by one order of magnitude, with Glu and Lys increasing activity the most. [70,74] Further development of these models in structured scaffolds will need to address the current synthetic scheme, which results in symmetrical substitution of the complexes, as well as the dynamics of the complex during the catalytic cycle.

Electron-transfer modules

Hydrogenases generally contain an electron-transfer module containing iron-sulfur clusters in proximity of their redox-active catalytic site. These cofactors are also found in other complex catalytic machinery such as hydrogenases, nitrogenases, and photosystem I (PSI), making them highly relevant in designing proteins for fuel

production. A number of different groups have made recent advances in the incorporation of these electron transfer modules into peptides.

Iron-sulfur clusters are found in a wide range of forms in nature, including [2Fe-2S], [3Fe-4S], [4Fe-4S] and higher order clusters; of these, [4Fe-4S] cubane-type clusters are the most abundant (Figure 1.5).[87] These moieties are formed in proteins via coordination of iron through Cys side chains with bridging inorganic sulfur atoms. In many biological systems, [4Fe-4S] clusters are found aligned to create an electron conduit that shuffles electrons to and from the active site.

Along with their ability to function as electron transfer modules, iron-sulfur clusters also play a role in other processes, such as catalysis, iron level regulation and storage, as well as transport of ligands within the cell; they are also used in the multi-electron chemistry of proton reduction, sulfite reduction, and elemental nitrogen reduction. [88,89] Here, we will focus on the use of iron-sulfur clusters for the purposes of electron transfer.

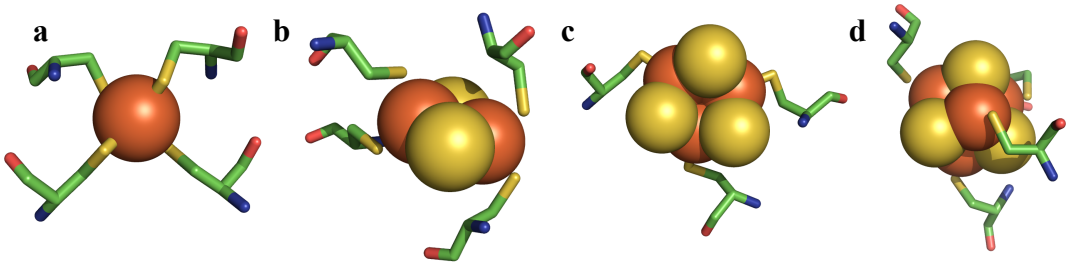

Figure 1.5: Structure of [Fe-S] clusters of different nuclearity. a) [Fe-S_4] center in Rubredoxin (PDB ID 1IU5), b) [Fe_2S_2] center from Spinach Ferredoxin (PDB ID

1A70) c) [3Fe-4S] cluster from [Ni-Fe] Hydrogenase (PDB ID 1H2R), d) [4Fe-4S] clusters from ferredoxins [PDB ID 2FDN)

Despite containing isostructural [4Fe-4S] clusters, iron-sulfur proteins exhibit redox potentials ranging from -700 mV to +450 mV, and have been shown to utilize three different redox states: $[4Fe\text{-}4S]^{3+/2+/1+}$.[90] It is believed that the electrostatic environment of amino acids surrounding the cluster, the hydrogen bonding interactions of bridging S-atoms, and the accessibility of the cluster to the solvent influence the potential observed for a particular cluster in a given context.[88] Due to their inherent structural complexity and to the necessity of a proteinogenic environment for existence in nature, a substantial amount of scientific effort has been dedicated to elucidating the structure-function relationship of iron-sulfur proteins in natural as well as *de novo* designed proteins. [91-94]

Work in natural proteins has not been able to fully elucidate the relationship between structure and iron-sulfur clusters redox potentials. Point mutagenesis work on the well studied ferredoxin proteins and the unique Rieske cluster has given some insight into the mechanisms by which nature has tuned iron-sulfur cluster redox potentials to particular functions. [91,93,94] Generally, it has been seen that introduction of positive charges into the proximity of the iron-sulfur clusters shifts the redox potential more positive, while the opposite holds true for introduction of negative charges. While the charges in proximity to each cluster can greatly affect the redox potential, it is also believed that hydrogen bonding to the polar peptide backbone significantly alters the apparent redox potentials. [93,95] It has been suggested that it is this hydrogen bonding that differentiates the two types of [4Fe-4S] clusters, those that employ a +3 to +2 transition, and those that employ a +2 to +1 transition (HiPiP vs Ferredoxin clusters), as the more

hydrogen bonds to Ferredoxin clusters allow for stabilization of higher electron density.[96] Although natural systems have lead to these general *a priori* trends, natural systems are limited in the information that can be obtained from them, as often multiple variables are changed at once. *De novo* design offers reliable systems to study these trends, to determine the contribution of each of these components in determining the redox potential of iron-sulfur clusters.

Iron-sulfur cluster binding sites have been incorporated into proteins that do not naturally bind this cofactor by using computational methods,[97] or reconstituted into minimalistic sequence motifs derived from natural proteins. Early work on [4Fe-4S] binding peptides was based on a conserved CXXCXXC sequence motif found in native cluster binding proteins such as the ferredoxins. It was shown that these peptides can generally incorporate iron sulfur clusters via *in situ* incorporation, in which the cluster is believed to form from inorganic precursors with β-mercaptoethanol ligands followed by an entropically driven exchange with the peptide, which acts as a chelating agent and releases the β-mercaptoethanol ligands. These early designs were reviewed recently.[90] Briefly, sequence alignment studies, confirmed by experimental characterization, narrowed the consensus sequence to CIACGAC. [98,99]

In the quest for increased structural and functional complexity, sequences adapted from the minimalistic motif CXXCXXC have been used as loops in helical hairpins. The Dutton lab engineered heme binding maquettes to design a helix-loop-helix motif that coordinates two hemes and one iron-sulfur cluster, and suggested that this motif dimerized into a four-helix bundle. The redox potential of the cluster, determined via spectroelectrochemical experiments, was -350 mV, which is comparable to that of natural

ferredoxins; it appears that the cluster's properties are not affected by the neighboring heme. A few possible models were put forward based on sequence information, and it is quite likely that the protein is a molten globule; no evidence was found for coupling between cofactors.[100]

This concept was adapted to reconstruct bridged metal assemblies based on the A-cluster of carbon monoxide dehydrogenase, which contains a cubane iron-sulfur cluster bridged to a Ni(II) site.[101] Using the ferredoxin consensus sequence, the Holm lab designed a series of four peptides that explored different ligand coordination spheres around the nickel. All the peptides bound a preformed cubane cluster with apparent 1:1 stoichiometry, and two of the peptides also bound nickel; it was not possible though to infer structural information from the available spectroscopic data.

Other efforts have focused on modeling the [4Fe-4S] clusters found in PSI, which contains three clusters, deemed F_X, F_A, and F_B. The F_x cluster is characterized by a pseudosymmetric arrangement in which the Cys ligands are contributed in pairs by the two subunits of the PsaA/PsaB heterodimer. Scott *et al*.[102] inserted the 10-amino acid consensus sequence CDGPGRGGTC as loops in helical hairpins designed to pair up into a four-helix bundle, so that the two loops coordinated a cubane cluster at one end of the bundle. The resulting protein displays a redox potential of -422 mV, reflecting the solvent exposed location of the cluster. In contrast, models of the F_A and F_b clusters had remained elusive. Utilizing the consensus binding sequence of CxxCxxCxxxCP found in PSI, Lubitz *et al.* modeled the individual binding sites of both F_A and F_B onto 16 amino acid peptides.[103] After cluster incorporation, the peptides showed similar redox potentials to the natural clusters, at -440 mV and -470 mV, and also irreversibly bound to PSI. This

approach has been extended recently to the incorporation of the less abundant Fe_3S_4 cluster through mutation of a single, ligating Cys residue to a Ser; further mutations in the variable portion of the consensus sequence were shown to modulate the efficiency of cluster incorporation as well as the relative preference for [4Fe-4S] vs [3Fe-4S].[92]

Recently, a computational methodology that starts from the geometric requirements of the metal was used to design a protein that incorporates an iron-sulfur cluster. [104,105] The natural symmetry of [4Fe-4S] clusters was extended to the four Cys making up the first coordination sphere, and then a four-helix bundle was built around the site. Notably, incorporation of the cluster into their artificial protein stabilizes the overall fold, leading to the conclusion that the designed a-helices are integral in cluster incorporation. The authors subsequently added to this peptide an empirically designed heme binding site. The new model successfully bound both the cluster and heme, although the latter with very low affinity. Throughout this series, though, oligomerization of the helical peptides was a large problem, affecting the functionality of the peptides.

Conclusions.

Since the first *de novo* designed proteins were reported 25 years ago, the field has advanced tremendously. This progress is mainly tied to the continuing optimization of computational algorithms and methods, which have emerged as a reliable approach to the design of protein structures and functions. [59,106,107] Indeed, relatively simple principles have been established for the development of stable and well-defined proteins[108-110] metalloproteins[111,112] and membrane proteins, [113-115] [116]paving the way for the design of

functional proteins[117,118] Recent success stories include the design of transferases,[119] hydrolases, [120-122] and oxidoreductases. [123-125] Building on these achievements, the field is now moving towards end-use inspired applications, with energy production emerging as one of the societal needs.

Scope of this thesis:

As mentioned in the above discussion, there has been a tremendous amount of work aimed at developing modular, biomimetic, and artificial proton reduction machinery for the development of a renewable energy source. Majority of these efforts are based on an organometallic platform, which has its own benefits. Most organometallic complexes are relatively easy to synthesize and characterize. Most importantly, majority of organometallic complexes can tolerate relatively harsh conditions such as organic solvents, high pressure and temperatures, which is beneficial in determining catalytic mechanism and other physicochemical properties of the catalyst. However, most of the time, resulting organometallic complexes are not compatible with aqueous solvent, an ideal solvent for proton reducion and utilizes a different mechanism than the natural enzyme. On the other end of spectrum, enzymes work under ambient conditions and are extremely efficient. But, difficulty in heterologous expression and oxygen sensitivity makes the native enzyme inapplicable for biotechnological purposes. In this thesis, we have taken a chemical biology approach where, we combine best of both worlds. We have attached simplistic synthetic organometallic unit to de novo designed and natural proteins utilizing a bottom up approach. This approach introduces the much-awaited modularity in the system, where the nature of organometallic complex can be varied as desired. On the other hand, native enzyme like interactions including secondary sphere

interactions can be introduced using the protein matrix, which appears to be otherwise herculean on completely synthetic organometallic complexes. We have also shown that multiredox cofactor binding protein can be engineered, which can be later introduced to close proximity of the catalytic site using principles of supramolecular protein designing, thus introducing real enzyme like properties in engineered system.

Chapter 2 and 3 of this thesis describes general design principles of multiredox cofactor binding protein and their characterization. Chapter 4 describes proof of concept hypothesis for designing proton reduction catalyst in a minimalistic peptide based model and our current effort of designing more elaborate protein matrix around the active site. In Chapter 5, we discuss this methodology extended to natural protein using a host guest approach.

REFERENCES:

(1) Cammack, R., Frey, M., and Robson, R. (2001) Hydrogen As a Fuel: Learning From Nature. Taylor and Francis, London.

(2) Amao, Y. (2011) Solar Fuel Production Based on the Artificial Photosynthesis System. ChemCatChem 3, 458–474.

(3) Gust, D., Moore, T. A., and Moore, A. L. (2012) Realizing artificial photosynthesis. Faraday Discuss. 155, 9–26.

(4) Gust, D., Moore, T. A., and Moore, A. L. (2009) Solar Fuels via Artificial Photosynthesis. Acc. Chem. Res. 42, 1890–1898.

(5) Wydrzynski, T. J., and Hillier, W. (2009) Molecular Solar Fuels. RCS, Cambridge, UK.

(6) Vignais, P. M., Billoud, B., and Meyer, J. (2001) Classification and phylogeny of hydrogenases. FEMS Microbiol. Rev. 25, 455–501.

(7) Vignais, P. M., and Billoud, B. (2007) Occurrence, Classification, and Biological Function of Hydrogenases: An Overview. Chem. Rev. 107, 4206–4272.

(8) Meyer, J. (2007) [FeFe] hydrogenases and their evolution: a genomic perspective. Cell. Mol. Life Sci. 64, 1063–1084.

(9) Shima, S., and Ermler, U. (2011) Structure and Function of [Fe]-Hydrogenase and its Iron–Guanylylpyridinol (FeGP) Cofactor. Eur. J. Inorg. Chem. 2011, 963–972.

(10) Shima, S., and Thauer, R. K. (2007) A third type of hydrogenase catalyzing H2 activation. Chem. Rec. 7, 37–46.

(11) Fontecilla-Camps, J. C., Volbeda, A., Cavazza, C., and Nicolet, Y. (2007) Structure/function relationships of [NiFe]- and [FeFe]-hydrogenases. 107, 4273–4303.

(12) Vincent, K. A., Parkin, A., and Armstrong, F. A. (2007) Investigating and Exploiting the Electrocatalytic Properties of Hydrogenases. Chem. Rev. 107, 4366–4413.

(13) Frey, M. (2002) Hydrogenases: Hydrogen-Activating Enzymes. ChemBioChem 3, 153–160.

(14) de Lacey, A. L., Fernandez, V. M., Rousset, M., and Cammack, R. (2007) Activation and Inactivation of Hydrogenase Function and the Catalytic Cycle: Spectroelectrochemical Studies. Chem. Rev. 107, 4304–4330.

(15) Volbeda, A., Charon, M.-H., Piras, C., Hatchikian, E. C., Frey, M., and Fontecilla-Camps, J. C. (1995) Crystal structure of the nickel-iron hydrogenase from Desulfovibrio

gigas. Nature 373, 580–587.

(16) Peters, J. W., Lanzilotta, W. N., Lemon, B. J., and Seefeldt, L. C. (1998) X-ray Crystal Structure of the Fe-Only Hydrogenase (CpI) from Clostridium pasteurianum to 1.8 Angstrom Resolution. Science 282, 1853–1858.

(17) Nicolet, Y., Piras, C., Legrand, P., Hatchikian, C. E., and Fontecilla-Camps, J. C. (1999) Desulfovibrio desulfuricans iron hydrogenase: the structure shows unusual coordination to an active site Fe binuclear center. Structure 7, 13–23.

(18) Nicolet, Y., de Lacey, A. L., Vernède, X., Fernandez, V. M., Hatchikian, E. C., and Fontecilla-Camps, J. C. (2001) Crystallographic and FTIR Spectroscopic Evidence of Changes in Fe Coordination Upon Reduction of the Active Site of the Fe-Only Hydrogenase from Desulfovibrio desulfuricans. J. Am. Chem. Soc. 123, 1596–1601.

(19) Happe, R. P., Roseboom, W., Pierik, A. J., Albracht, S. P. J., and Bagley, K. A. (1997) Biological activition of hydrogen. Nature 385, 126–126.

(20) Bagley, K. A., Duin, E. C., Roseboom, W., Albracht, S. P. J., and Woodruff, W. H. (1995) Infrared-Detectable Group Senses Changes in Charge Density on the Nickel Center in Hydrogenase from Chromatium vinosum. Biochemistry 34, 5527–5535.

(21) Pierik, A. J., Hulstein, M., Hagen, W. R., and Albracht, S. P. J. (1998) A low-spin iron with CN and CO as intrinsic ligands forms the core of the active site in [Fe]-hydrogenases. Eur J Biochem 258, 572–578.

(22) Hoffmann, P. (2012) Tomorrow's Energy: Hydrogen, Fuel Cells, and Prospects for a Cleaner Planet. MIT Press, Cambridge, MA.

(23) Bingham, A. S., Smith, P. R., and Swartz, J. R. (2012) Evolution of an [FeFe] hydrogenase with decreased oxygen sensitivity. Int. J. Hydrogen Energy 37, 2965–2976.

(24) Stapleton, J. A., and Swartz, J. R. (2010) Development of an In Vitro Compartmentalization Screen for High-Throughput Directed Evolution of [FeFe] Hydrogenases. PLoS ONE 5, 1–8.

(25) Liu, T., DuBois, D. L., and Bullock, R. M. (2013) An iron complex with pendent amines as a molecular electrocatalyst for oxidation of hydrogen. Nat. Chem. 5, 228–233.

(26) Camara, J. M., and Rauchfuss, T. B. (2011) Combining acid-base, redox and substrate binding functionalities to give a complete model for the [FeFe]-hydrogenase. Nat. Chem. 4, 26–30.

(27) Ogo, S., Ichikawa, K., Kishima, T., Matsumoto, T., Nakai, H., Kusaka, K., and Ohhara, T. (2013) A Functional [NiFe]Hydrogenase Mimic That Catalyzes Electron and Hydride Transfer from H2. Science 339, 682–684.

(28) Wilson, A. D., Newell, R. H., McNevin, M. J., Muckerman, J. T., Rakowski DuBois, M., and DuBois, D. L. (2005) Hydrogen Oxidation and Production Using Nickel-Based Molecular Catalysts with Positioned Proton Relays. J. Am. Chem. Soc. 128, 358–366.

(29) Smith, S. E., Yang, J. Y., DuBois, D. L., and Bullock, R. M. (2012) Reversible Electrocatalytic Production and Oxidation of Hydrogen at Low Overpotentials by a Functional Hydrogenase Mimic. Angew. Chem. 124, 3206–3209.

(30) Le Goff, A., Artero, V., Jousselme, B., Tran, P. D., Guillet, N., Métayé, R., Fihri, A., Palacin, S., and Fontecave, M. (2009) From Hydrogenases to Noble Metal–Free Catalytic Nanomaterials for H2 Production and Uptake. Science 326, 1384–1387.

(31) Cammack, R. (1999) Bioinorganic chemistry: Hydrogenase sophistication. Nature 397, 214–215.

(32) Mulder, D. W., Shepard, E. M., Meuser, J. E., Joshi, N., King, P. W., Posewitz, M. C., Broderick, J. B., and Peters, J. W. (2011) Insights into [FeFe]-hydrogenase structure, mechanism, and maturation. Structure 19, 1038–1052.

(33) Peters, J. W., and Broderick, J. B. (2012) Emerging Paradigms for Complex Iron-Sulfur Cofactor Assembly and Insertion. Annu. Rev. Biochem. 81, 429–450.

(34) Böck, A., King, P. W., Blokesch, M., and Posewitz, M. C. (2006) Advances in Microbial Physiology, in Advances in Microbial Physiology (Robert, K. P., Ed.), pp 1–225. Academic Press.

(35) Nicolet, Y., Lemon, B. J., Fontecilla-Camps, J. C., and Peters, J. W. (2000) A novel FeS cluster in Fe-only hydrogenases. Trends Biochem. Sci 25, 138–143.

(36) Lemon, B. J., and Peters, J. W. (1999) Binding of Exogenously Added Carbon Monoxide at the Active Site of the Iron-Only Hydrogenase (CpI) from Clostridium pasteurianum. Biochemistry 38, 12969–12973.

(37) Lespinat, P. A., Berlier, Y., Fauque, G., Czechowski, M., Dimon, B., and Le Gall, J. (1986) The pH dependence of proton-deuterium exchange, hydrogen production and uptake catalyzed by hydrogenases from sulfate-reducing bacteria. Biochimie 68, 55–61.

(38) Darensbourg, M. Y., Lyon, E. J., Zhao, X., and Georgakaki, I. P. (2003) The organometallic active site of [Fe]hydrogenase: Models and entatic states. Proc. Natl. Acad. Sci. USA 100, 3683–3688.

(39) Winkler, M., Esselborn, J., and Happe, T. (2013) Molecular basis of [FeFe]-hydrogenase function: An insight into the complex interplay between protein and catalytic cofactor. Biochim. Biophys. Act - Bioenerg. in press.

(40) Kubas, G. J. (2007) Fundamentals of H2 Binding and Reactivity on Transition Metals Underlying Hydrogenase Function and H2 Production and Storage. Chem. Rev.

107, 4152–4205.

(41) Bruschi, M., Greco, C., Bertini, L., Fantucci, P., Ryde, U., and Gioia, L. D. (2010) Functionally Relevant Interplay between the Fe4S4 Cluster and CN− Ligands in the Active Site of [FeFe]-Hydrogenases. J. Am. Chem. Soc. 132, 4992–4993.

(42) Liu, Z.-P., and Hu, P. (2002) A Density Functional Theory Study on the Active Center of Fe-Only Hydrogenase: Characterization and Electronic Structure of the Redox States. J. Am. Chem. Soc. 124, 5175–5182.

(43) Darensbourg, M. Y., and Bethel, R. D. (2012) Biomimetic chemistry: Merging the old with the new. Nat. Chem. 4, 11–13.

(44) Knorzer, P., Silakov, A., Foster, C. E., Armstrong, F. A., Lubitz, W., and Happe, T. (2012) Importance of the Protein Framework for Catalytic Activity of [FeFe]-Hydrogenases. J. Biol. Chem. 287, 1489–1499.

(45) Pandey, A. S., Harris, T. V., Giles, L. J., Peters, J. W., and Szilagyi, R. K. (2008) Dithiomethylether as a Ligand in the Hydrogenase H-Cluster. J. Am. Chem. Soc. 130, 4533–4540.

(46) Lyon, E. J., Georgakaki, I. P., Reibenspies, J. H., and Darensbourg, M. Y. (1999) Carbon Monoxide and Cyanide Ligands in a Classical Organometallic Complex Model for Fe-Only Hydrogenase. Angew. Chem. Int. Ed. 38, 3178–3180.

(47) Schmidt, M., Contakes, S. M., and Rauchfuss, T. B. (1999) First Generation Analogues of the Binuclear Site in the Fe-Only Hydrogenases: Fe2(μ-SR)2(CO)4(CN)22. J. Am. Chem. Soc. 121, 9736–9737.

(48) Le Cloirec, A., C Davies, S., J Evans, D., L Hughes, D., J Pickett, C., P Best, S., and Borg, S. (1999) A di-iron dithiolate possessing structural elements of the carbonyl/cyanide sub-site of the H-centre of Fe-only hydrogenase. Chem. Commun. 0, 2285–2286.

(49) Erdem, Ö. F., Schwartz, L., Stein, M., Silakov, A., Kaur-Ghumaan, S., Huang, P., Ott, S., Reijerse, E. J., and Lubitz, W. (2011) A Model of the [FeFe] Hydrogenase Active Site with a Biologically Relevant Azadithiolate Bridge: A Spectroscopic and Theoretical Investigation. Angew. Chem. Int. Ed. 50, 1439–1443.

(50) Singleton, M. L., Crouthers, D. J., Duttweiler, R. P. 3., Reibenspies, J. H., and Darensbourg, M. Y. (2011) Sulfonated diiron complexes as water-soluble models of the [Fe-Fe]-hydrogenase enzyme active site. Inorganic chemistry 50, 5015–5026.

(51) Barton, B. E., Olsen, M. T., and Rauchfuss, T. B. (2010) Artificial hydrogenases. Curr. Opin. Biotechnol. 21, 292–297.

(52) Tard, C., and Pickett, C. J. (2009) Structural and Functional Analogues of the Active

Sites of the [Fe]-, [NiFe]-, and [FeFe]-Hydrogenases. Chem. Rev. 109, 2245–2274.

(53) Ezzaher, S., Gogoll, A., Bruhn, C., and Ott, S. (2010) Directing protonation in [FeFe] hydrogenase active site models by modifications in their second coordination sphere. Chem. Commun. 46, 5775–5777.

(54) Surawatanawong, P., Tye, J. W., Darensbourg, M. Y., and Hall, M. B. (2010) Mechanism of electrocatalytic hydrogen production by a di-iron model of iron-iron hydrogenase: a density functional theory study of proton dissociation constants and electrode reduction potentials. Dalton Trans. 39, 3093–3104.

(55) Wang, F., Wang, W.-G., Wang, X.-J., Wang, H.-Y., Tung, C.-H., and Wu, L.-Z. (2011) A Highly Efficient Photocatalytic System for Hydrogen Production by a Robust Hydrogenase Mimic in an Aqueous Solution - Wang - 2011 - Angewandte Chemie International Edition - Wiley Online Library. Angew. Chem. Int. Ed. 50, 3193–3197.

(56) Wang, W.-G., Wang, F., Wang, H.-Y., Tung, C.-H., and Wu, L.-Z. (2012) Electron transfer and hydrogen generation from a molecular dyad: platinum(II) alkynyl complex anchored to [FeFe] hydrogenase subsite mimic. Dalton Trans. 41, 2420–2426.

(57) Singleton, M. L., Reibenspies, J. H., and Darensbourg, M. Y. (2010) A cyclodextrin host/guest approach to a hydrogenase active site biomimetic cavity. J. Am. Chem. Soc. 132, 8870–8871.

(58) Hsieh, C.-H., Erdem, Ö. F., Harman, S. D., Singleton, M. L., Reijerse, E., Lubitz, W., Popescu, C. V., Reibenspies, J. H., Brothers, S. M., Hall, M. B., and Darensbourg, M. Y. (2012) Structural and Spectroscopic Features of Mixed Valent FeIIFeI Complexes and Factors Related to the Rotated Configuration of Diiron Hydrogenase. J. Am. Chem. Soc. 134, 13089–13102.

(59) DeGrado, W. F., Summa, C. M., Pavone, V., Nastri, F., and Lombardi, A. (1999) De novo design and structural characterization of metalloproteins. Annu. Rev. Biochem. 68, 779–819.

(60) He, C., Wang, M., Zhang, X., Wang, Z., Chen, C., Liu, J., Åkermark, B., and Sun, L. (2004) An Unusual Cyclization in a Bis(cysteinyl-S) Diiron Complex Related to the Active Site of Fe-Only Hydrogenases. Angew. Chem. 116, 3655–3658.

(61) de Hatten, X., Bothe, E., Merz, K., Huc, I., and Metzler-Nolte, N. (2008) A Ferrocene–Peptide Conjugate as a Hydrogenase Model System. Eur. J. Inorg. Chem. 2008, 4530–4537.

(62) de Hatten, X., Cournia, Z., Huc, I., Smith, J. C., and Metzler-Nolte, N. (2007) Force-Field Development and Molecular Dynamics Simulations of Ferrocene–Peptide Conjugates as a Scaffold for Hydrogenase Mimics. Chem. Eur. J. 13, 8139–8152.

(63) de Hatten, X., Weyhermüller, T., and Metzler-Nolte, N. (2004) Ferrocenoyl peptides

with sulfur-containing side chains: synthesis, solid state and solution structures. J. Organomet. Chem. 689, 4856–4867.

(64) Jones, A. K., Lichtenstein, B. R., Dutta, A., Gordon, G., and Dutton, P. L. (2007) Synthetic Hydrogenases: Incorporation of an Iron Carbonyl Thiolate into a Designed Peptide. J. Am. Chem. Soc. 129, 14844–14845.

(65) Sano, Y., Onoda, A., and Hayashi, T. (2011) A hydrogenase model system based on the sequence of cytochrome c: photochemical hydrogen evolution in aqueous media. Chem. Commun. (Camb.) 47, 8229–8231.

(66) Sano, Y., Onoda, A., and Hayashi, T. (2011) Photocatalytic hydrogen evolution by a diiron hydrogenase model based on a peptide fragment of cytochrome c556 with an attached diiron carbonyl cluster and an attached ruthenium photosensitizer. J. Inorg. Biochem. 108, 159–162.

(67) Apfel, U.-P., Volkers, P., Tard, C., Kowol, C. R., Rauchfuss, T. B., Pickett, C. J., Halpin, Y., Kloss, F., Kuebel, J., Goerls, H., Vos, J. G., Keppler, B. K., Morera, E., Lucente, G., and Weigand, W. (2007) Extending the motif of the [FeFe]-hydrogenase active site models: Protonation of Fe-2(NR)(2)(CO)(6-x)L-x species. J. Inorg. Biochem. 101, 1748–1751.

(68) Roy, S., Shinde, S., Hamilton, G. A., Hartnett, H. E., and Jones, A. K. (2011) Artificial [FeFe]-Hydrogenase: On Resin Modification of an Amino Acid to Anchor a Hexacarbonyldiiron Cluster in a Peptide Framework. Eur. J. Inorg. Chem. (Darensbourg, M. Y., and Weigand, W., Eds.) 2011, 1050–1055.

(69) Helm, M. L., Stewart, M. P., Bullock, R. M., DuBois, M. R., and DuBois, D. L. (2011) A Synthetic Nickel Electrocatalyst with a Turnover Frequency Above 100,000 s-1 for H2 Production. Science 333, 863–866.

(70) Jain, A., Lense, S., Linehan, J. C., Raugei, S., Cho, H., DuBois, D. L., and Shaw, W. J. (2011) Incorporating peptides in the outer-coordination sphere of bioinspired electrocatalysts for hydrogen production. Inorganic chemistry 50, 4073–4085.

(71) O'Hagan, M., Ho, M. H., Yang, J. Y., Appel, A. M., Rakowski DuBois, M., Raugei, S., Shaw, W. J., DuBois, D. L., and Bullock, R. M. (2012) Proton delivery and removal in [Ni(P(R)2N(R')2)2]2+ hydrogen production and oxidation catalysts. J. Am. Chem. Soc. 134, 19409–19424.

(72) O'Hagan, M., Shaw, W. J., Raugei, S., Chen, S., Yang, J. Y., Kilgore, U. J., DuBois, D. L., and Bullock, R. M. (2011) Moving protons with pendant amines: proton mobility in a nickel catalyst for oxidation of hydrogen. J. Am. Chem. Soc. 133, 14301–14312.

(73) Pool, D. H., Stewart, M. P., O'Hagan, M., Shaw, W. J., Roberts, J. A., Bullock, R. M., and DuBois, D. L. (2012) Acidic ionic liquid/water solution as both medium and proton source for electrocatalytic H2 evolution by [Ni(P2N2)2]2+ complexes. Proc. Natl.

Acad. Sci. USA 109, 15634–15639.

(74) Shaw, W. J., Helm, M. L., and DuBois, D. L. (2013) A modular, energy-based approach to the development of nickel containing molecular electrocatalysts for hydrogen production and oxidation. Biochim. Biophys. Acta.1827, 1123-1139.

(75) Jacques, P.-A., Artero, V., Pecaut, J., and Fontecave, M. (2009) Cobalt and nickel diimine-dioxime complexes as molecular electrocatalysts for hydrogen evolution with low overvoltages. Proc. Natl. Acad. Sci. USA 106, 20627–20632.

(76) Zhang, P., Jacques, P.-A., Chavarot-Kerlidou, M., Wang, M., Sun, L., Fontecave, M., and Artero, V. (2012) Phosphine Coordination to a Cobalt Diimine–Dioxime Catalyst Increases Stability during Light-Driven H2 Production. Inorganic chemistry 51, 2115–2120.

(77) Fourmond, V., Canaguier, S., Golly, B., Field, M. J., Fontecave, M., and Artero, V. (2011) A nickel-manganese catalyst as a biomimic of the active site of NiFe hydrogenases: a combined electrocatalytical and DFT mechanistic study. Energy Environ. Sci. 4, 2417–2427.

(78) Canaguier, S., Fourmond, V., Perotto, C. U., Fize, J., Pecaut, J., Fontecave, M., Field, M. J., and Artero, V. (2013) Catalytic hydrogen production by a Ni-Ru mimic of NiFe hydrogenases involves a proton-coupled electron transfer step. Chem. Commun. 49, 5004–5006.

(79) McCormick, T. M., Han, Z., Weinberg, D. J., Brennessel, W. W., Holland, P. L., and Eisenberg, R. (2011) Impact of Ligand Exchange in Hydrogen Production from Cobaloxime-Containing Photocatalytic Systems. Inorganic chemistry 50, 10660–10666.

(80) McNamara, W. R., Han, Z., Yin, C. J., Brennessel, W. W., Holland, P. L., and Eisenberg, R. (2012) Cobalt-dithiolene complexes for the photocatalytic and electrocatalytic reduction of protons in aqueous solutions. Proc. Natl. Acad. Sci. USA 109, 15594–15599.

(81) McNamara, W. R., Han, Z., Alperin, P. J., Brennessel, W. W., Holland, P. L., and Eisenberg, R. (2011) A Cobalt–Dithiolene Complex for the Photocatalytic and Electrocatalytic Reduction of Protons. J. Am. Chem. Soc. 133, 15368–15371.

(82) Du, P., Schneider, J., Luo, G., Brennessel, W. W., and Eisenberg, R. (2009) Visible light-driven hydrogen production from aqueous protons catalyzed by molecular cobaloxime catalysts. Inorganic chemistry 48, 4952–4962.

(83) Eckenhoff, W. T., McNamara, W. R., Du, P., and Eisenberg, R. (2013) Cobalt complexes as artificial hydrogenases for the reductive side of water splitting. Biochim. Biophys. Act - Bioenerg. 1827, 958–973.

(84) Shaw, W. J. (2012) The Outer-Coordination Sphere: Incorporating Amino Acids and

Peptides as Ligands for Homogeneous Catalysts to Mimic Enzyme Function. Cat. Rev. - Sci. Eng. 54, 489–550.

(85) Reback, M. L., Ginovska-Pangovska, B., Ho, M.-H., Jain, A., Squier, T. C., Raugei, S., Roberts, J. A. S., and Shaw, W. J. (2013) The Role of a Dipeptide Outer-Coordination Sphere on H2-Production Catalysts: Influence on Catalytic Rates and Electron Transfer. Chem. Eur. J. 19, 1928–1941.

(86) Jain, A., Reback, M. L., Lindstrom, M. L., Thogerson, C. E., Helm, M. L., Appel, A. M., and Shaw, W. J. (2012) Investigating the Role of the Outer-Coordination Sphere in [Ni(PPh2NPh-R2)2]2+ Hydrogenase Mimics. Inorganic chemistry 51, 6592–6602.

(87) Fontecave, M. (2006) Iron-sulfur clusters: ever-expanding roles. Nat. Chem. Biol. 2, 171–174.

(88) Beinert, H. (1997) Iron-Sulfur clusters: Nature's modular, multipurpose structures. Science 277, 653–659.

(89) Klausner, R. D., and Rouault, T. A. (1993) A double life: cytosolic aconitase as a regulatory RNA binding protein. Molecular biology of the cell 4, 1–5.

(90) Koay, M. S., Antonkine, M. L., Gartner, W., and Lubitz, W. (2008) Modelling low-potential [Fe4S4] clusters in proteins. Chem. Biodivers. 5, 1571–1587.

(91) Brereton, P. S., Verhagen, M. F., Zhou, Z. H., and Adams, M. W. (1998) Effect of iron-sulfur cluster environment in modulating the thermodynamic properties and biological function of ferredoxin from Pyrococcus furiosus. Biochemistry 37, 7351–7362.

(92) Hoppe, A., Pandelia, M. E., Gartner, W., and Lubitz, W. (2011) [Fe(4)S(4)]- and [Fe(3)S(4)]-cluster formation in synthetic peptides. Biochim. Biophys. Acta 1807, 1414–1422.

(93) Klingen, A. R., and Ullmann, G. M. (2004) Negatively charged residues and hydrogen bonds tune the ligand histidine pKa values of Rieske iron-sulfur proteins. Biochemistry 43, 12383–12389.

(94) Beck, B. W., Xie, Q., and Ichiye, T. (2001) Sequence determination of reduction potentials by cysteinyl hydrogen bonds and peptide pipoles in [4Fe-4S] ferredoxins. Biophysical journal 81, 601–613.

(95) Kolling, D. J., Brunzelle, J. S., Lhee, S., Crofts, A. R., and Nair, S. K. (2007) Atomic resolution structures of rieske iron-sulfur protein: role of hydrogen bonds in tuning the redox potential of iron-sulfur clusters. Structure 15, 29–38.

(96) Backes, G., Mino, Y., Loehr, T., Meyer, T., Cusanovich, M. A., Sweeney, W. V., Adman, E. T., and Sanders-Loehr, J. (1991) The enviornment of Fe4S4 clusters in ferredoxins and high-potential iron proteins. New information from x-ray crystallography

and resoance raman spectroscopy. J. Am. Chem. Soc. 113, 2055–2064.

(97) Coldren, C. D., Hellinga, H. W., and Caradonna, J. P. (1997) The rational design and construction of a cuboidal iron–sulfur protein. Proc. Natl. Acad. Sci. USA 94, 6635–6640.

(98) Mulholland, S. E., Gibney, B. R., Rabanal, F., and Dutton, P. L. (1998) Characterization of the fundamental protein ligand requirements of [4Fe-4S](2+/+) clusters with sixteen amino acid maquettes. J. Am. Chem. Soc. 120, 10296–10302.

(99) Mulholland, S. E., Gibney, B. R., Rabanal, F., and Dutton, P. L. (1999) Determination of nonligand amino acids critical to [4Fe-4S]2+/+ assembly in ferredoxin maquettes. Biochemistry 38, 10442–10448.

(100) Gibney, B. R., Mulholland, S. E., Rabanal, F., and Dutton, P. L. (1996) Ferredoxin and ferredoxin-heme maquettes. Proceedings of the National Academy of Sciences of the United States of America 93, 15041–15046.

(101) Laplaza, C. E., and Holm, R. H. (2001) Helix-loop-helix peptides as scaffolds for the construction of bridged metal assemblies in proteins: the spectroscopic A-cluster structure in carbon monoxide dehydrogenase. J. Am. Chem. Soc. 123, 10255–10264.

(102) Scott, M. P., and Biggins, J. (1997) Introduction of a [4Fe-4S (S-cys)4]+1,+2 iron-sulfur center into a four-alpha helix protein using design parameters from the domain of the Fx cluster in the Photosystem I reaction center. Protein Sci. 6, 340–346.

(103) Antonkine, M. L., Breitenstein, C., Epel, B., Bill, E., Gärtner, W., and Lubitz, W. (2008) De novo Peptides Modeling the Binding Sites of [4Fe-4S] Clusters in Photosystem I. Photosynthesis. Energy from the Sun; 14th International Congress on Photosynthesis 1257–1260.

(104) Grzyb, J., Xu, F., Nanda, V., Luczkowska, R., Reijerse, E., Lubitz, W., and Noy, D. (2012) Empirical and computational design of iron-sulfur cluster proteins. Biochim. Biophys. Acta 1817, 1256–1262.

(105) Grzyb, J., Xu, F., Weiner, L., Reijerse, E. J., Lubitz, W., Nanda, V., and Noy, D. (2010) De novo design of a non-natural fold for an iron-sulfur protein: alpha-helical coiled-coil with a four-iron four-sulfur cluster binding site in its central core. Biochim. Biophys. Acta 1797, 406–413.

(106) Koga, N., Tatsumi-Koga, R., Liu, G., Xiao, R., Acton, T. B., Montelione, G. T., and Baker, D. (2012) Principles for designing ideal protein structures. Nature 491, 222–227.

(107) Guntas, G., Purbeck, C., and Kuhlman, B. (2010) Engineering a protein–protein interface using a computationally designed library. Proc. Natl. Acad. Sci. USA.

(108) Samish, I., MacDermaid, C. M., Perez-Aguilar, J. M., and Saven, J. G. (2011) Theoretical and Computational Protein Design. Annu. Rev. Phys. Chem. 62, 129–149.

(109) Nanda, V., and Koder, R. L. (2010) Designing artificial enzymes by intuition and computation. Nat. Chem. 2, 15–24.

(110) Suárez, M., and Jaramillo, A. (2009) Challenges in the computational design of proteins. J. R. Soc. Interface.

(111) Peacock, A. F. A., Iranzo, O., and Pecoraro, V. L. (2009) Harnessing natures ability to control metal ion coordination geometry using de novo designed peptides. Dalton Trans. 0, 2271–2280.

(112) Ghosh, D., and Pecoraro, V. L. (2005) Probing metal–protein interactions using a de novo design approach. Curr Opin Chem Biol 9, 97–103.

(113) Senes, A. (2011) Computational design of membrane proteins. Curr. Opin. Struct. Biol. 21, 460–466.

(114) Ghirlanda, G. (2009) Design of membrane proteins: toward functional systems. Curr Opin Chem Biol 13, 643–651.

(115) Shinde, S., Cordova, J., Woodrum, B., and Ghirlanda, G. (2012) Modulation of function in a minimalist heme-binding membrane protein. J Biol Inorg Chem 17, 557–564.

(116) Yin, H., Slusky, J. S., Berger, B. W., Walters, R. S., Vilaire, G., Litvinov, R. I., Lear, J. D., Caputo, G. A., Bennett, J. S., and DeGrado, W. F. (2007) Computational Design of Peptides That Target Transmembrane Helices. Science 315, 1817–1822.

(117) Koder, R. L., Anderson, J. L. R., Solomon, L. A., Reddy, K. S., Moser, C. C., and Dutton, P. L. (2009) Design and engineering of an O2 transport protein. Nature 458, 305–309.

(118) Reig, A. J., Pires, M. M., Snyder, R. A., Wu, Y., Jo, H., Kulp, D. W., Butch, S. E., Calhoun, J. R., Szyperski, T. G., Solomon, E. I., and DeGrado, W. F. (2012) Alteration of the oxygen-dependent reactivity of de novo Due Ferri proteins. Nat. Chem. 4, 900–906.

(119) Wilcoxen, K. M., Leman, L. J., Weinberger, D. A., Huang, Z.-Z., and Ghadiri, M. R. (2007) Biomimetic Catalysis of Intermodular Aminoacyl Transfer. J. Am. Chem. Soc. 129, 748–749.

(120) Khare, S. D., Kipnis, Y., Greisen, P. J., Takeuchi, R., Ashani, Y., Goldsmith, M., Song, Y., Gallaher, J. L., Silman, I., Leader, H., Sussman, J. L., Stoddard, B. L., Tawfik, D. S., and Baker, D. (2012) Computational redesign of a mononuclear zinc metalloenzyme for organophosphate hydrolysis. Nat. Chem. Biol. 8, 294–300.

(121) Der, B. S., Edwards, D. R., and Kuhlman, B. (2012) Catalysis by a De Novo Zinc-Mediated Protein Interface: Implications for Natural Enzyme Evolution and Rational Enzyme Engineering. Biochemistry 51, 3933–3940.

(122) Zastrow, M. L., PeacockAnna, F. A., Stuckey, J. A., and Pecoraro, V. L. (2012) Hydrolytic catalysis and structural stabilization in a designed metalloprotein. Nat. Chem. 4, 118–123.

(123) Faiella, M., Andreozzi, C., de Rosales, R. T. M., Pavone, V., Maglio, O., Nastri, F., DeGrado, W. F., and Lombardi, A. (2009) An artificial di-iron oxo-protein with phenol oxidase activity. Nat. Chem. Biol. 5, 882–884.

(124) Faiella, M., Maglio, O., Nastri, F., Lombardi, A., Lista, L., Hagen, W. R., and Pavone, V. (2012) Inside Cover: De Novo Design, Synthesis and Characterisation of MP3, A New Catalytic Four-Helix Bundle Hemeprotein (Chem. Eur. J. 50/2012). Chem. Eur. J. 18, 15890–15890.

(125) Lichtenstein, B. R., Farid, T. A., Kodali, G., Solomon, L. A., Anderson, J. L., Sheehan, M. M., Ennist, N. M., Fry, B. A., Chobot, S. E., Bialas, C., Mancini, J. A., Armstrong, C. T., Zhao, Z., Esipova, T. V., Snell, D., Vinogradov, S. A., Discher, B. M., Moser, C. C., and Dutton, P. L. (2012) Engineering oxidoreductases: maquette proteins designed from scratch. Biochem. Soc. Trans. 40, 561–566.

CHAPTER 2

DE NOVO DESIGN OF AN ARTIFICIAL BIS-[4FE-4S] BINDING PROTEIN

Anindya Roy,[a] Iosifina Sarrou [a], Michael D. Vaughn [a] Andrei V. Astashkin [b], and Giovanna Ghirlanda*[a]

[a] Department of Chemistry and Biochemistry, Arizona State University, Tempe, AZ 85287-1604; [b] Department of Chemistry and Biochemistry, University of Arizona, Tucson, AZ, 85721

Reproduced by permission from Biochemistry, 2013, 52 (43), 7586-7594

KEYWORDS. De novo design, metalloproteins, iron-sulfur clusters, EPR, pulsed ELDOR, coiled coil.

ABSTRACT. In nature, protein subunits containing multiple iron-sulfur clusters often mediate the delivery of reducing equivalents from metabolic pathways to the active site of redox proteins. Thus, the de novo design of redox active proteins should include the engineering of a conduit for delivery of electrons to and from the active site, in which multiple redox-active centers are arranged in a controlled manner. Here, we describe a

designed three-helix protein, DSD-bis[4Fe-4S], that coordinates two iron-sulfur clusters within its hydrophobic core. The design exploits the pseudo two-fold symmetry of the protein scaffold, DSD, which is a homodimeric three-helix bundle. Starting from the sequence of the parent peptide, eight leucine residues per dimer in the hydrophobic core are mutated to cysteine to provide the first coordination sphere for cubane-type iron-sulfur clusters. Incorporation of two clusters per dimer is readily achieved by *in situ* reconstitution, and imparts increased stability to thermal denaturation compared to the apo form of the peptide as assessed by CD monitored thermal denaturation. The presence of [4Fe-4S] clusters in intact proteins is confirmed by UV-vis spectroscopy, gel filtration, analytical ultracentrifugation, and EPR spectroscopy. Pulsed electron-electron double resonance (ELDOR) experiments have detected the magnetic dipole interaction between the two clusters of about 0.7 MHz, which is consistent with the expected inter-cluster distance of ~36 Å. Taken together, our data demonstrate the successful design of an artificial multi-FeS cluster protein with evidence of cluster-cluster interaction. The design principles implemented here can be extended to the design of multi-cluster molecular wires.

Introduction.

[Fe-S] cluster proteins represent one of the most abundant and functionally pliable classes of proteins: they carry out a wide variety of biological functions including catalysis, oxygen sensing, and electron transfer.[1-5] The chemical properties of the [Fe-S] clusters, such as low redox potential and high oxygen sensitivity, their prevalence, and their structural and functional flexibility, suggest that they emerged during early evolution.[6-8] Most frequently, [Fe-S] clusters act as donors or acceptors of electrons at a wide range of potentials, and they are organized in protein-embedded redox chains that function as relays for the transfer of electrons from soluble protein partners to catalytic centers in complex, often multiunit, proteins.[9-14]

The most common type of [Fe-S] cluster, the [4Fe-4S] cubane-like structure, is generally coordinated by four cysteines in a variety of protein folds, often in a combination of loops and secondary structure elements.[7,15] A common fold is that of the ferredoxins, small soluble electron carrier proteins that can contain one or two clusters coordinated by four conserved cysteines.[7,16,17] The two-cluster ferredoxin-like fold is also found in the PsaC subunit of Photosystem I[18,19] and in hydrogenases as part of the accessory iron-sulfur cluster binding domain, which regulates long range electron transfer to/from the active site (H-cluster).[13,20-23]

Over the years, a substantial amount of scientific effort has been dedicated to elucidating the structure-function relationship of different clusters with their protein counterpart in natural and de novo designed model systems. Model proteins designed to coordinate an iron sulfur cluster generally utilize loop regions to accommodate the

cluster, resembling the sequence and topology found in most of the natural proteins.[8,15,24-26] Computational approaches have been used to position an idealized cluster into a designed 4-helix coiled coil[5,27,28] or into the structure of natural proteins[27,29]. These models were designed to contain a single iron-sulfur cluster, either isolated within the protein scaffold or in proximity to a second cofactor.[5,30,31] When functioning as electron conduits, however, iron-sulfur clusters are generally arranged in chains of two or more.[9-14]

As a first step towards constructing bioinspired functional redox proteins encompassing an electron transfer domain and a catalytic domain,[15,32,33] we have engineered a model system that contains two [4Fe-4S] clusters embedded in the hydrophobic core of a de novo designed helical three-helix bundle. We present here the design, synthesis and characterization of this model system, DSD-bis[4Fe-4S], demonstrating for the first time the incorporation of two clusters at a defined distance. This approach can be extended to the design of other systems, in which the intercluster distance can be modulated by exploiting the geometric properties of α-helical coiled coils.[1,3,5,15,34,35]

Materials and Methods

Chemicals. Chemicals were purchased from Sigma Aldrich; Fmoc protected amino acids for solid phase peptide synthesis were purchased from Novabiochem. All reactions were performed under an inert environment either using a Schlenk line or in a glovebox (Coy Scientific), unless otherwise noted. All buffers/solutions were degassed extensively by purging with N_2 prior to their transfer to the glovebox.

Protein Design.

Models of DSD-4Cys and DSD-bis[4Fe-4S] were built in MacPyMol[6,36,37] starting from the coordinates of DSD (PDB ID 1G6U). Leucines 9, 12, 22, and 43 in DSD were mutated to cysteine, and side chain orientations were selected among the backbone-dependent favorable rotamers in MacPyMol. Disembodied [4Fe-4S] cluster and four cysteines that form the primary coordination sphere were obtained from *Thermoatoga maritima* tryptophanyl t-RNA synthase (PDB ID 2G36) and manually docked onto DSD-4Cys using pairwise alignment in MacPyMol. Finally, new bonds were created using the Build function.The models of DSD-4Cys, DSD-bis[4Fe-4S], and the original DSD structure were analyzed with Q-Sitefinder,[9,36,37] which identifies and measures the volume of cavities using PDB files as input.

Peptide synthesis and purification.

DSD-4Cys, which is comprised of 49 amino acids, was synthesized on a Liberty microwave-assisted solid phase peptide synthesizer (CEM). Peptide synthesis was performed using standard Fmoc/t-Bu/Trt protecting strategy on a Rink amide resin; the N-terminus of the peptide was acetylated. Cleavage from the resin and simultaneous removal of side chain protecting groups was achieved by treatment with 94% TFA, 2.5% water 2.5% EDT, 1% TIS. The crude peptide was purified by HPLC on a C-18 semi-preparative column (Vydac, 1cm x 25cm), using gradient elution with solvent system A (100% water and 0.1% TFA) and B (95% Acetonitrile, 5% water and 0.1%TFA) at 4 ml/min flow-rate. Peptide purity was confirmed by re-injecting appropriate fractions on

analytical C-18 column; the molecular weight of the peptide was verified by MALDI-TOF mass spectrometry. Peptides used for further experiments were >99% pure.

Direct incorporation of [4Fe-4S] cluster into the synthesized peptides.

All the reactions were performed in an anaerobic chamber (Coy Scientific) under an inert atmosphere. Cluster incorporation was performed following an established protocol.[15,35] Briefly, a 120 mM solution of DSD-4Cys peptide in 100 mM Tris-HCl, pH=8.5, 2 M urea, was treated with 0.8% (v/v) BME for 2 hours. To this solution iron (III) chloride ($FeCl_3$) and a freshly prepared solution of sodium sulfide (Na_2S) in water were added in 30-min intervals to a final concentration of 30 mM. The resulting dark brown solution was incubated overnight at 4°C under N_2. The reaction mixture was then passed through a PD10 G25 desalting column (GE healthcare) pre-equilibrated with 50 mM Tris-HCl buffer, pH=7.5, to exclude all non-protein, low molecular weight contaminants and salts. Appropriate fractions were collected in 1 ml increments and subjected to characterization.

UV-Vis Spectroscopy.

UV-Vis spectra were recorded on a Perkin-Elmer Lambda-35 spetrophotomether in anaerobic conditions using a sealed cuvette with a 1 cm path length.

MALDI-TOF Spectroscopy:

Cluster incorporation was carried out as described in the main text. After overnight incubation, the reaction mixture was passed through a G-25, PD10 desalting column pre-equilibrated with100 mM NH4HCO3, pH=7.5. Appropriate fractions were collected and

used to prepare MALDI samples anaerobically. Specifically, 2 μL of protein sample were mixed 2 μl of matrix stock (alpha-Cyano-4-hydroxycinnamic acid in 0.1% TFA in water) and dried on a sample plate in the glove box. The plate was transferred in an argon-filled small chamber and transferred out of the glove box for MALDI characterization. MALDI-TOF (Matrix Assisted Laser Desorption Ionization-Time of Flight) spectrometry was carried out using a Applied Biosystems DE-STR MALDI-TOF instrument under linear/positive ionization mode.

Gel filtration.

The oligomerization states of DSD-4Cys and DSD-bis[4Fe-4S], were determined on a G-25 gel filtration column using an Agilent Technologies 1260 Insight FPLC system. The apo peptide was treated with 10 fold molar excess DTT at 4°C to prevent disulfide formation. DSD-bis[4Fe-4S] was kept under anaerobic conditions prior to injection. The assignment of the elution peak to dimer was confirmed by analytical centrifugation.

Circular dichroism (CD) Spectroscopy.

CD spectroscopy of the apo and holo-peptides was carried out on a JASCO J-815 spectropolarimeter. Spectra were recorded from 240 nm to 190 nm in 1 nm increments at protein concentrations of 0.050 mM and 0.025mM in 10 mM Tris-HCl, pH 7.5, using a quartz cuvette with a pathlength of 1 mm; the final spectra are the average of three data sets. Thermal unfolding curves were monitored by following the CD signal at 222 nm as a function of temperature from 4°C to 96°C. Holo DSD-bis[4Fe-4S] peptide samples

were handled in an airtight cuvette to exclude air during the course of the experiment. CD spectra of DSD-4Cys were recorded in presence of excess reducing agent (TCEP) to prevent oxidation of the cysteine side chains.

Electron paramagnetic resonance (EPR) spectroscopy.

Appropriate fractions from the PD10 column were concentrated using a centrifuge concentrator with a MW cutoff of 3,000 Da (GE Healthcare). The pH values of the samples were then adjusted to pH 10 by addition of 1 M glycine buffer, and the samples were reduced by addition of 100 mM $Na_2S_2O_4$ in 1 M glycine buffer, pH 10. Aliquots (150 mL) of the reduced samples were transferred to quartz EPR tubes, flash frozen by immersion in liquid nitrogen, and stored at 77 K until EPR characterization.

Continuous wave (CW) EPR experiments were performed on the X-band EPR spectrometer Elexsys E500 (Bruker). Pulsed EPR experiments were performed on a home-built broadband (2-18 ∪ 26-40 GHz) pulsed EPR spectrometer[16,36,38] at the microwave (mw) frequencies of about 9.6 GHz. The measurement temperature was 15 K. Detailed experimental conditions are given in Figure captions.

Cluster quantification.

For each preparation, percentage yield of cluster incorporation was estimated by UV-vis, using e of 5,500 $M^{-1}cm^{-1}$ per protein at 280 nm and of 16,000 $M^{-1}cm^{-1}$ per cluster at 410 nm.[18] Cluster incorporation was assessed quantitatively by measuring independently the concentration of iron and of peptide in identical samples. First, DSD-bis[4Fe-4S] samples were further purified by anion exchange chromatography on a Q-sepharose FF column

(GE health care), using 100 mM Tris, pH 8.5 as equilibration buffer, and 100mM NaCl, 100 mM Tris, pH 8.5 as elution buffer. The samples were split in two portions: one was used to measure peptide concentration by amino acid analysis (Proteomics Department, University of California, Davis), and the second was used to determine iron concentration by ferrozine assay.[20] Incorporation of EPR active, reduced cluster was determined by EPR spin quantification. Briefly, a concentrated DSD-bis[4Fe-4S] sample was divided in two parts, one of which was submitted for peptide concentration determination by amino acid analysis. The second portion was prepared for EPR spectroscopy as described above, and subjected to spin quantification by comparing the double integral of the CW EPR spectrum of $[4Fe\text{-}4S]^{+}$ recorded at 7 K with the spectrum of 5 mM Cu(II) nitrate recorded at 21 K (at lower temperatures the Cu(II) EPR signal saturated even at the lowest accessible mw power of 0.2 mW). The estimated concentration of $[4Fe\text{-}4S]^{+}$ was then compared with the DSD protein concentration evaluated using amino acid analysis for the same sample (accounting for dilutions).

Results and discussion

Design of model peptide

DSD-bis[4Fe-4S] was designed by using as a scaffold a dimeric three helix bundle originally designed to probe domain swapping (Domain Swapped Dimer, DSD, PDB ID 1G6U). In DSD, two identical peptides each form a helical hairpin, in which one of the helices is approximately twice the other in length. The long helices from two monomers pair up in an antiparallel manner, while the two shorter helices dock against the dimer formed by the long helices. An approximate 2-fold symmetry axis is located

between the two short helices (Figure 2.1). The fold is stabilized by a leucine-rich hydrophobic core and by salt bridges positioned at the helix-helix interfaces to impart specificity.

The arrangement of the two monomers in DSD is reminiscent of the internal pseudo two-fold symmetry found in two-cluster ferredoxins, which have long been thought to derive from gene duplication events and domain swapping[8]. Ferrodoxins comprise two repeats of a 29-residue sequence, and adopt the so-called ferredoxin fold defined by a babbab secondary structure. In the 2-cluster bacterial ferredoxins, each of the two symmetric clusters is coordinated by three sequentially contiguous cysteines contained in the loop, between the helix and the second beta sheet. A fourth distal cysteine, which is located in the helix of the second sequence repeat, completes the first coordination sphere of the cluster. The sequence motif is CXXCXXC…….C. Mirroring this arrangement, we designed a binding site, in which three of the coordinating cysteines belong to a monomer, while the fourth one is provided by the second monomer. DSD-bis[4Fe-4S], however, differs from the ferredoxins both in its highly helical secondary structure and in its dimeric oligomerization state. To ensure a correct selection of cysteine rotamers, we docked a natural [4Fe-4S] cluster and its primary coordination sphere into the hydrophobic core of DSD. This "metal-first" approach has been successfully used to insert iron sulfur clusters in natural and designed proteins.[5,27] We referred to the cluster found in *Thermotoga maritima* tryptophanyl t-RNA synthase (PDB 2G36),[29] which has been used by Grzyb et al. as a starting point to model a symmetrized cluster.[5] The cluster is coordinated through a C……..C…. CXXC sequence motif, in which the CXXC residues are part of a helix, as assessed by backbone dihedral angles, while the two

additional cysteines are found at the base of inter-helix loops and are in non-helical conformation. The distances between the backbone atoms of the cysteines are compatible with the regular three-helix coiled coil geometry of DSD. Accordingly, once we overlaid the CXXC motif with the LXXL motif that forms the core of DSD, the Ca carbons of the remaining two cysteines then overlapped with the Ca of leucines forming the core of native DSD. Several core positions corresponding to different layers within the coiled coil were possible matches for the geometry of the 4-cysteine motif; we selected the alignment that results in minimal clashes and supports the correct rotamers for the cysteine side chains (see Methods). We evaluated the impact of four Leu to Cys mutations and of cluster insertion on the integrity of the peptide scaffold by analysing the models with Q-Sitefinder,[9] and comparing the results to the X-ray structure of DSD. This analysis revealed the presence of a 58 $Å^3$ cavity in the core of DSD-4Cys corresponding to the cluster binding site, and smaller pockets to the side. This central cavity is completely occupied by the [4Fe-4S] cluster in the model of DSD-bis[4Fe-4S], which presents only the small pockets to the side. DSD-bis[4Fe-4S] resembles the original DSD structure, which contains no cavities in the core, and identical side pockets.

The cluster-binding site is located at one end of the bundle; because of the symmetry of the scaffold, the site is replicated in the second half (Figure 2.1). The sequence of the monomeric peptide contains 4 Leu to Cys mutations, three of which are contiguous in the sequence, and a fourth one that is distal; we have named the peptide DSD-4Cys. The peptide was synthesized by solid phase peptide synthesis (SPPS) and purified as described in Materials and Methods.

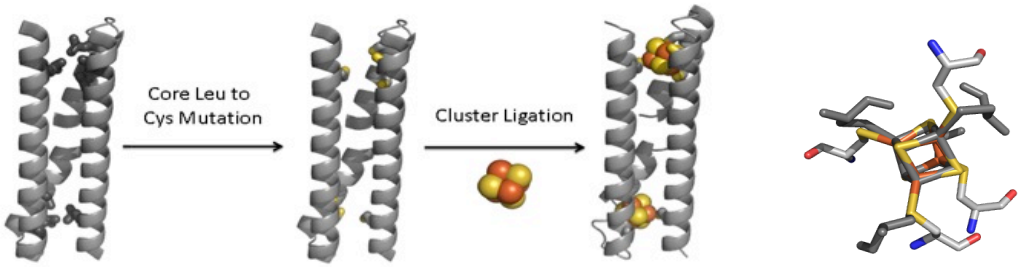

DSD: SLAALKSE**L**QA**L**KKEGFSPEE**L**AALESELQALEKKLAALKSK**L**QALKG

DSD-4Cys: SLAALKSE**C**QA**C**KKEGFSPEE**C**AALESELQALEKKLAALKSK**C**QALKGW

Figure 2.1. Design of DSD-bis[4Fe-4S]. (Top) The crystal structure of DSD (PDB ID: 2G6U) serves as a starting point. The [4Fe-4S] cluster from *Thermotoga maritima*, including the four cysteines comprising its first coordination sphere, was docked in the core of DSD. Appropriate core leucine residues in the hydrophobic core were mutated to cysteines. The first coordination sphere of DSD-bis[4Fe-4S] displays an excellent agreement with the natural coordination sphere of the cluster. (Bottom) Sequences of DSD and DSD-4Cys; mutations to the DSD sequence in DSD-4Cys are highlighted in bold. A tryptophan was inserted at the C terminal to facilitate concentration assessment.

Assembly of DSD-bis[4Fe-4S].

We reconstituted the clusters into the apo DSD-4Cys peptide using a well established in situ synthetic procedure under anaerobic conditions.[15] Briefly, the reconstitution reaction was carried out with ferric chloride and sodium sulfide in aqueous buffer (pH 8.5) in the presence of 2-mercaptoethanol and 2 M urea that serves to partially unfold DSD-4Cys, permitting access to the cysteines located in the hydrophobic core. Cluster incorporation is entropically favorable, and proceeds by ligand exchange between

the four preorganized cysteines and the more basic 2-mercaptoethanol that initially ligate the cluster.[15,34,35]

The UV-vis spectrum of the resulting DSD-bis[4Fe-4S] protein shows broad absorptions at 415 nm and 360 nm, which arise from sulfur to iron charge transfer excitations in oxidized [4Fe-4S] clusters; the absorption at 415 nm disappears upon reduction with sodium dithionate (Figure 2.2). The positions of the maxima are red-shifted compared with inorganic [4Fe-4S] clusters, consistent with a cluster shielded from aqueous environment. These spectral features and redox dependent behavior are typical of iron sulfur cluster proteins.[36,37] The ratio of absorbance at 410 nm to 280 nm is 0.76, within the 0.7-0.8 range usually observed in natural proteins.[36,37] Based on these values we estimate the stoichiometry at 1:1 peptide:cluster, consistent with a dimeric peptide coordinating two clusters.

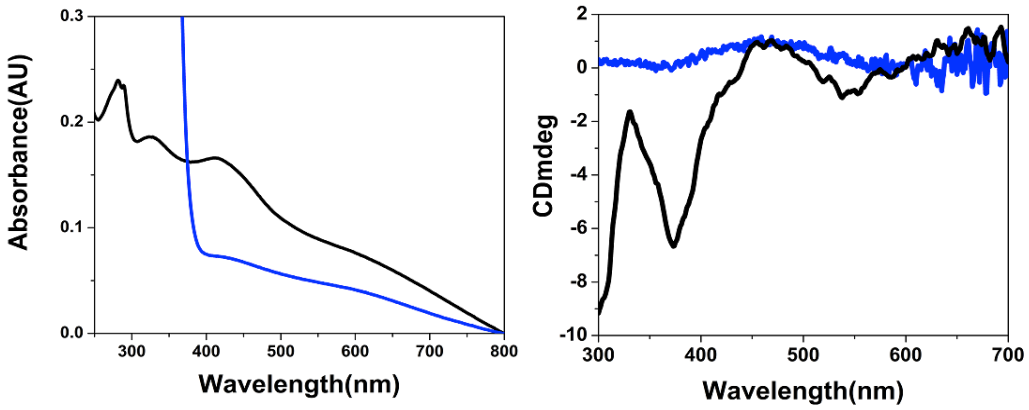

Figure 2.2. (Left). Optical absorption spectrum of reconstituted DSD-bis[4Fe-4S] in the oxidized state (black line) showing bands at 324 nm and 415 nm. The reduced state (blue line) shows the loss of 415 nm absorption after reduction. (Right). Circular dichroism

spectrum in the visible region of reconstituted, oxidized DSD-bis[4Fe-4S] (black line): the induced dichroic absorption in correspondence to the optical absorption in the visible indicates that the cluster is in a chiral environment. No signal is observed in the 300-700 nm range for DSD-4Cys.

We further characterized the redox behavior of DSD-bis[4Fe-4S] by cyclic voltammetry (Figure 2.3). In the presence of 4 mM neomycin as stabilizer, we observed a cathodic wave at -478mV vs SHE, which is in the range observed for natural cubane-type iron-sulfur clusters.[35] However, the absence of anodic wave indicates electrochemical irreversibility of the process under these conditions.

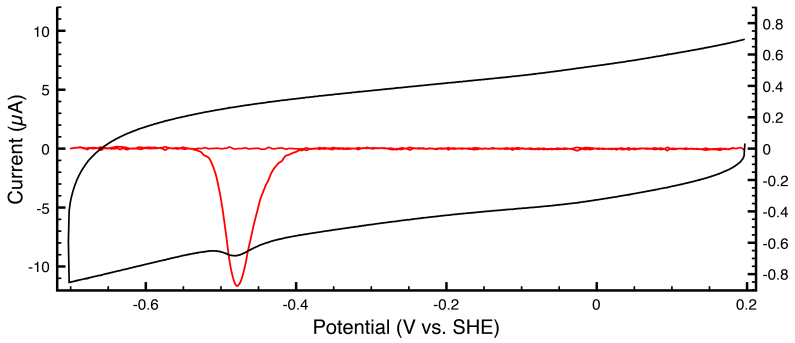

Figure 2.3: Cyclic Volatamogram of DSD_2[4Fe-4S] cluster in solution in presence of 4mM Neomycin with glassy carbon working electrode, platinum mesh counter electrode and saturated calomel reference electrode, scan rate 100mV/s. In the absence of neomycin, no electrochemical response was observed.

Protein folding and stability.

We verified that DSD-4Cys and DSD-bis[4Fe-4S] fold into dimers, as observed in the structure of DSD, by gel filtration, monitoring elution at wavelengths of 220 nm, 280 nm, and 410 nm. The two proteins have identical elution profiles dominated by a single

peak at 30 minutes, consistent with the presence of a single species with a molecular weight of a dimer (Figure 2.4). Furthermore, sedimentation velocity experiments by analytical ultracentrifugation of DSD-4Cys yielded an apparent molecular weight in excellent agreement with that expected for a dimer (12.4 kDa vs 10.6 kDa respectively) at a loading concentration of 100 mM, thus indicating that the protein forms a stable dimer in the micromolar range (Figure 2.4). The sedimentation data confirm our assignment of the peaks observed in the gel filtration elution profile to dimers.

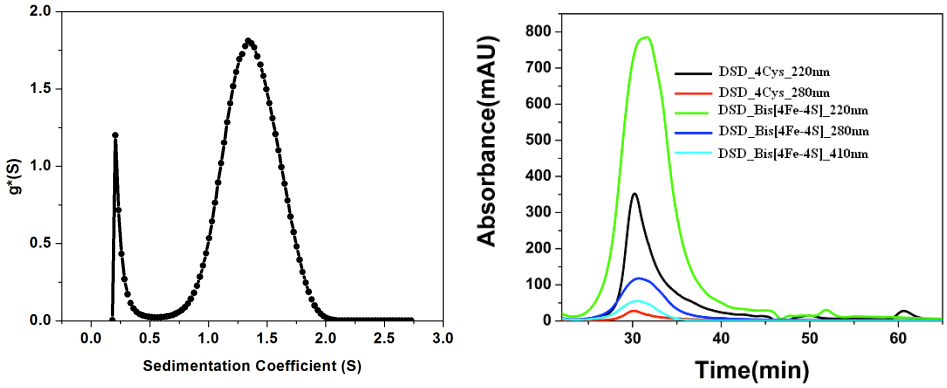

Figure 2.4: Oligomeric state of Apo and Holo peptide, on the left analytical ultracentrifugation data for apo peptide showing one major peak in solution; on the right panel, gel filtration data for apo and holo peptide showing same retention time for apo and holo peptide confirming dimeric nature of the system.

Cluster incorporation was also monitored by MALDI-TOF spectroscopy as shown in Figure 2.5. A broad peak centered around 11310 was observed corresponding to the dimeric peptide bound to two [4Fe-4S] clusters . A small peak was also observed centered around 5655 which we assign as a doubly charged species of the DSD-Bis[4Fe-4S]. No peak corresponding to dimeric apo DSD-4C (expected mass 10620) was observed in this sample. A sharp peak around 5314.44 dalton corresponding to DSD_4C was observed for the apo peptide.

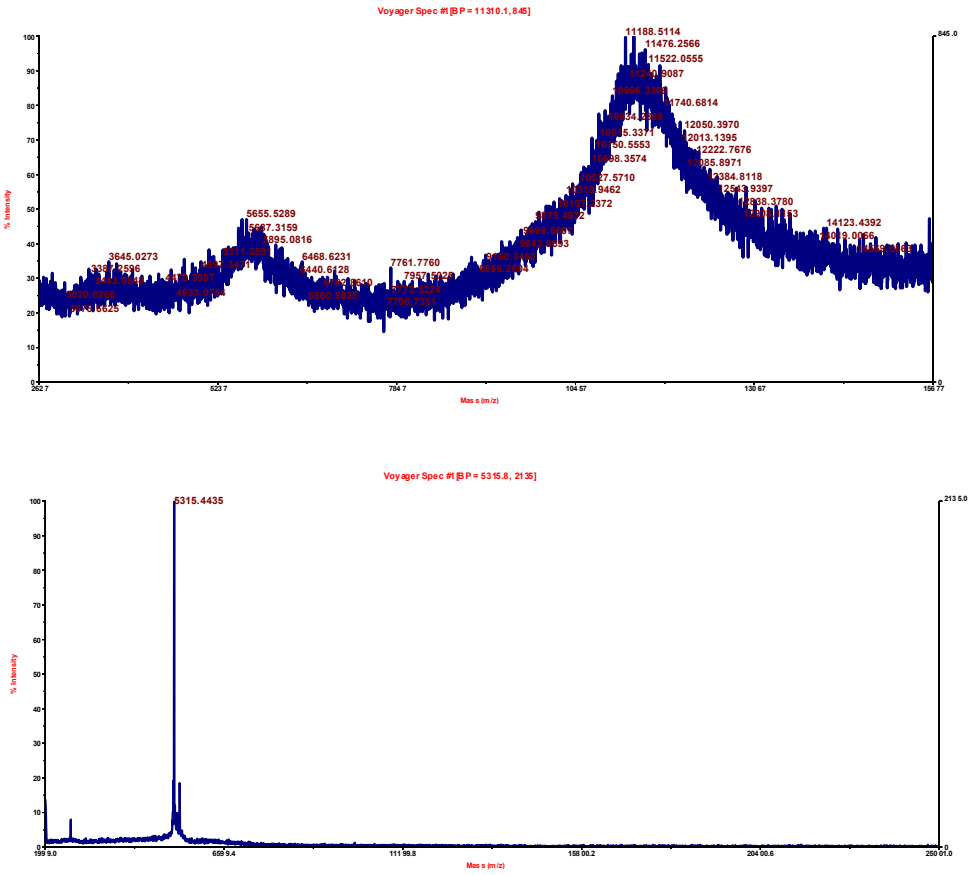

Figure 2.5: MALDI-TOF spectrum of DSD-Bis[4Fe-4S]: A broad peak centered around 11310 was observed corresponding to the dimeric peptide bound to two [4Fe-4S] clusters . A small peak was also observed centered around 5655 which we assign as a doubly

charged species of the DSD-Bis[4Fe-4S]. No peak corresponding to dimeric apo DSD-4C (expected mass 10620) was observed in this sample.

The impact of mutations on the structure of DSD in the apo DSD-4Cys and in the reconstituted DSD-bis[4Fe-4S] was verified by CD spectroscopy. Analysis of the models of DSD-4Cys and DSD-bis[4Fe-4S] shows that exchanging the hydrophobic side chain of leucine with the smaller, polar side chain of cysteine results in a polar cavity in the core of the bundle. The dimensions of the cavity calculated using Qsite-Finder are compatible with the cubane iron sulfur cluster; further, coordination by the cysteines to the iron-sulfur cluster stabilizes the fold and replaces hydrophobic interactions.

The secondary structure content of the apo DSD-4Cys and of the reconstituted DSD-bis[4Fe-4S] was evaluated by analysing the corresponding CD spectra. Similarly to DSD, both spectra contain bands at 190 nm, 208 nm, and 222 nm typical of alpha-helical proteins. The spectra are indistinguishable, indicating that the secondary structure of the protein is not distorted significantly upon insertion of the [4Fe-4S] cluster. The visible portion of the CD spectrum of DSD-bis[4Fe-4S] is dominated by a complex feature, comprising a narrow negative signal at approximately 360 nm and a broader one centred at 560 nm, which arises from the [4Fe-4S] clusters and resembles the spectra of ferredoxins.[36,38] Such signature for DSD-bis[4Fe-4S] corroborates the evidence for successful incorporation of the cluster.

To further evaluate the impact of modifications on DSD in the apo DSD-4Cys and in the reconstituted DSD-bis[4Fe-4S], we have investigated their thermal denaturation by monitoring the decrease of the helical signal at 222 nm as a function of temperature. A comparison of the melting curves (see Figure 2.6) reveals conspicuous differences in

stability. The thermal denaturation of DSD-bis[4Fe-4S] is irreversible, as partial denaturation results in a loss of the cofactor, thus precluding a rigorous thermodynamic analysis aimed at extrapolating folding parameters: the following discussion is thus limited to comparison of denaturation profiles and apparent melting points (T_m).

We chose DSD as a starting scaffold because of its remarkable thermal stability. DSD retains over 90% of its helical structure at temperatures as high as 94 ˚C: a complete unfolding transition was observed only by subjecting DSD to thermal denaturation in the presence of 3 M guanidinium chloride.[2,4,39] Not surprisingly, substituting eight leucines per dimer with cysteines in the hydrophobic core of DSD-4Cys results in loss of stability. In contrast to DSD, the thermal denaturation curve of DSD-4Cys shows unfolding even in the absence of guanidinium chloride; the protein, however, is still very stable, with an apparent T_m of 50 °C. Incorporation of the cluster into DSD-4Cys recovers the thermal stability: as shown in Figure 2.6, DSD-bis[4Fe-4S] is more than 90% folded at 80 ˚C; the apparent T_m is 87 ˚C. As the temperature increases above 80 ˚C, though, the protein undergoes rapid unfolding and loss of the cluster, as evident from the observation of iron precipitate.

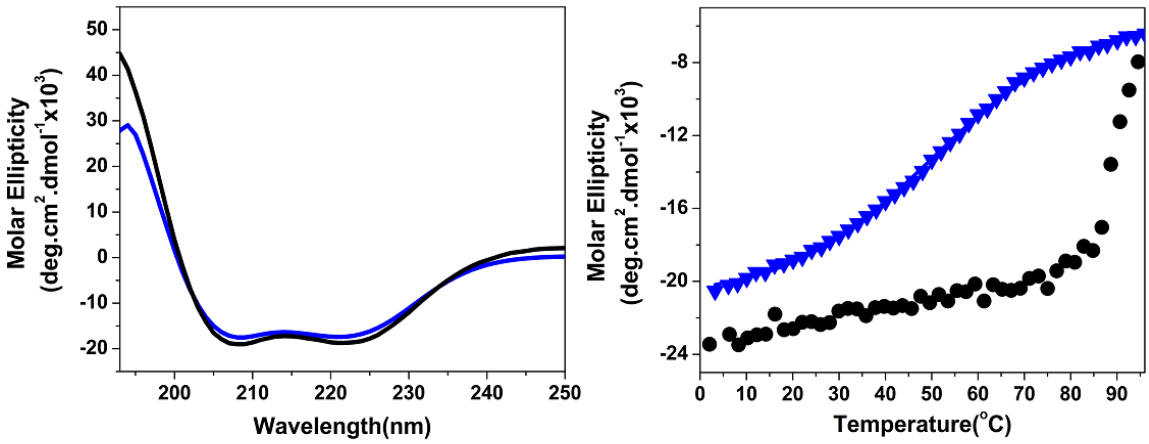

Figure 2.6. CD spectra in the UV range recorded at 22 ˚C (left) and thermal denaturation curves (right) of DSD-4Cys (blue lines) and DSD-bis[Fe4S4] (black lines). The denaturation curves are obtained by monitoring the loss of helical signal by CD at 222 nm while increasing the temperature.

EPR spectroscopy

The CW EPR spectrum obtained for the DSD-bis[4Fe-4S] sample reduced with dithionite (shown in Figure 2.7) exhibits the principal g-values of (g_x, g_y, g_z) =(1.879, 1.943, 2.058), with g_{iso} = 1.965, and is similar to the spectra of $[4Fe\text{-}4S]^+$ clusters described in the literature[7,8,35], which confirms the presence of intact [4Fe-4S] clusters bound to DSD. The temperature dependence of the EPR amplitude (Figure 2.7) shows a nearly exclusive population of the ground state with S = 1/2 at the temperatures below 15 K. The temperature dependence presented in Figure 2.7 is typical of $[4Fe\text{-}4S]^+$ clusters and it can be used to obtain information about the energies and multiplicities of the excited states.[10-14,40] Spin quantification of the reduced, EPR active clusters revealed that the $[4Fe\text{-}4S]^+$/protein concentration ratio is about 56%. In contrast, cluster quantification

on an identical sample carried out using the ferrozine assay to assess iron content yielded incorporation of 73.5 %. Such difference could be explained by the challenge of completely reducing the clusters in the EPR sample.

In order to obtain an additional proof of the pairwise binding of the [4Fe-4S] clusters to the DSD protein, we used the pulsed electron-electron double resonance

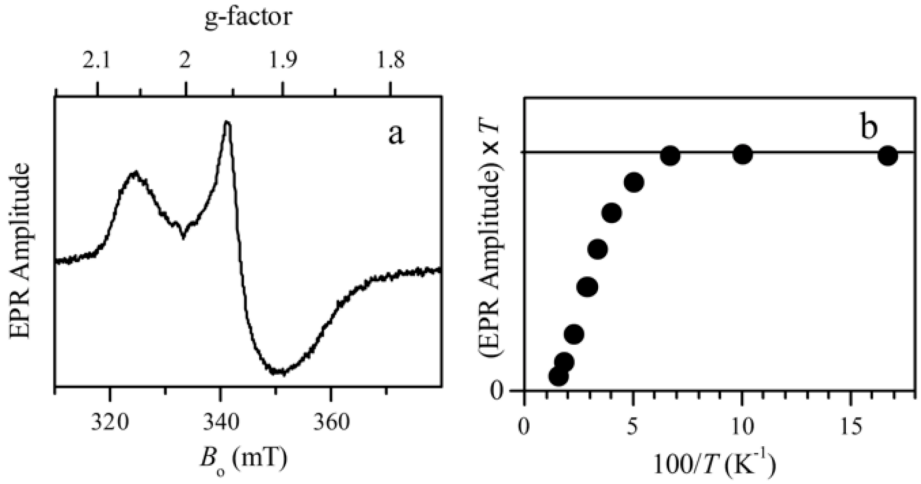

Figure 2.7: a) EPR spectrum of DSD-bis[4Fe-4S] reduced with sodium dithionite. Experimental conditions: mw frequency, 9.340 GHz; mw power, 2 mW; field modulation amplitude, 0.5 mT; temperature, 15 K. b) Temperature dependence of the EPR amplitude under non-saturating conditions (mw power, 0.2 mW). The horizontal line corresponds to the temperature dependence described by the Curie law (no low-lying excited states).

(ELDOR) technique that detects a magnetic dipole interaction between the paramagnetic centers.[7,41] Pulsed ELDOR and related techniques are routinely used to determine the distances between paramagnetic centers (spin labels, native radicals, and/or metal centers) in biological systems.[7,17,42-49] In particular, pulsed ELDOR was employed to study the electron transfer systems containing [FeS] clusters and to obtain information

about the relative spatial arrangement of the electron transfer carriers and the electronic structure of the [FeS] clusters themselves.[19,43,50,51]

In the pulsed ELDOR experiment, the pumping mw frequency, n_{pmp}, was set in resonance with the maximum of the ESE field sweep spectrum (g_y position). The observation frequency, n_{obs}, was 93 MHz higher, which corresponds to the observation EPR position shifted by ~ 3.3 mT toward g_z (Figure 2.8). Since the characteristic width of the EPR spectrum (~17 mT) is much greater than the pumping mw excitation width (~1.5 mT for the 12 ns pumping mw pulse), the ELDOR effect was expected to be very small, especially taking into account the incomplete pairing of the EPR-active $[4Fe\text{-}4S]^+$ clusters and possible (and unpredictable) orientational selectivity effects. With the distance between the [4Fe-4S] cluster binding sites of about 30 Å in the model, the dipole interaction constant was expected to be not very large, under ~ 4 MHz (see below). Therefore, we have used in our experiments the three-pulse ELDOR sequence (based on the two-pulse observation sequence),[13,21-23,41] which offers somewhat better sensitivity than the four-pulse one.[15,24-26,52] The pulsed ELDOR measurements were performed at the temperature of 15 K, where the population of the excited states is still negligible (see Figure 2.7), but the longitudinal relaxation time is already short enough to enable the measurements with a reasonably fast pulse repetition rate of 500 Hz.

The experimental ELDOR trace is presented in Figure 2.8 (solid trace). It exhibits the oscillations with the high frequency of ~ 15 MHz (~ 70 ns period), which represent a residual electron spin echo envelope modulation (ESEEM) at the Zeeman frequency of ^1H. Such a residual ESEEM is often observed in ELDOR experiments with insufficiently large frequency separation between n_{obs} and n_{pmp}.[5,28,44] In addition, a fast-

damping low-frequency oscillation is observed with the first minimum at $t' \sim 700$ ns (where t' is the time interval between the first observation pulse and the pumping pulse). This oscillation arises from the dipole interaction between the $[4Fe\text{-}4S]^+$ clusters, which follows from the facts that the $[4Fe\text{-}4S]^+$ clusters only exist as a protein-bound species, and no such oscillation was observed for the samples with low $[4Fe\text{-}4S]^+$ / protein concentration ratios resulting in negligible probability of the pair formation.

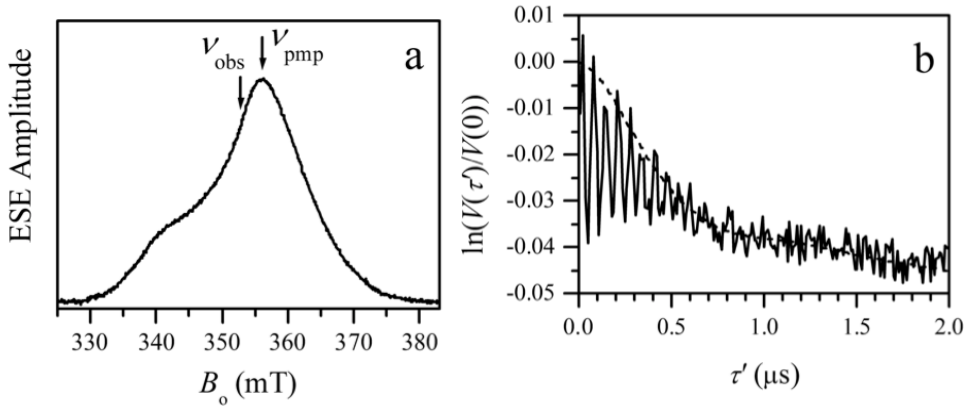

Figure 2.8. a) Two-pulse ESE field sweep spectrum of reduced DSD-bis[4Fe-4S]. Experimental conditions: mw frequency, 9.640 GHz; mw pulses, 15 and 20 ns; time interval between the mw pulses, t = 200 ns; temperature, 10 K. b) Solid trace, experimental pulsed ELDOR trace obtained using the three-pulse sequence. Experimental conditions: n_{obs} = 9.733 GHz; n_{pmp} = 9.640 GHz; B_o = 356.1 mT (EPR signal maximum for n_{pmp}); observation mw pulses, 15 and 20 ns; pumping mw pulse, 12 ns; temperature, 10 K. To suppress the residual ^{1}H ESEEM, the time interval between the observation pulses, t, was varied from 2 ms to 2.3 ms with the step of 10 ns, and the ELDOR traces were summed up. Dashed trace, numerical simulation (see text for details).

The characteristic frequency of the low-frequency oscillation assigned to the dipole interaction between the clusters is only about 0.7 MHz (as estimated from the position of the first minimum). In a point dipolar approximation, this dipole interaction would correspond to the distance of ~42 Å, significantly longer than the structurally reasonable distance of ~30-35 Å. The dashed trace in Figure 2.8 shows the simulation (using a simple point dipolar model and neglecting any possible orientational selectivity) for the uniform distance distribution from 36.5 Å to 51.5 Å ($\langle R \rangle$ = 44 Å, DR = 15 Å). The simulated pairwise effect is superimposed on the exponential decay from the uniformly distributed spins.

In order to explain this discrepancy, one has to take into account that the [4Fe-4S]$^{+}$ clusters represent mixed valence systems, with the total dipole interaction being a weighted sum of the contributions of the interactions between the individual ions.[27,43,50,51] Therefore, representing the whole cluster by a single point dipole is not appropriate, and the spins of the individual ions and the way they are coupled together have to be considered explicitly. The spin coupling scheme for the [4Fe-4S]$^{+}$ cluster was described elsewhere.[30,31,53] Briefly, the total spin S = 1/2 results from antiferromagnetic coupling of two pairs of ferromegnatically-coupled ions, Fe(II)-Fe(II) (S = 4) and Fe(II)-Fe(III) (S = 9/2). The spin projection factors that determine the statistical weights of individual dipole interactions are -4/3 for the ions of Fe(II)-Fe(II) pair and 11/6 for the ions of Fe(II)-Fe(III) pair (the iron ions in this pair are actually equivalent and have the charge of 2.5). A simple estimate (see Supporting Information) shows that the dipole interaction between two such clusters located at the distance of about 32.5 Å can be from ~0.4 MHz

to ~5 MHz, depending on their relative orientation. The observed frequency of about 0.7 MHz is closer to the lower limit of this range, which indicates that the clusters are approximately oriented by the Fe(II)-Fe(II) pairs towards each other.

The above considerations demonstrate that while it may be possible for mixed-valence systems to explain the observed dipole interaction constant, solving the opposite problem of deriving a unique distance from the dipole interaction constant may not be feasible.

Conclusions

In this work we exploited the pseudo-two fold symmetry of DSD, a de novo designed dimeric three-helix bundle, to generate a model protein that contains two iron-sulfur clusters in the hydrophobic core. Starting with the primary coordination sphere of a natural [4Fe-4S] cuboidal cluster, we replaced leucines in the three helix bundle with coordinating cysteines in the appropriate side chain rotamers to satisfy cluster coordination. The substitutions result in the formation of a hydrophilic cavity in the protein core, which is then filled by insertion of the cluster. Our data show that the mutations are structurally conservative, resulting in highly helical dimeric proteins both in the apo and holo state. The folding stability of the proteins is found to be in the order DSD-4Cys< DSD-bis[4Fe-4S] <DSD, thus mirroring the trend in core hydrophobicity and packing. Further, we showed that DSD-bis[4Fe-4S] contains two intact cubane iron-sulfur clusters located at the intended distance.

The design approach adopted here replaces the hydrophobic core of a scaffold protein with a sterically compatible metal binding center, and has been validated in

several systems.[5,10-14,27,54-63] Helical systems derived from the coiled coil motif have proven particularly adept to accommodate metal binding sites, because the inter-helix distances in the core is compatible with typical bond length in metal-ligand complexes. Further, the regular structure repeat of the coiled coil lends itself to parametrization and thus to computational design.[3,32,33] Towards the goal of generating artificial molecular wires capable of transferring electrons to an active site center, coiled coil present the advantage that a metal binding site can be easily moved along the longitudinal axis of the scaffold simply by replicating the sequence motif in a modular fashion. Here, we demonstrated the incorporation of those design principles in a model system that contains two clusters at fixed distance. The design principles could be further extended to tailor intercluster distances, and/or to add additional cofactors.

REFERENCES

(1) Woolfson, D. N., Bartlett, G. J., Bruning, M., and Thomson, A. R. (2012) New currency for old rope: from coiled-coil assemblies to α-helical barrels. *Curr. Opin. Struct. Biol.*22, 432-441.

(2) Lill, R. (2009) Function and biogenesis of iron-sulphur proteins. *Nature 460*, 831–838.

(3) Crick, F. H. C. (1953) The packing of α-helices: simple coiled-coils. *Acta crystallographica 6*, 689–697.

(4) Beinert, H. (1997) Iron-Sulfur clusters: Nature's modular, multipurpose structures. *Science 277*, 653–659.

(5) Grzyb, J., Xu, F., Weiner, L., Reijerse, E. J., Lubitz, W., Nanda, V., and Noy, D. (2010) De novo design of a non-natural fold for an iron-sulfur protein: alpha-helical coiled-coil with a four-iron four-sulfur cluster binding site in its central core. *Biochim. Biophys. Acta 1797*, 406–413.

(6) Delano, W. L. (2005) MacPymol: a PyMol-based Molecular Graphics Application for MacOS X. Delano Scientific, LLC, South San Francisco, CA, USA.

(7) Meyer, J. (2008) Iron-sulfur protein folds, iron-sulfur chemistry, and evolution. *J Biol Inorg Chem 13*, 157–170.

(8) Eck, R. V., and Dayhoff, M. O. (1966) Evolution of the structure of ferredoxin based on living relics of primitive amino Acid sequences. *Science 152*, 363–366.

(9) Laurie, A. T. R., and Jackson, R. M. (2005) Q-SiteFinder: an energy-based method for the prediction of protein-ligand binding sites. *Bioinformatics (Oxford, England) 21*, 1908–1916.

(10) Hinchliffe, P., and Sazanov, L. A. (2005) Organization of iron-sulfur clusters in respiratory complex I. *Science 309*, 771–774.

(11) Sazanov, L. A., and Hinchliffe, P. (2006) Structure of the hydrophilic domain of respiratory complex I from Thermus thermophilus. *Science 311*, 1430–1436.

(12) Jordan, P., Fromme, P., Witt, H. T., Klukas, O., Saenger, W., and Krauss, N. (2001) Three-dimensional structure of cyanobacterial photosystem I at 2.5 A resolution. *Nature 411*, 909–917.

(13) Peters, J., Peters, J., Lanzilotta, W., Lanzilotta, W., Lemon, B., Lemon, B., Seefeldt, L., and Seefeldt, L. (1998) X-ray crystal structure of the Fe-only hydrogenase (Cpl) from Clostridium pasteurianum to 1.8 angstrom resolution. *Science 282*, 1853–1858.

(14) Fontecilla-Camps, J. C., Volbeda, A., Cavazza, C., and Nicolet, Y. (2007) Structure/function relationships of [NiFe]- and [FeFe]-hydrogenases. *107*, 4273–4303.

(15) Antonkine, M. L., Maes, E. M., Czernuszewicz, R. S., Breitenstein, C., Bill, E., Falzone, C. J., Balasubramanian, R., Lubner, C., Bryant, D. A., and Golbeck, J. H. (2007) Chemical rescue of a site-modified ligand to a [4Fe-4S] cluster in PsaC, a bacterial-like dicluster ferredoxin bound to Photosystem I. *Biochim. Biophys. Acta 1767*, 712–724.

(16) Astashkin, A. V., Enemark, J. H., and Raitsimring, A. (2006) 26.5–40 GHz Ka-band pulsed EPR spectrometer. *Concepts in Magnetic Resonance Part B: Magnetic Resonance Engineering 29B*, 125–136.

(17) Krishna, S. S., Sadreyev, R. I., and Grishin, N. V. (2006) A tale of two ferredoxins: sequence similarity and structural differences. *BMC Struct. Biol. 6*, 8.

(18) Hoppe, A., Pandelia, M. E., Gartner, W., and Lubitz, W. (2011) [Fe(4)S(4)]- and [Fe(3)S(4)]-cluster formation in synthetic peptides. *Biochim. Biophys. Acta 1807*, 1414–1422.

(19) Antonkine, M. L., and Golbeck, J. H. (2006) Abstract - SpringerLink. *Photosystem I*.

(20) Carter, P. (1971) Spectrophotometric determination of serum iron at the submicrogram level with a new reagent (ferrozine). *Anal Biochem 40*, 450–458.

(21) Mulder, D. W., Shepard, E. M., Meuser, J. E., Joshi, N., King, P. W., Posewitz, M. C., Broderick, J. B., and Peters, J. W. (2011) Insights into [FeFe]-hydrogenase structure, mechanism, and maturation. *Structure 19*, 1038–1052.

(22) Nicolet, Y., Piras, C., Legrand, P., Hatchikian, C. E., and Fontecilla-Camps, J. C. (1999) Desulfovibrio desulfuricans iron hydrogenase: the structure shows unusual coordination to an active site Fe binuclear center. *Structure 7*, 13–23.

(23) Dubini, A., Mus, F., Seibert, M., Grossman, A. R., and Posewitz, M. C. (2009) Flexibility in anaerobic metabolism as revealed in a mutant of Chlamydomonas reinhardtii lacking hydrogenase activity. *J. Biol. Chem. 284*, 7201–7213.

(24) Scott, M. P., and Biggins, J. (1997) Introduction of a [4Fe-4S (S-cys)4]+1,+2 iron-sulfur center into a four-alpha helix protein using design parameters from the domain of the Fx cluster in the Photosystem I reaction center. *Protein Sci. 6*, 340–346.

(25) Antonkine, M. L., Koay, M. S., Epel, B., Breitenstein, C., Gopta, O., Gärtner, W., Bill, E., and Lubitz, W. (2009) Synthesis and characterization of de novo designed peptides modelling the binding sites of [4Fe-4S] clusters in photosystem I. *Biochim. Biophys. Acta 1787*, 995–1008.

(26) Kennedy, M. L., and Gibney, B. R. (2002) Proton coupling to [4Fe-4S](2+/+) and [4Fe-4Se](2+/+) oxidation and reduction in a designed protein. *J. Am. Chem. Soc. 124*, 6826–6827.

(27) Coldren, C. D., Hellinga, H. W., and Caradonna, J. P. (1997) The rational design and construction of a cuboidal iron–sulfur protein. *Proc. Natl. Acad. Sci. USA 94*, 6635–6640.

(28) Grzyb, J., Xu, F., Nanda, V., Luczkowska, R., Reijerse, E., Lubitz, W., and Noy, D. (2012) Empirical and computational design of iron-sulfur cluster proteins. *Biochim. Biophys. Acta 1817*, 1256–1262.

(29) Han, G. W., Yang, X. L., McMullan, D., Chong, Y. E., Krishna, S. S., Rife, C. L., Weekes, D., Brittain, S. M., Abdubek, P., Ambing, E., Astakhova, T., Axelrod, H. L., Carlton, D., Caruthers, J., Chiu, H. J., Clayton, T., Duan, L., Feuerhelm, J., Grant, J. C., Grzechnik, S. K., Jaroszewski, L., Jin, K. K., Klock, H. E., Knuth, M. W., Kumar, A., Marciano, D., Miller, M. D., Morse, A. T., Nigoghossian, E., Okach, L., Paulsen, J., Reyes, R., van den Bedem, H., White, A., Wolf, G., Xu, Q., Hodgson, K. O., Wooley, J., Deacon, A. M., Godzik, A., Lesley, S. A., Elsliger, M. A., Schimmel, P., and Wilson, I. A. (2010) Structure of a tryptophanyl-tRNA synthetase containing an iron-sulfur cluster. *Acta crystallographica. Section F, Structural biology and crystallization communications 66*, 1326–1334.

(30) Laplaza, C. E., and Holm, R. H. (2001) Helix-loop-helix peptides as scaffolds for the construction of bridged metal assemblies in proteins: the spectroscopic A-cluster structure in carbon monoxide dehydrogenase. *J. Am. Chem. Soc. 123*, 10255–10264.

(31) Gibney, B. R., Mulholland, S. E., Rabanal, F., and Dutton, P. L. (1996) Ferredoxin and ferredoxin-heme maquettes. *Proceedings of the National Academy of Sciences of the United States of America 93*, 15041–15046.

(32) Roy, A., Madden, C., and Ghirlanda, G. (2012) Photo-induced hydrogen production in a helical peptide incorporating a [FeFe] hydrogenase active site mimic. *Chem. Commun. (Camb.)* 48, 9816-9818.

(33) Faiella, M., Roy, A., Sommer, D. J., and Ghirlanda, G. Design of functional proteins: towards artificial hydrogenases. *Biopolymers-peptide science*.100, 558-571.

(34) Beinert, H. (2000) Iron-sulfur proteins: ancient structures, still full of surprises. *J Biol Inorg Chem 5*, 2–15.

(35) Koay, M. S., Antonkine, M. L., Gartner, W., and Lubitz, W. (2008) Modelling low-potential [Fe4S4] clusters in proteins. *Chem. Biodivers. 5*, 1571–1587.

(36) Sweeney, W. V., and Rabinowitz, J. C. (1980) Proteins containing 4Fe-4S clusters: an overview. *Annu. Rev. Biochem. 49*, 139–161.

(37) Jin, Z., Heinnickel, M., Krebs, C., Shen, G., Golbeck, J. H., and Bryant, D. A. (2008) Biogenesis of Iron-Sulfur Clusters in Photosystem I: Holo-NfuA from the Cyanobacterium Synochococcus Sp. PCC 7002 rapidly and efficiently transfers [4Fe-4S] clusters to apo-PSac in vitro. *J. Biol. Chem. 283*, 28426–28435.

(38) Bertini, I., Gray, H. B., Lippard, S. J., and Valentine, J. S. (1994) Bioinorganic chemistry.

(39) Ogihara, N. L., Ghirlanda, G., Bryson, J. W., Gingery, M., DeGrado, W. F., and Eisenberg, D. (2001) Design of three-dimensional domain-swapped dimers and fibrous oligomers. *Proceedings of the National Academy of Sciences of the United States of America 98*, 1404–1409.

(40) Papaefthymiou, G. C., Frankel, R. B., and Foner, S. (1980) Magnetic Properties of [Fe 4 S 4(SR) 4] 3- Clusters. *J. Phys. Colloques.*41, 493-494.

(41) Milov, A. D., Maryasov, A. G., and Tsvetkov, Y. D. (1998) Pulsed electron double resonance (PELDOR) and its applications in free-radicals research. *Applied Magnetic Resonance*. 15, 107-143.

(42) Schiemann, O., and Prisner, T. F. (2007) Long-range distance determinations in biomacromolecules by EPR spectroscopy. *Quarterly Reviews of Biophysics 40*, 1–53.

(43) Astashkin, A. V., Seravalli, J., Mansoorabadi, S. O., Reed, G. H., and Ragsdale, S. W. (2006) Pulsed electron paramagnetic resonance experiments identify the paramagnetic intermediates in the pyruvate ferredoxin oxidoreductase catalytic cycle. *J. Am. Chem. Soc. 128*, 3888–3889.

(44) Jeschke, G. (2012) DEER Distance Measurements on Proteins, in *Annual Review of Physical Chemistry, Vol 63* (Johnson, M. A., and Martinez, T. J., Eds.), 419–446.

(45) Swanson, M. A., Kathirvelu, V., Majtan, T., Frerman, F. E., Eaton, G. R., and Eaton, S. S. (2009) DEER Distance Measurement Between a Spin Label and a Native FAD Semiquinone in Electron Transfer Flavoprotein. *J. Am. Chem. Soc. 131*, 15978.

(46) Sen, K. I., Wu, H., Backer, J. M., and Gerfen, G. J. (2010) The Structure of p85ni in Class IA Phosphoinositide 3-Kinase Exhibits Interdomain Disorder. *Biochemistry 49*, 2159–2166.

(47) Astashkin, A. V., Rajapakshe, A., Cornelison, M. J., Johnson-Winters, K., and Enemark, J. H. (2012) Determination of the Distance between the Mo(V) and Fe(III) Heme Centers of Wild Type Human Sulfite Oxidase by Pulsed EPR Spectroscopy. *Journal of Physical Chemistry 116*, 1942–1950.

(48) Gordon-Grossman, M., Kaminker, I., Gofman, Y., Shai, Y., and Goldfarb, D. (2011) W-Band pulse EPR distance measurements in peptides using Gd3+-dipicolinic acid derivatives as spin labels. *Physical Chemistry Chemical Physics 13*, 10771–10780.

(49) Lovett, J. E., Bowen, A. M., Timmel, C. R., Jones, M. W., Dilworth, J. R., Caprotti, D., Bell, S. G., Wong, L. L., and Harmer, J. (2009) Structural information from orientationally selective DEER spectroscopy. *Physical Chemistry Chemical Physics 11*, 6840–6848.

(50) Elsasser, C., Brecht, M., and Bittl, R. (2002) Pulsed electron-electron double resonance on multinuclear metal clusters: Assignment of spin projection factors based on the dipolar interaction. *J. Am. Chem. Soc. 124*, 12606–12611.

(51) Elsaesser, C., Brecht, M., and Bittl, R. (2005) Treatment of spin-coupled metal-centres in pulsed electron-electron double-resonance experiments. *Biochem. Soc. Trans. 33*, 15–19.

(52) Martin, R. E., Pannier, M., Diederich, F., Gramlich, V., Hubrich, M., and Spiess, H. W. (1998) Determination of end-to-end distances in a series of TEMPO diradicals of up to 2.8 nm length with a new four-pulse double electron electron resonance experiment. *Angew. Chem. Int. Ed. 37*, 2834–2837.

(53) Torres, R. A., Lovell, T., Noodleman, L., and Case, D. A. (2003) Density functional and reduction potential calculations of Fe4S4 clusters. *J. Am. Chem. Soc. 125*, 1923–1936.

(54) Zastrow, M. L., PeacockAnna, F. A., Stuckey, J. A., and Pecoraro, V. L. (2012) Hydrolytic catalysis and structural stabilization in a designed metalloprotein. *Nat. Chem. 4*, 118–123.

(55) Salgado, E. N., Radford, R. J., and Tezcan, F. A. (2010) Metal-directed protein self-assembly. *Acc. Chem. Res. 43*, 661–672.

(56) Cordova, J. M., Noack, P. L., Hilcove, S. A., Lear, J. D., and Ghirlanda, G. (2007) Design of a functional membrane protein by engineering a heme-binding site in glycophorin A. *J. Am. Chem. Soc. 129*, 512–518.

(57) Shinde, S., Cordova, J., Woodrum, B., and Ghirlanda, G. (2012) Modulation of function in a minimalist heme-binding membrane protein. *J Biol Inorg Chem 17*, 557–564.

(58) Calhoun, J. R., Nastri, F., Maglio, O., Pavone, V., Lombardi, A., and DeGrado, W. F. (2005) Artificial diiron proteins: from structure to function. *Biopolymers 80*, 264–278.

(59) Shiga, D., Funahashi, Y., Masuda, H., Kikuchi, A., Noda, M., Uchiyama, S., Fukui, K., Kanaori, K., Tajima, K., Takano, Y., Nakamura, H., Kamei, M., and Tanaka, T. (2012) Creation of a binuclear purple copper site within a de novo coiled-coil protein.

Biochemistry 51, 7901–7907.

(60) Chakraborty, S., Iranzo, O., Zuiderweg, E. R. P., and Pecoraro, V. L. (2012) Experimental and theoretical evaluation of multisite cadmium(II) exchange in designed three-stranded coiled-coil peptides. *J. Am. Chem. Soc. 134*, 6191–6203.

(61) Der, B. S., Machius, M., Miley, M. J., Mills, J. L., Szyperski, T. A., and Kuhlman, B. (2011) Metal-mediated affinity and orientation specificity in a computationally designed protein homodimer. *J. Am. Chem. Soc 134,* 375-385

(62) Ghirlanda, G. (2009) Design of membrane proteins: toward functional systems. *Curr Opin Chem Biol 13*, 643–651.

(63) Ghirlanda, G., Osyczka, A., Liu, W., Antolovich, M., Smith, K. M., Dutton, P. L., Wand, A. J., and DeGrado, W. F. (2004) De novo design of a D2-symmetrical protein that reproduces the diheme four-helix bundle in cytochrome bc1. *J. Am. Chem. Soc. 126*, 8141–8147.

CHAPTER 3

DE NOVO DESIGN AND SYNTHESIS OF AN ARTIFICIAL SYNTHETIC FERREDOXIN: TOWARDS TAILOR MADE REDOX PROTEIN

Anindya Roy, Dayn Joseph Sommer, Robert A. Schmitz, Chelsea Brown, Andrei Astachkine and Giovanna Ghirlanda*

Department of Chemistry and Biochemistry, Arizona State University, Tempe, Az

Introduction:

In nature, redox proteins often employ chains of varied [Fe-S] clusters to shuttle electrons from electron donors to electron acceptors in which individual clusters are placed at distances from one another optimal to allow electronic coupling between them, increasing the rate of electron transfer between the two. Examples of these multi-cluster proteins are the [Fe-Fe] and [Ni-Fe] hydrogenases, enzymes responsible for reversible proton reduction.[1] The active site of these enzymes is deeply buried in protein matrix and electronically coupled to the surface of the protein via a series of suitably spaced [4Fe-4S] clusters [Figure 3.1]. In many hydrogenases , these 2[4Fe-4S] clusters are ensconced into a ferredoxin fold ('βαββαβ' fold) [Figure 3.1].[2,3] In this fold, a single polypeptide chain folds into two domains that bind each of the 2[4Fe-4S] clusters. The structure often exhibits a pseudo two-fold symmetry that is indicative of ancient sequence/gene duplication.[2] Despite of their structural similarity, 2[4Fe-4S] cluster binding proteins differ substantially in their physico-chemical properties. This diversity emerges from the difference in primary amino acid sequence of the ferredoxins and the specific stereo-electronic properties of the environment surrounding the clusters. Owing to their notable

importance in redox and non-redox catalysis, there has been a substantial amount of work in the field of *de novo* design attempting to model clusters into peptide based model system, in order to mimic the natural cluster environment, with the long term aim to incorporate these model peptides into engineered redox enzymes.[4-10] However, most of these peptides have been designed to incorporate a single, electronically isolated cluster, limiting their usefulness as electron conduits *in vitro*. To address this problem, we recently developed a general method to design bis-[4Fe-4S] cluster binding peptide using symmetry parameters. We have shown, as a proof of concept, that multiple [4Fe-4S] clusters can be incorporated inside the hydrophobic core

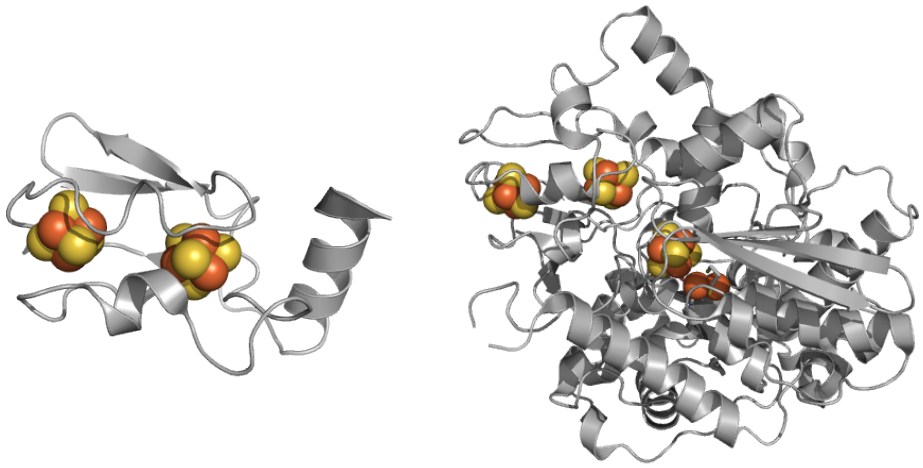

Figure 3.1: Structure of [FeFe] hydrogenase from *Desulfovibrio desulfuricans* (PDB 1HFE). The ferrodoxin-like domain is highlighted on the left. All molecular figures were created with PyMOL (DeLano, W.L. (2002). The PyMOL Molecular Graphics System).

of a helical bundle separated by a predetermined distance.[11] Following up on that work, we deigned here characterization of a variant peptide that moves the two clusters to within 12 Å of one another, a biologically relevant distance for effective electron transfer.

This designed system shows proof-of-concept redox activity, implicating its use in engineered redox proteins.

Experimental:

Peptide Synthesis and Purification

Peptides were synthesized on a Liberty microwave-assisted solid phase peptide synthesizer (CEM). The synthesis was carried out utilizing standard Fmoc protection procedures. Briefly, Rink Amide resin was doubly deprotected using 20% piperidine, 0.1 M HOBt in DMF. Following deprotection, appropriate amounts of 0.45 M HBTU in DMF, 2M Ethyl-Diisopropylamine (DIEA) in N-Methyl-2-Pyrrolidone, and 0.2 M Fmoc protected amino acid (Novabiochem) were added to the reaction vessel, followed by irradiation with microwaves to pre established temperatures according to CEM protocols. Peptides were acetylated at the N-terminus via addition of acetic anhydride in coupling conditions.

Peptides were cleaved from resin utilizing 94% TFA, 2.5% H_2O, 2.5% EDT, and 10% TIS for 3 hours, followed by precipitation with cold ether. Crude, lyophilized peptide was purified utilizing C18 preparatory reverse-phase high performance liquid chromatography (HPLC), with a linear gradient of 99.9% water with 0.1% TFA to 95% acetonitrile, 4.9% water, and 0.1% TFA and a flow rate of at 10 mL/min. Peptide identity was confirmed by matrix-assisted laser desorption ionization time-of-flight mass spectrometry (MALDI-TOF-MS) and purity by C18 analytical HPLC. Peptide was lyophilized to yield a white powder, >99% purity.

Cluster Incorporation

Iron-sulfur clusters were incorporated into peptide variants following well-established methodologies.[5,11] All reactions were performed in an anaerobic chamber (Coy Scientific), with a 95% N_2 and 5% H_2 environment. To a solution of 150 μM peptide in 100 mM Tris-HCl, pH 8.5, was added sequentially in 20 minute intervals to a final concentration: 0.8% (v/v) β-mercaptoethanol, 3 mM ferric chloride ($FeCl_3$, and 3 mM sodium sulfide (Na_2S). Peptide was incubated overnight at 4 °C anaerobically.

The dark brown solution was subjected to desalting utilizing a PD10 G25 column (GE Healthcare) that was preequillibrated with 100 mM Tris, pH 7.5. The holo protein was characterized immediately or flash frozen and stored at -80 °C.

Gel Filtration

Size exclusion chromatography was performed on a G-25 gel filtration column fit to an Agilent Technologies 1260 Insight FPLC system. To a column pre-equilibrated in 100 mM Tris-HCl, pH 7.5, was injected 200 μL of 150 μM apo or holo peptide. Apo peptide was pre-treated with t*ris*(2-carboxyethyl)phosphine (TCEP) 30 minutes before injection to eliminate any disulfides formed from air oxidation.

Circular Dichroism Spectroscopy

Spectra were recorded on a JASCO J-815 spectropolarimeter in the range of 260-190 nm. Data were recorded every 1 nm and averaged over 3 scans in a 1 mm path length, quartz cuvette. The holo-peptide was placed in a sealed cuvette to maintain an anaerobic environment. Concentration of apo and holo-peptide was kept at 50 μM in 100

mM Tris, pH 7.5. Apo-peptide measurements contained an excess amount of TCEP to remove any disulfides formed. Chemical denaturations were performed through iterative additions of an 8 M stock of Guanidinium-HCl, followed by mixing and incubation for 5 minutes to allow equilibration.

Electron Paramagnetic Resonance Spectroscopy

Holo-peptide obtained from PD10 desalting was concentrated in a 3000 MWCO centrifuge concentrator to approximately 1 mM peptide concentration. Reduced samples were adjusted to pH 10 by addition of 100 mM sodium dithionite in 1 M glycine buffer, to a final concentration of 10 mM dithionite. EPR samples were prepared by addition of 10% (v/v) glycerol as a cryoprotectant to either oxidized or reduced samples, and placed in quartz EPR tubes. Samples were flash frozen and stored under liquid N_2 until measurement.

Samples were measured on a X-band EPR spectrometer Elexsys E500 (Bruker), utilizing continuous wave methodology (mw frequency, 9.340 GHz; mw power, 2 mW; field modulation amplitude, 0.5 mT). Measurement temperatures ranged from 5-50 K.

Synthesis of water-soluble porphyrin analogue:

5,10,15,20-tetrakis(4-diethylmalonatemethylphenyl)porphyrin was synthesized following a previously published method.[12] Zinc insertion was achieved by modifying a literature procedure [13]for related compounds, using $Zn(OAc)_2.2H_2O$ in THF for 12 h at 60 ºC. The esters were cleaved following a procedure for a similar compound.[14] The water-soluble, malonate-functionalized porphyrin was characterized by mass spectrometry and NMR in D_2O, and then used for transient absorption spectroscopy.

Transient Absorption Spectroscopy:

Nanosecond transient absorption measurements were acquired on a flash photolysis set-up using a pulsed laser source and a pump-probe optical set-up. Excitation was provided from an optical parametric oscillator pumped by the third harmonic (352 nm)of a Nd:YAG laser (Ekspla NT 342B). The pulse width was 4-5 ns, and the repetition rate was 10 Hz. The signal was detected by a Proteus spectrometer (Ultrafast Systems). The instrument response function was 4-5 ns. Transient data analysis was carried out using in-house program ASUFIT. Simple exponentials were fit one wavelength at a time.

Cytochrome C_{550} Reduction Assay

PD10 fractions of the holo-peptide were reduced via slow addition of dithionite, monitoring the loss of signal at 410 nm. After no more change was seen, and a slight dithionite signal arose at 300 nm, the holo-peptide was subjected to a PD10 column. The first 1.5 mL of the total 3.5 mL elution volume were concentrated to a protein concentration of 300 μM. To 500μL of a solution of Cytochome C_{550} isolated from *Thermosynechococcus elongatus* (7 μM protein concentration as assayed by absorbance at 550 nm, ε_{550} = 21000 M^{-1} cm^{-1}) was added 1 μL of reduced holo-peptide. After each addition, UV-Vis spectra were obtained with an Ocean Optics USB4000 detector with an USB-ISS-UV-Vis light source attached. Data were fit to linear regression curves before and after saturation to determine the mole equivalents required to obtain full reduction of the heme.

Results and discussion:

Protein Design and Synthesis:

DSD-Fdm was designed following a similar protocol as described before. [11] Briefly, We searched for leucine residues arranged at i, i+3 positions inside the hydrophobic core of the helical bundle of DSD [15](PDB Code 1G6U) that is compatible with ligating a [4Fe-4S] cluster at the N-term of the helix. The first coordination sphere of [4Fe-4S] cluster binding site from *Thermotoga maritima* (PDB ID 2G36)[16] was then docked manually inside the hydrophobic core of the DSD to find other two positions geometrically compatible to chelate the [4Fe-4S] clusters (Figure 3.2). This resulted in translation of the cluster binding site one heptad down, along the axis of the 3-helix bundle as compared to our previous design.[11] Owing to the inherent two-fold symmetry of the designed protein, DSD-Fdm, incorporates two [4Fe-4S] clusters in the hydrophobic core which is reminiscent of the natural ferredoxin fold. Mutation of eight core leucine to cystine initially causes formation of a polar cavity inside the helical bundle in the apo peptide, while the cavity gets completely occupied by the clusters in holo Peptide [Figure 3.2]. Resulting 49 amino acid residue peptide was synthesized utilizing standard Fmoc chemistry with Microwave-Assisted Solid Phase Peptide Synthesis with high yield and homogeneity. Crude peptide was purified via reverse-phase HPLC to >95% purity, as assessed by analytical HPLC. Identity of the construct was confirmed with MALDI-TOF Mass Spectrometry.

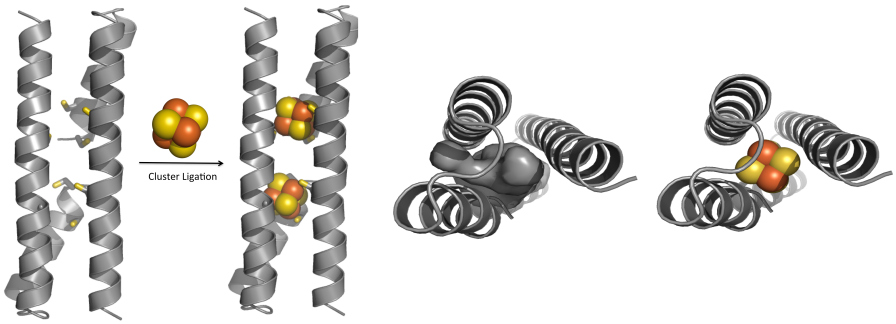

DSD: SLAALKSELQALKKEGFSPEELAALESELQALEKKLAALKSKLQALKG

DSD-Fdm: SCAACKSELQALKKEGFSPEELAALESECQALEKKCAALKSKLQALKGW

Figure 3.2: Design Strategy for DSD-Fdm (Left Panel); Polar cavity generated by Leucine to Cystine mutation gets filled by [4Fe-4S] cluster (Top View, right panel)

Cluster Incorporation, Protein Structure and Stability:

We performed *in situ* cluster incorporation reaction following standard protocol. [5,11] Briefly, β-mercaptoethanol reduced peptide was incubated overnight with 20 molar equivalents of $FeCl_3$ and Na_2S. This entropically favorable reaction was quenched via desalting on a PD10 column, removing unbound Fe and S equivalents. In agreement with previously characterized peptides, the holo DSD-Fdm shows broad absorbance at 415 and 360 nm, characteristic of [Fe-S] cluster charge transfer bands, which disappear upon reduction (Figure 3.3). This parameters are typical of a cuboidal [4Fe-4S] cluster [17,18] where as-incorporated $[4Fe\text{-}4S]^{2+}$ cluster undergo dithionite mediated reduction to $[4Fe\text{-}4S]^{1+}$.

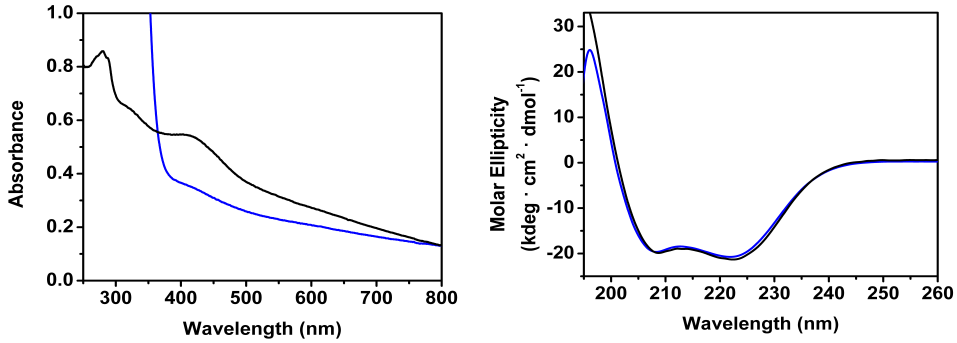

Figure 3.3: UV-Vis (left panel) spectra of holo DSD-Fdm before and after dithionite reduction. CD Spectra of apo and holo DSD-Fdm in the UV range showing two minima around 222nm and 208nm.

We investigated the oligomeric state for apo and holo DSD-Fdm using a combinatorial analytical centrifugation and gel filtration approach. Apo-DSD-Fdm exists predominantly in dimeric form in solution at ~100μM loading concentration (data not shown). When analyzed by gel filtration, both apo and holo DSD-Fdm elutes at comparable volume of elution buffer as shown in Figure 3.4. For holo peptide, the elution profile contains an additional absorbance at 410 nm, indicating the presence of the [4Fe-4S] cluster.

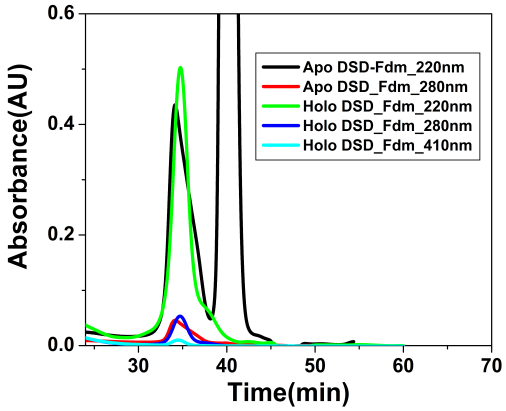

Figure 3.4: Gel filtration data of Apo and Holo DSD-Fdm. Both Apo and Holo peptide elutes at similar elution volume, confirming same oligomeric state.

The peak centered around 40 min for apo peptide comes from TCEP.HCl used for reduction, which was confirmed from a blank injection of TCEP.HCl by itself (data not shown).

The presence of two clusters was subsequently confirmed through characterization of Fe and protein concentration. Utilizing the same sample, analysis of Fe content via a Ferrozine assay and protein concentration via a Bradford assay, we found that the peptide contains 4.3 ± 0.9 Fe/monomer. Variation in Fe concentration may arise from non-specific binding of Fe^{2+} to the exterior of the DSD-Fdm peptide.

We investigated the secondary structure of both apo and holo DSD-Fdm using far-UV Circular Dichroism (CD) spectroscopy. Both the apo and holo DSD-Fdm shows two minima centered around 208nm and 222nm, indicative of high helical content of both peptides (Figure 3.3 right panel). Cluster incorporation does not interfere with the folding of the peptide, which is reflected by the similar molar ellipticity value of the holo peptide as compared to the apo peptide.

We also assessed the stability of the apo and holo peptide towards chemical denaturation procedure in circular dichroism. Briefly, molar ellipticity of apo and holo peptide was monitored

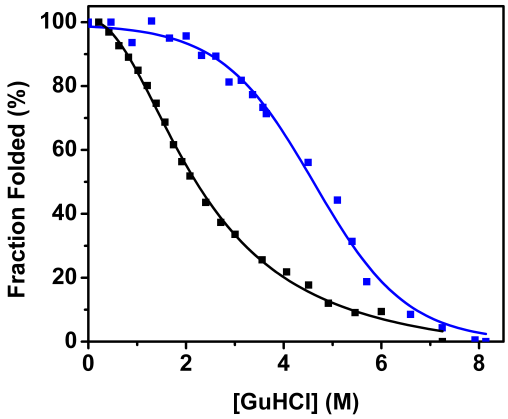

Figure 3.5: Guanidine.HCl melt of apo and holo DSD-Fdm monitored by CD at 222nm. Apo peptide denatures at 2.1 M Gdn.HCl (black line), and holo peptide denatures at 4.4 M Gdn.HCl (blue line)

at 222nm as a function of increasing concentration of a chaotropic agent(Guanidine hydrochloride). We observed a remarkable and unambiguous increase in stability towards denaturant was observed for holo DSD-Fdm compared to apo DSD-Fdm, as shown in Figure 3.5. The midpoint of denaturation for the apo peptide is at 2.1 M Gdn.HCl concentration, while for the holo DSD-Fdm it is at 4.4 M Gdn.HCl concentration. On a qualitative level, though, this increase in stability can be attributed to the formation of four cystine-SH to [Fe] bonds per peptide upon cluster incorporation.

.

EPR Spectroscopy and redox properties of the cluster:

In vitro reconstitution of cuboidal iron sulfur proteins results in formation of $[4Fe\text{-}4S]^{2+}$ clusters , which are EPR silent because of antiferromagnetic coupling of unpaired spins.

Accordingly reconstituted holo DSD-Fdm shows no EPR signal, where as upon dithionite reduction a rhombic signal arises confirming incorporation of an intact [4Fe-4S] cluster (Figure3.6). The signal with a g_{iso} value= 1.97 (g_x=1.91, g_y=1.95, g_z=2.06), is consistent with a S=1/2 system.[2,19,20]

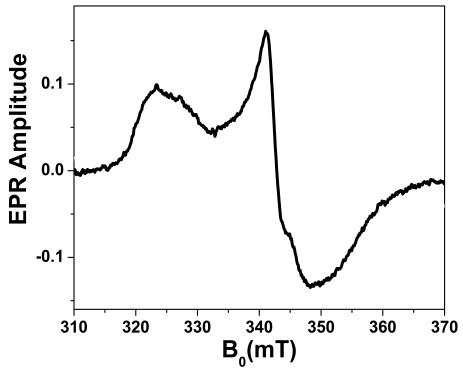

Figure 3.6: CW EPR spectra of dithionite-reduced holo DSD-Fdm, Experimental conditions, Temperature 12 K, Microwave Frequency 9.340GHz, Microwave Power 2mW.

In general, 2[4Fe-4S] containing ferredoxin type proteins, where two clusters are within 11-13 Å of each other, exhibit a spin-spin interaction in EPR spectra giving rise to more complex features as compared to magnetically isolated clusters. The EPR spectra observed in our system, shows no such features indicating no detectable spin-spin interaction. This can be due to the orientational selectivity or incomplete reduction of the second cluster.

We also probed the redox properties of DSD-Fdm using cyclic voltammetry. A solution of DSD-Fdm in 100mM Tris, pH 7.5, 100mM NaCl shows no observable redox process by cyclic voltametry in the range from 0 to -1 (V) vs SHE, presumably because of the absence of interaction between electrode surface and the electroactive species. To solve this issue we used neomycin, which has long been used to stabilize and enhance

interaction of ferredoxin type protein with electrode surface.[21,22] After addition of 3.5 mM neomycin, we observed a quasi-reversible process with a cathodic and anodic wave centered around -0.438 and -0.521 V vs SHE respectively, as shown in Figure 3.7. The estimated redox potential value -0.479 V vs SHE falls in the reported window for low potential [4Fe-4S] clusters in literature confirming presence of a $[4Fe\text{-}4S]^{2+/1+}$ cluster.

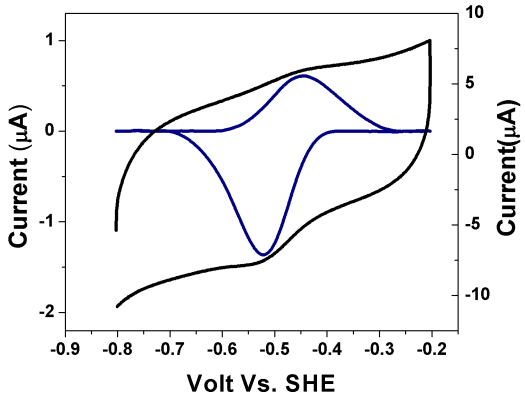

Figure 3.7: Cyclic Voltammogram of DSD-Fdm in presence of 3.5 mM neomycin using Ag/AgCl reference electrode, glassy carbon working electrode and a platinum mesh counter electrode; scan rate 100 mV/s .

In nature, ferredoxin-type proteins are involved in numerous electron transfer processes leading up to redox catalysis.[23-26] Thus, designed systems should also have these capabilities with the ultimate aim of engineering bio-hybrid catalysts that incorporate artificial and natural counterpart, each with fine tunable redox properties. Keeping this in mind, we turned our effort to investigate electron transfer properties of holo DSD-Fdm, with external redox active species. Firstly, in order to assess the possibility of the holo-DSD-Fdm to function in dye-sensitized solar cells, we characterized the kinetics of electron transfer from a porphyrin photosensitizer to the oxidized cluster utilizing

Nanosecond Transient Absorption Spectroscopy. In the presence of the holo-peptide, the triplet state of the utilized porphyrin was quenched 3.4 times faster relative to the porphyrin in the presence of the apo-protein, indicating interaction with the clusters. Experiments were done to probe the possibility of

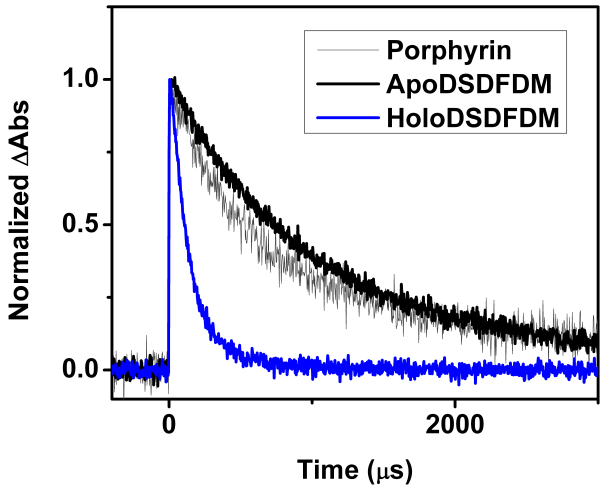

Figure 3.8: Normalized spectra of Porphyrin 1, apo-protein, and holoprotein. Porphyrins in solution were excited at their Q-band (560 nm) and their triplet state (450 nm) lifetimes were probed. Porphyrin and apo-protein had similar lifetimes, ca. 1400 μs, while the holo-protein had a significantly quenched triplet lifetime, ca. 100 μs. This quenching is most likely due to Dexter-type energy transfer from the porphyrin to the FeS cluster.

electron transfer between the P^* and the [4Fe-4S], but no oxidized porphyrin could be detected (Figure 3.8). This result points to the possibility of triplet-triplet energy transfer. Because this type of energy transfer is dipole-forbidden, the exchange mechanism must be of the Dexter type, which requires the donor and acceptor to be within 10 Å for sufficient orbital overlap to occur.

Finally, as a proof-of-concept study for the ability of this construct to be incorporated into a *de novo* designed, fully functional redox enzyme, the ability to transfer an electron to oxidized cytochome C was assayed. holo DSD-Fdm was reduced

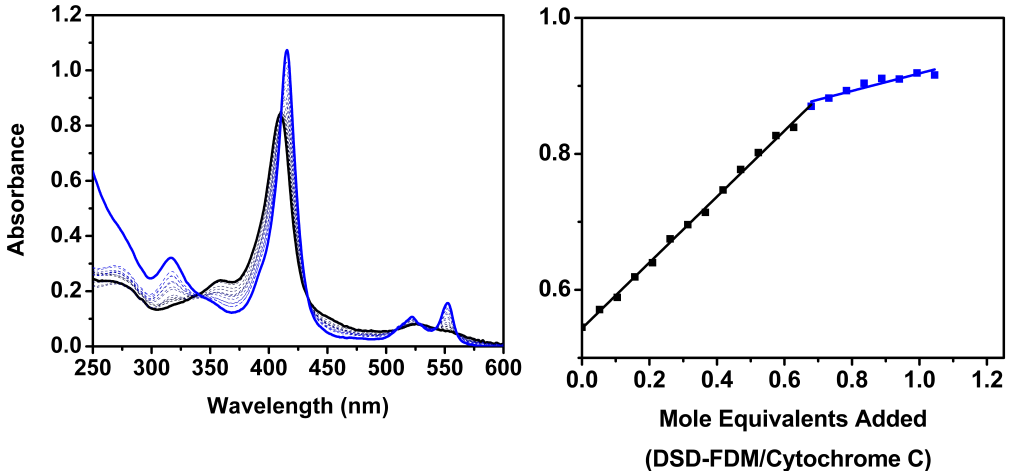

Figure 3.9: Electron Transfer Study between reduced holo DSD-Fdm and Cyt-C: UV-Vis titration of reduced DSD-Fdm to a solution of air oxidized Cyt-C (left panel),
by sequential addition of sodium dithionite, monitoring the loss of absorbance at 410 nm, stopping addition after no more change in signal was seen. Reduced peptide was desalted on a PD10 column to remove possible dithionite excess, and concentrated to an appropriate molarity.

The reduced peptide was then titrated into an air-oxidized Cytochrome C_{550} sample, isolated from *Thermosynechococcus elongatus*, while monitoring the UV-Vis spectra. The change in absorbance in the Soret and q-bands indicate reduction of the protein-bound heme. Fitting the data of the change of absorbance as a function of molar equivalents of holo DSD-Fdm indicated an approximate 1:1 molar ratio of reduction.
In this second design, we have extended our previous effort [11] to design a more realistic artificial model of electron transfer protein assembly where redox active species are

separated by a distance biologically relevant for effective electron transfer . Using symmetry property of a *de novo* designed homo-dimeric protein DSD [15], we rationally designed 2[4Fe-4S] cluster binding site in the hydrophobic core the helical bind. Total 8-leucine residues in the core were designed to be replaced by 8-cystine residues that serve as ligands to the [4Fe-4S] clusters. Resulting peptide binds 2[4Fe-4S] clusters with high yield and both apo and holo peptides are highly helical and dimeric in nature. Cofactor binding induces a significant amount of stability towards chemical denaturation, as often seen in designed metalloproteins. [27] Most importantly, for the first time, we show here de novo designed Holo DSD-Fdm is able to partake in electron transfer process involving an excited photosensitizer and also soluble, biologically relevant, small electron transfer protein, Cyt-C. This artificial redox proteins opens up new avenue for designing redox catalysts in a modular way, where different component of an engineered redox pathway can be disembodied and fine-tuned as desired for optimization of the whole system.

REFERENCES:

(1) Fontecilla-Camps, J. C., Volbeda, A., Cavazza, C., and Nicolet, Y. (2007) Structure/function relationships of [NiFe]- and [FeFe]-hydrogenases. *107*, 4273–4303.

(2) Meyer, J. (2008) Iron-sulfur protein folds, iron-sulfur chemistry, and evolution. *J Biol Inorg Chem 13*, 157–170.

(3) Orengo, C. A., and Thornton, J. M. Protein Families and their Evolution- A structural Perspective. *Annual Reviews 74,*867-900.

(4) Scott, M. P., and Biggins, J. (1997) Introduction of a [4Fe-4S (S-cys)4]+1,+2 iron-sulfur center into a four-alpha helix protein using design parameters from the domain of the Fx cluster in the Photosystem I reaction center. *Protein Sci. 6*, 340–346.

(5) Antonkine, M. L., Maes, E. M., Czernuszewicz, R. S., Breitenstein, C., Bill, E., Falzone, C. J., Balasubramanian, R., Lubner, C., Bryant, D. A., and Golbeck, J. H. (2007) Chemical rescue of a site-modified ligand to a [4Fe-4S] cluster in PsaC, a bacterial-like dicluster ferredoxin bound to Photosystem I. *Biochim. Biophys. Acta 1767*, 712–724.

(6) Antonkine, M. L., Koay, M. S., Epel, B., Breitenstein, C., Gopta, O., Gärtner, W., Bill, E., and Lubitz, W. (2009) Synthesis and characterization of de novo designed peptides modelling the binding sites of [4Fe-4S] clusters in photosystem I. *Biochim. Biophys. Acta 1787*, 995–1008.

(7) Kennedy, M. C., Kent, T. A., Emptage, M., Merkle, H., Beinert, H., and Münck, E. (1984) Evidence for the formation of a linear [3Fe-4S] cluster in partially unfolded aconitase. *J. Biol. Chem. 259*, 14463–14471.

(8) Grzyb, J., Xu, F., Weiner, L., Reijerse, E. J., Lubitz, W., Nanda, V., and Noy, D. (2010) De novo design of a non-natural fold for an iron-sulfur protein: alpha-helical coiled-coil with a four-iron four-sulfur cluster binding site in its central core. *Biochim. Biophys. Acta 1797*, 406–413.

(9) Coldren, C. D., Hellinga, H. W., and Caradonna, J. P. (1997) The rational design and construction of a cuboidal iron–sulfur protein. *Proc. Natl. Acad. Sci. USA 94*, 6635–6640.

(10) Gibney, B. R., Mulholland, S. E., Rabanal, F., and Dutton, P. L. (1996) Ferredoxin and ferredoxin-heme maquettes. *Proceedings of the National Academy of Sciences of the*

United States of America 93, 15041–15046.

(11) Roy, A., Sarrou, I., Astashkin, A., and Ghirlanda, G. (2013) De novo Design of an Artificial bis-[4Fe-4S] Binding Protein. *Biochemistry 53*,43, 7586-7594.

(12) Sherman, B. D., Pillai, S., Kodis, G., Bergkamp, J., Mallouk, T. E., Gust, D., Moore, T. A., and Moore, A. L. (2011) A porphyrin-stabilized iridium oxide water oxidation catalyst. *Can. J. Chem. 89*, 152–157.

(13) Loewe, R. S., Ambroise, A., Muthukumaran, K., Padmaja, K., Lysenko, A. B., Mathur, G., Li, Q., Bocian, D. F., Misra, V., and Lindsey, J. S. (2004) Porphyrins Bearing Mono or Tripodal Benzylphosphonic Acid Tethers for Attachment to Oxide Surfaces. *J. Org. Chem. 69*, 1453–1460.

(14) Guldi, D. M., Zilbermann, I., Anderson, G., Li, A., Balbinot, D., Jux, N., Hatzimarinaki, M., Hirsch, A., and Prato, M. (2004) Multicomponent redox gradients on photoactive electrode surfaces. *Chem. Commun. (Camb.)* 726–727.

(15) Ogihara, N. L., Ghirlanda, G., Bryson, J. W., Gingery, M., DeGrado, W. F., and Eisenberg, D. (2001) Design of three-dimensional domain-swapped dimers and fibrous oligomers. *Proceedings of the National Academy of Sciences of the United States of America 98*, 1404–1409.

(16) Han, G. W., Yang, X. L., McMullan, D., Chong, Y. E., Krishna, S. S., Rife, C. L., Weekes, D., Brittain, S. M., Abdubek, P., Ambing, E., Astakhova, T., Axelrod, H. L., Carlton, D., Caruthers, J., Chiu, H. J., Clayton, T., Duan, L., Feuerhelm, J., Grant, J. C., Grzechnik, S. K., Jaroszewski, L., Jin, K. K., Klock, H. E., Knuth, M. W., Kumar, A., Marciano, D., Miller, M. D., Morse, A. T., Nigoghossian, E., Okach, L., Paulsen, J., Reyes, R., van den Bedem, H., White, A., Wolf, G., Xu, Q., Hodgson, K. O., Wooley, J., Deacon, A. M., Godzik, A., Lesley, S. A., Elsliger, M. A., Schimmel, P., and Wilson, I. A. (2010) Structure of a tryptophanyl-tRNA synthetase containing an iron-sulfur cluster. *Acta crystallographica. Section F, Structural biology and crystallization communications 66*, 1326–1334.

(17) Sweeney, W. V., and Rabinowitz, J. C. (1980) Proteins containing 4Fe-4S clusters: an overview. *Annu. Rev. Biochem. 49*, 139–161.

(18) Jin, Z., Heinnickel, M., Krebs, C., Shen, G., Golbeck, J. H., and Bryant, D. A. (2008) Biogenesis of Iron-Sulfur Clusters in Photosystem I:Holo-NfuA from the Cyanobacterium Synchococcus Sp. PCC 70002 rapidly and efficiently transfers [4Fe-4S] clusters to apo PSac in vitro. *J. Biol. Chem. 283*, 28426–28435.

(19) Koay, M. S., Antonkine, M. L., Gartner, W., and Lubitz, W. (2008) Modelling low-potential [Fe4S4] clusters in proteins. *Chem. Biodivers. 5*, 1571–1587.

(20) Eck, R. V., and Dayhoff, M. O. (1966) Evolution of the structure of ferredoxin based on living relics of primitive amino Acid sequences. *Science 152*, 363–366.

(21) Duff, J. L. C., Breton, J. L. J., Butt, J. N., Armstrong, F. A., and Thomson, A. J. (1996) Novel redox chemistry of [3Fe-4S] clusters : Electrochemical characterization of the all-Fe (II) form of the [3Fe-4S] cluster generated reversibly in various proteins and its spectroscopic investigation in Sulfolobus acidocaldarius ferredoxin. *J. Am. Chem. Soc. 118*, 8593–8603.

(22) Armstrong, F. A., George, S. J., Thomson, A. J., Yates, M. G., (1988)Direct electrochemistry in the characterisation of redox proteins: Novel properties of Azotobacter 7Fe ferredoxin. *FEBS lett. 234,*1, 107-110

(23) Tagawa, K., and Arnon, D. I. (1968) Oxidation-reduction potentials and stoichiometry of electron transfer in ferredoxins. *Biochim. Biophys. Act - Bioenerg. 153*, 602–613.

(24) Mulder, D. W., Shepard, E. M., Meuser, J. E., Joshi, N., King, P. W., Posewitz, M. C., Broderick, J. B., and Peters, J. W. (2011) Insights into [FeFe]-hydrogenase structure, mechanism, and maturation. *Structure 19*, 1038–1052.

(25) Kurisu, G., Kusunoki, M., Katoh, E., Yamazaki, T., Teshima, K., Onda, Y., Kimata-Ariga, Y., and Hase, T. (2001) Structure of the electron transfer complex between ferredoxin and ferredoxin-NADP+ reductase. *Nat. Struct Biol. 8*, 117–121.

(26) Hanke, G. T., Satomi, Y., Shinmura, K., Takao, T., and Hase, T. (2011) A screen for potential ferredoxin electron transfer partners uncovers new, redox dependent interactions. *Biochimica et Biophysica Acta (BBA) - Proteins and Proteomics 1814*, 366–374.

(27) Zastrow, M. L., PeacockAnna, F. A., Stuckey, J. A., and Pecoraro, V. L. (2012) Hydrolytic catalysis and structural stabilization in a designed metalloprotein. *Nat. Chem. 4*, 118–123.

CHAPTER 4

PHOTO-INDUCED HYDROGEN PRODUCTION IN A HELICAL PEPTIDE INCORPORATING A [FE-FE] HYDROGENASE ACTIVE SITE MIMIC

Anindya Roy, Christopher Madden, and Giovanna Ghirlanda*

Department of Chemistry and Biochemistry, Arizona State University, Tempe, AZ

Reproduced by permission from The Royal Society of Chemistry

Chem. Commun., 2012,48, 9816-9818

Abstract:

There is growing interest in the development of protein-based hydrogenase mimetics for solar fuel production. Here, we present a di-iron hexacarbonyl dithiolate center anchored via an artificial amino acid to a model helical peptide, and we evaluate the impact of the amino acid on the helical content. The peptide-anchored complex catalyses the photo-induced production of hydrogen with high efficiency.

Introduction:

Natural hydrogenases catalyse the reduction of protons to molecular hydrogen reversibly under mild conditions. The relevance of this reaction to energy production, and in particular to sustainable fuel production, has spurred considerable interest around these enzymes, in particular [Fe-Fe] and [Ni-Fe] hydrogenases. The first structures of [Fe-Fe] hydrogenase revealed an unusual coordination sphere surrounding an asymmetric di-iron

site: a series of [4Fe-4S] clusters that shuttle the reducing electrons to the catalytic site, termed the H-cluster (Figure 4.1a), which contains a [4Fe-4S] cluster and a [Fe-Fe] site coordinated by a non-protein dithiolate bridging ligand as well as carbon monoxide (CO) and cyanide (CN) ligands (Figure 4.1b).[1,2] The site is anchored to the protein through a cysteine that bridges the proximal iron-sulfur cluster and one iron.

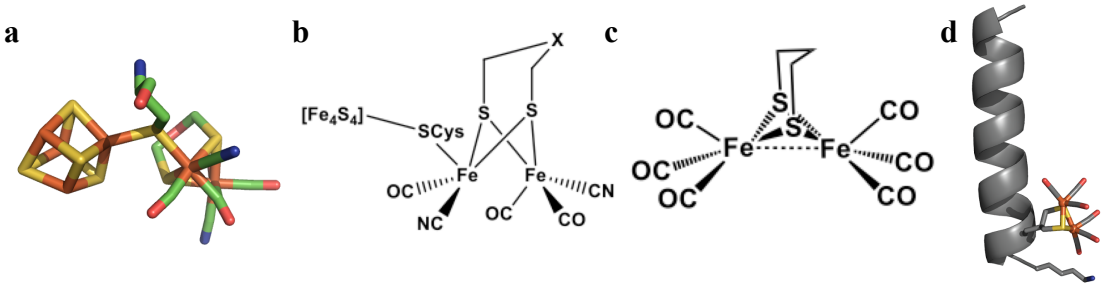

e) K16Dt: YGGKAAAAKAAAAKA**D$_t$**AAK

K16L: YGGKAAAAKAAAAKA**L**AAK

Figure 4.1: a) Active site structure of [Fe-Fe] hydrogenase from Clostridium pasteurianum (CpI, PDB ID 1FEH); b) Chemical Structure of the active site; c) Organometallic mimetic complex of [Fe-Fe] hydrogenase active site, d) Model peptide **K16Dt-Fe$_2$(CO)$_6$** ; e) Sequence of **K16Dt** and **K16L**.

Over the years, parallel work on the natural enzyme and on organometallic model compounds has elucidated several features that characterize the active site and the catalytic cycle of the di-iron site. Increasingly complex bio-inspired organometallic systems, in particular, have explored modifications of structural mimics derived from a (μ-S-(CH$_2$)$_3$-S)[Fe$_2$(CO)$_6$] center (Figure 4.1c). [3-11]

Several of these organometallic model compounds demonstrate moderate catalytic activity, albeit with rates much slower than the natural enzymes, under significantly

harsher conditions (typically in organic or organic/aqueous co-solvents and strong acids), and with unfavorable energetics (high overpotentials). The differences in activity between the natural enzymes and the organometallic complexes are ascribed to the protein matrix, which stabilizes a catalytically active "rotated" conformation of the distal iron and facilitates the reaction by rapidly transferring electrons and a proton to the active site.[12-17] The role of a conserved hydrophobic H-pocket (domain) in stabilizing the H-cluster is becoming increasingly clear: analysis of conserved residues provides a blueprint for designing artificial proteins capable of stabilizing the H-cluster.[15]

Artificial model proteins have been used successfully as a bridging ground between organometallic models and natural proteins in a variety of metalloproteins.[18-28] Initial work to anchor a di-iron hexacarbonyl site to a peptide framework via the thiol moiety of cysteine has relied on CXXC motifs found in helical structures [12,29,30], either engineered into a simple model [30] or found in two natural proteins, Cyt *c* and cyt c_{556}.[12,29] Remarkably, the latter constructs displayed photocatalyzed hydrogen production in aqueous media in the presence of a sacrificial electron donor.

Here, we describe an alternative approach that utilizes an artificial amino acid containing a 1,3 dithiol moiety as an anchor to covalently secure the H –cluster at any position in an artificial protein scaffold. With this strategy, we can incorporate the amino acid into any peptide sequence, regardless of its fold. Conversely, direct incorporation of the amino acid in a complex scaffold allows us to design for solubility, as well as explicitly plan specific interactions to the [Fe-Fe] cluster.

Experimental:

All reactions were performed under argon to ensure an inert environment. All chemicals were purchased from Sigma-Aldrich, Alfa-Asar and Fisher scientific. All NMR spectra are recorded either in $CDCl_3$ or in CD_3OD unless otherwise mentioned in Varian 400MHz instrument. Triethylamine was distilled over KOH and stored over KOH under argon. All other anhydrous solvents were purchased from Sigma-Aldrich. Fmoc and side chain protected Amino acids were purchased from Novabiochem.

Synthesis of 1B:

Compound **1A** [31] (1g , 2.10 mmol) was dissolved in 6 mL dry DMSO in an oven dried round bottom flask. **Acetamidomethylthiol** [32] (880 mg, 8.4 mmol) of was treated with 201mg (8.4 mmol) of NaH in 7.5 ml of dry DMSO. Resulting solution was stirred under argon for 15 min after which it was added to the previous solution in a drop wise fashion. The mixture was stirred until all the reactants were consumed and monitored by TLC (generally for 3 hrs). Following the completion of the reaction, 200 ml water was added to the reaction mixture and extracted with ethyl acetate. The organic layer was separated and washed with (5×100) ml of distilled water. Organic layer was dried over $MgSO_4$ and solvent was evaporated to dryness under reduced pressure. Resulting colorless oil was purified on a silica gel column using (1:1) CH_2Cl_2: Acetone. R_f=0.63(CH_2Cl_2: Acetone=1:1). Yield=700mg (67%), 1H NMR ($CDCl_3$) δ ppm 7.35 (b, 1H), 6.84(b, 1H), 5.25 (d,*J*=9.6 Hz, 2H), 4.37 (m, 2H), 4.31 (m,2H), 4.05 (m,1H), 2.84(m,2 H),2.46 (m, 2H), 1.97 (s,3H), 1.96 (s,3H),1.73(m,2H), 1.41(s,9H),1.37 (s,9H). 13C ($CDCl_3$) δ ppm 171.65, 170.30, 156.07, 82.40, 80.21, 51.86, 41.02, 39.92, 37.08, 34.69, 33.86, 33.01,

28.30, 27.96, 23.21, 23.16. HRMS Calculated for $C_{21}H_{40}N_3O_6S_2$ (M^+) 494.3364, obtained 494.3359.

Synthesis of 1C:

Compound **1B (**150 mg, 0.304 mmol) was treated with 0.3 ml (3.9mmol) of TFA and 0.155 ml (0.76 mmol) of triisopropylsilane in a round bottom flask under strictly anaerobic condition. After 3 hours TFA was evaporated under reduced pressure and the resulting oily residue was triturated with ether to yield a white precipitate, which was filtered and washed with another portion of ether. The compound was used for next step without any further purification.

Synthesis of 1D:

The solid precipitate of **1C** was transferred to a new round bottom flask and dissolved in 2 ml of 10% $NaHCO_3$. To this stirring solution under argon, 119 mg (0.353 mmol) of Fmoc-Osu dissolved in 0.70 ml of THF was added drop wise with vigorous stirring. The resulting solution was stirred overnight under argon. The organic layer was evaporated under reduced pressure and pH of the aqueous layer was adjusted to ~4 by the addition of 10% citric acid solution. The aqueous layer was then extracted with (5×100) ml of ethyl acetate. Combined organic layer was dried over $MgSO_4$ and evaporated under reduced pressure. Resulting solid was purified on a silica gel column using (1:1) CH_2Cl_2 : Acetone. R_f=0.33 (CH_2Cl_2: Acetone=1:1), Yield=54mg (32% over two steps) 1H NMR (CD_3OD) δ ppm 7.67 (d, J=8Hz, 2H), 7.53 (d, J=8Hz, 2H), 7.27 (t, J=8Hz,2H), 7.19 (t,J=7.36,2H), 4.31 (m,1H), 4.30-4.0 (m,7H), 2.68-2.57(m,4H),2.0-1.92 (m,8H) 1.63 (m,1H).13C (CD3OD) δ ppm 171.92, 171.89, 156.99, 143.91, 143.70, 141.14, 127.37, 126.74, 124.75, 124.71, 119.53, 66.37, 53.79, 40.30, 40.10, 35.46, 34.35, 34.13, 33.19,

21.36. HRMS Calculated for $C_{27}H_{33}N_3O_6S_2$ ($M+Na^+$) *m/Z*=582.1735, obtained 582.1709, ($M+K^+$) = 598.1436, obtained 598.1448.

Synthesis of the Peptides:

All peptides were synthesized in a CEM Liberty SPS automated peptide synthesizer on a PAL-ChemMatrix resin using standard Fmoc-based SPPS with a slight variation for **K16Dt** in 0.1 mmol scale. All of the amino acids were double coupled at all positions. For **K16Dt**, first three amino acids were coupled using the synthesizer after which the resin was removed from the synthesizer and manually deprotected using 20% piperdine in DMF. Then it was coupled with 2.5 fold excess of **1D**, using standard coupling conditions for 12 hours. Cleaving a small portion of resin and then characterizing the mass of the system, completion of the reaction was monitored. The resin was then put back in the synthesizer and rest of the synthesis was carried out as usual. All the peptides were manually deprotected and then acetylated in the N-terminus. For **K16Dt**, the Acm protecting group on the side chain was cleaved using I_2 (15 equivalent excess) in DMF for 2 hours on the resin. For **K16L**, the peptide was cleaved from the resin using 95% TFA, 2.5% water and 2.5% TIPS. **K16Dt** was cleaved from the resin using 94% TFA, 2.5% water, 2.5% BME, 1% TIPS. Following the cleavage the resin was filtered off and collected TFA was evaporated using a stream of nitrogen through the solution. Ice-cold ether was added to the residue, which resulted in a white precipitate that was centrifuged and the resulting pallet was collected after decanting the ether. The solid precipitate was dissolved in water and lyophilized to get a white fluffy powder. Peptides were purified on a Vydac-C18 semiprep column using A (0.1% TFA in water) and B (95% acetonitrile, 5% water and 0.1% TFA) solvent system. For **K16Dt**, after lyopholization it was

dissolved in water and a large excess of TCEP was added to the solution to avoid oxidation of the dithiol unit. Appropriate fractions from HPLC purification were collected and lyophilized. Mass of the peptides was confirmed in MALDI and purity of the peptides was checked by re-injecting them on a C-18 analytical peptide. All the peptides used for further experiments were at least 99% pure. Cluster incorporated peptide was also purified in a similar manner except no reducing agent was added to minimize cluster degradation.

Cluster Incorporation Reaction:

2.4 mg (1.2mmol) of **K16Dt** was dissolved in 0.5ml of degassed water in a round bottom flask fitted with a water condenser. To this solution, was added 4.44 mg (8.7 mmol) of $Fe_3(CO)_{12}$ dissolved in 1.7 ml of methanol. The reaction mixture was refluxed under argon for two hours. In the course of the reaction a change in color was observed from green to red. The solvent was evaporated under reduced pressure. Resulting brown solid was dissolved in 10 ml of water. 0.1 ml of this solution was centrifuged and the supernatant was injected on a Vydac C-18 analytical column to monitor the progress of the reaction. UV-Vis absorbance was monitored at 220 nm and 335 nm simultaneously to follow cluster incorporated peptide. Cluster incorporated peptide was purified on a Vydac semipreparative C-18 column using 5ml/min flow rate. Appropriate fractions were collected and lyopholyzed. Identity of the peptides was confirmed using MALDI-MS for apo peptides and ESI-MS for holo-peptide. Purity of the peptide was confirmed by reinjecting the purified peptides on a C-18 analytical column.

Protein Concentration determination:

For **K16L** and **K16Dt**, peptide concentration was determined from absorbance of at 276 nm (ε=1455). **K16Dt-[$Fe_2(CO)_6$]** has an absorption peak at 327 nm that overlaps with the absorption peak at 276 nm, so absorbance at 276 nm is not a correct reflection of peptide concentration. To determine the concentration of **K16Dt-[$Fe_2(CO)_6$]** two different techniques were employed. Firstly, a fluorimetric standardization curve was constructed using **K16Dt** as standard. Serial dilutions of stock **K16Dt** in 10 mM TRIS of 7.5 pH were made. Samples were excited at 276 nm and emission spectra were monitored in 280-400 nm range. A standard curve was constructed by plotting maximum emission intensity vs. concentration. From this standard curve, concentration of unknown **K16Dt-[$Fe_2(CO)_6$]** was determined. Peptide concentration of the same unknown sample was also determined using Amino Acid Analysis technique (UC-Davis proteomics facility). Concentrations determined from two different techniques were within 4% of each other.

FTIR:

FTIR spectra were recorded on a Bruker Vertex 70 series instrument by depositing a thin film on a CaF_2 window and drying it under vacuum. The optical chamber was flushed with Nitrogen for 15 minutes before each scan.

UV-Vis:

UV-Vis spectra were recorded using a Cary-50 UV–vis spectrometer in water.

CD Spectroscopy:

CD spectra were recorded in a JASCO J-815 spectropolarimeter. All the CD spectra were recorded in 10mM TRIS pH=7.5 buffer. For each peptide, CD spectra were recorded at

three different concentrations (30uM, 50uM and 100uM). Each spectra is an average of 6 accumulations. For **K16Dt**, the peptide was reduced with TCEP to exclude any kind of intermolecular or intramolecular covalent bond formation. For **K16Dt-[$Fe_2(CO)_6$]** the sample was dissolved in a degassed buffer solution to avoid aerial degradation of cluster. CD spectra were recorded for two different temperatures, 4°C and 20°C respectively. Fraction helix (f_{helix}) was determined using the following equation.

$$f_{helix} = \frac{[\theta]_{222}}{40000(1 - 2.5/N)}$$

Where [θ] is mean residue molar ellipticity at 222nm and N is the number of backbone amide bonds. Error in f_{helix} is reported as standard deviation of the mean. It is worthy to mention that our fraction helix deviate significantly from the reported value of equivalent peptides mainly because of the difference in conditions used to record the CD spectra. Most of the reported CD spectra for equivalent peptides are reported in 1 M NaCl, 1 mM sodium phosphate, 1 mM sodium citrate, and 1 mM sodium borate (pH 7) at 0 °C, where as all our spectra are recorded in 10mM TRIS, pH=7.5 buffer at 4°C and 20°C to get a better (S/N) below 200nm.

We monitored molar ellipticity at 222 nm as a function of temperature to evaluate the stability of the peptides to thermal denaturation. Qualitatively, we were able to observe enhanced stability of **K16Dt-[$Fe_2(CO)_6$]**; the lack of a folded baseline, however, prevented a rigorous analysis of thermodynamic parameters.

Photocatalytic Hydrogen Production:

In a typical photocatalytic hydrogen evolution experiment 9.33 uM **K16Dt-[$Fe_2(CO)_6$]** , 150uM Ru(bipyridine)$_3$,6H_2O and 50 mM ascorbate in 50 mM of citrate buffer of pH=

4.5 in total 1mL were taken in an airtight cuvette with 1 cm path length. All the solutions were degassed extensively to exclude any atmospheric oxygen. The cuvette was then irradiated with a 450W xenon lamp using a pyrex cutoff filter excluding wavelength <410nm and an IR cut off filter to exclude light > 700nm. The light intensity at the sample was maintained 1100 W/m^2 for all the experiments. For the control experiments, all the components of the reaction mixture were added in the same ratio except the photosensitizer i.e. $Ru(bpy)_3,6H_2O$. The Hydrogen evolved as a function of time was monitored by taking 100 μL of sample overhead gas with a gas tight syringe and injecting and analyzing on a GC (SRI instruments, Model no. 310C) using a 5Å molecular sieve column, a thermal conductivity detector and Ar carrier gas. The GC instrument was calibrated using a gas standard (1% H_2 and bulk N_2).

Electrochemistry:

All electrochemical studies were performed on CH-Instruments model 420B electrochemical workstation using a SCE reference electrode, a Pt-mesh counter electrode and a glassy carbon working electrode (3mm diameter). 100 mM citrate and 25mM NaCl buffer of desired pH (3.6, 4.0, 4.5, 5.0 and 5.5) was utilized to record the cyclic voltammogram. All scans were performed at 200mV/s scan rate. Catalyst concentration was 42 μM. A chemical degradation of the catalyst was observed after 1st scan that deposited on the electrodes. Continuous cleaning of the electrode was necessary to successfully repeat the electrochemical scans. An increase of current around -1.1V was observed as the pH of the solution was lowered. No current increase was observed with substoichiometric ratio of proton to catalyst.

Results and Discussion:

Peptide Design and Synthesis:

In the case of an alpha helix, pairwise side chain interactions are found for residues at *i, i+3* or *i, i+4* positions, which corresponds to one helical turn. To demonstrate this approach we designed peptide **K16Dt** (Figure 4.1d), based on the alanine-rich peptides developed by Baldwin and co-workers, which have been widely used as general host system to evaluate the effect on alpha helix formation of natural and unnatural amino acids.[33-35] To measure the effect of the unnatural amino acid, and of cluster incorporation, on helix formation we chose position 16 as the host position for the dithiol amino acid, which is a leucine in the original sequence (Figure 4.1e). The C terminal lysine 19 is in a *i, i+3* configuration, which allows for interactions with the unnatural amino acid and the reconstituted (μ-S-R-S)[$Fe_2(CO)_6$] complex. Interestingly, Lys 358 is found at a similar distance from the [Fe-Fe] cluster in the structure of *Clostridium pasterianum* hydrogenase (PDB ID 1FEH)[1].

First, we modified an existing synthetic scheme [31]which yielded (*S*)-2-amino-3-(1,2-dithiolan-4-yl)-propionic acid Boc-protected at the amine moiety and swapped it with Fmoc protection, which is more commonly used in solid phase synthesis. Additionally, we changed the thiolane S-S bond to an orthogonal protecting group, acetamidomethyl (Acm), on the two thiols (Scheme 4.1). With this modification, deprotection can occur on resin or off resin, as required for the synthesis. Amino acids containing 1,2-dithiolane moieties have been used to prepare peptides containing 2-3 amino acids by using Boc-compatible solution methods, however the small size of the peptide prevented the direct investigation of secondary structure elements. [36,37]

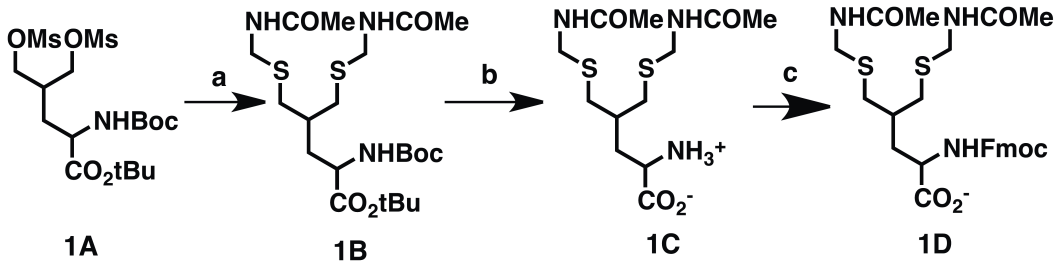

Scheme 4.1: Synthesis of Fmoc-protected artificial amino acid D_t: a) NaH, DMSO, AcmSH, 3 hours; b) TFA, TIPS, 3 hours; c) Fmoc-Osu, THF, Aq. $NaHCO_3$, 3 hours.

Direct incorporation of 2-(((9H-fluoren-9-yl)methoxy)carbonyl amino)-5-(acetamidomethylthio)-4-((acetamidomethylthio) methyl)pentanoic acid (Dt) into peptide **K16Dt** via microwave assisted solid phase peptide synthesis (SPPS) is readily achieved with high yields with peptide purification via reverse phase HPLC. **K16L**, which contains a leucine in place of the dithioleucine analog, was synthesized as a control (see Electronic Supplementary Information, ESI). The [2Fe-2S] cluster was incorporated into purified **K16Dt** by direct reaction with $Fe_3(CO)_{12}$ under strictly anaerobic conditions[38,39], and the product was purified by HPLC (Figure 4.2).

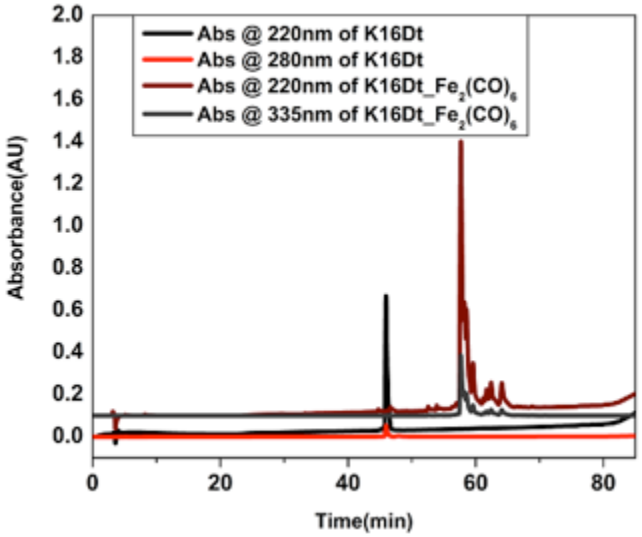

Figure 4.2: HPLC analysis of **K16Dt** and **K16Dt_$Fe_2(CO)_6$** on C-18 analytical column. The retention time for **K16Dt_$Fe_2(CO)_6$** increases by at least 12 minutes under the same

gradient condition, confirming increased hydrophobicity of cluster incorporated peptide as compared to the apo peptide.

UV-Vis, FTIR and CD Spectra:

The resulting **K16Dt-[$Fe_2(CO)_6$]** adduct displays a UV-vis spectrum characterized by an absorption maximum at 327 nm (ε=12931 $M^{-1}cm^{-1}$) and by a broader absorption band at 470 nm (ε=1082 $M^{-1}cm^{-1}$) (Figure 4.3, left panel). These features are consistent with the position and the intensity of absorption bands observed for model hydrogenase compounds containing (μ-S-R-S)$[Fe(CO)_3]_2$ clusters.[12,14]

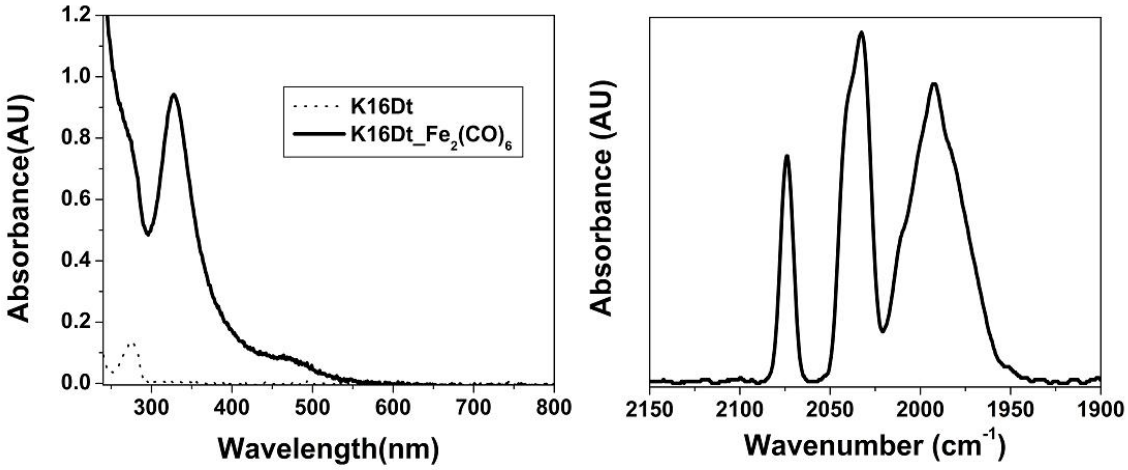

Figure 4.3: UV-Vis spectra of **K16Dt** and **K16Dt-$Fe_2(CO)_6$** (left panel); FTIR spectra of **K16Dt- $Fe_2(CO)_6$** (right panel).

We further characterized the peptide **K16Dt**-[**$Fe_2(CO)_6$**] adduct by FTIR, as the CO and CN^- ligands on the H-cluster of natural hydrogenases and of model compounds show characteristic absorption bands in the 1800-2200 cm^{-1} region. Consistent with the presence of an intact (μ-S-R-S)$[Fe(CO)_3]_2$ cluster, the FT-IR spectrum of **K16Dt-[$Fe_2(CO)_6$]** (Figure 4.3, right panel) contains bands at 1992, 2033, and 2074 cm^{-1} that can be assigned to the presence of CO ligands.[1,2,12,38] Additionally, electrospray

ionization mass spectrometry of peptide **K16Dt-[$Fe_2(CO)_6$]** reveals a mass of 2087 Da, which corresponds to the formation of a $[Fe(CO)_3]_2$ cluster.

Having established the presence of an intact (μ-S-R-S)$[Fe(CO)_3]_2$ cluster, we investigated its effect on the peptide secondary structure. We used circular dichroism (CD) spectroscopy to evaluate the secondary structure of each peptide. The spectra of peptides **K16L**, **K16Dt** and **K16Dt-[$Fe_2(CO)_6$]** recorded at 4 °C (Figure 4.4, left panel) are all dominated by minima at 208 nm and 222 nm of equal intensity, which are the hallmark of high alpha helix content. At 20 °C, the spectra of **K16L**, **K16Dt** reveal significant random coil component, while peptide **K16Dt-$Fe_2(CO)_6$** shows higher helical content. This assessment is confirmed by comparison of fraction helix values (f_{Helix}), (Table 1) calculated for each peptide using the mean residue molar ellipticity at 222 nm in 10 mM TRIS buffer at 7.5 pH.[33-35,40]

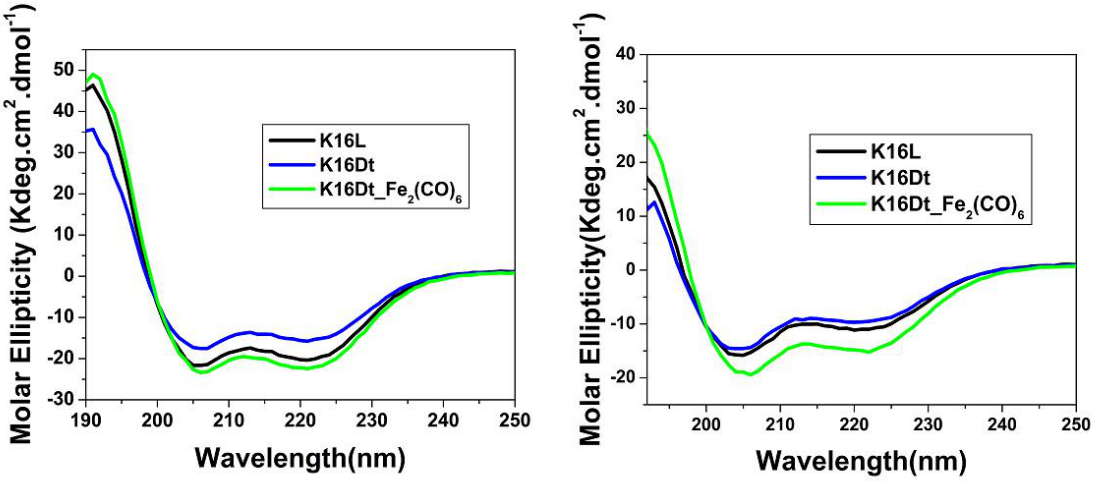

Figure 4.4: CD Spectra in UV region for the peptides at 4°C (left panel) and 20°C (right panel)

Table 1: Fraction helix of **K16Dt**, **K16L**, **K16Dt-[$Fe_2(CO)_6$]**

Peptide	f_{Helix} (4 °C)	f_{Helix} (20 °C)
K16Dt	**0.442±0.017**	**0.272±0.005**
K16L	**0.571±0.015**	**0.327±0.007**
K16Dt-[$Fe_2(CO)_6$]	**0.599±0.019**	**0.410±0.016**

Photo and Electrocatalytic hydrogen production:

Next, we demonstrated the ability of peptide **K16Dt-[$Fe_2(CO)_6$]** to catalyse photo-induced hydrogen production in the presence of a photosensitizer ($Ru(bpy)_3$) and a sacrificial electron donor (ascorbate). We observed visible light induced hydrogen production, measured by gas chromatography, with a turnover number (TON) of 84 in 2.30 hours for 9.33 μM **K16Dt-[$Fe_2(CO)_6$]** in the presence of a 15 fold excess of photosensitizer and 50 mM of ascorbate, in citrate buffer at pH 4.5 (Figure 4.5, left panel). Hydrogen production is completely abolished in absence of the photosensitizer, confirming the role of $Ru(bpy)_3$ as an essential partner in the photocatalysis. Although a direct comparison is complicated by different experimental conditions, this efficiency compares favourably with previous literature reports for di-iron hexacarbonyl complexes in similar conditions, which typically range from 10 to 100 TON at maximum catalytic efficiency.[13,15-17,29,41,42] We also characterized the redox properties of peptide **K16Dt-[$Fe_2(CO)_6$]** under aqueous conditions using cyclic voltammetry (CV). Similar to previous reports, peptide **K16Dt-[$Fe_2(CO)_6$]** shows an irreversible oxidation and reduction, the

latter approximately at -1.1 V (vs NHE).[14,43] The current intensity for the reductive event is strongly dependent on pH (Figure 4.5, right panel), which supports previously reported electrochemical studies in aqueous and mixed solvents. These results are consistent with the $Fe^{I}Fe^{I}/Fe^{I}Fe^{0}$ couple, which strongly depends on proton concentration.[3,12,29]

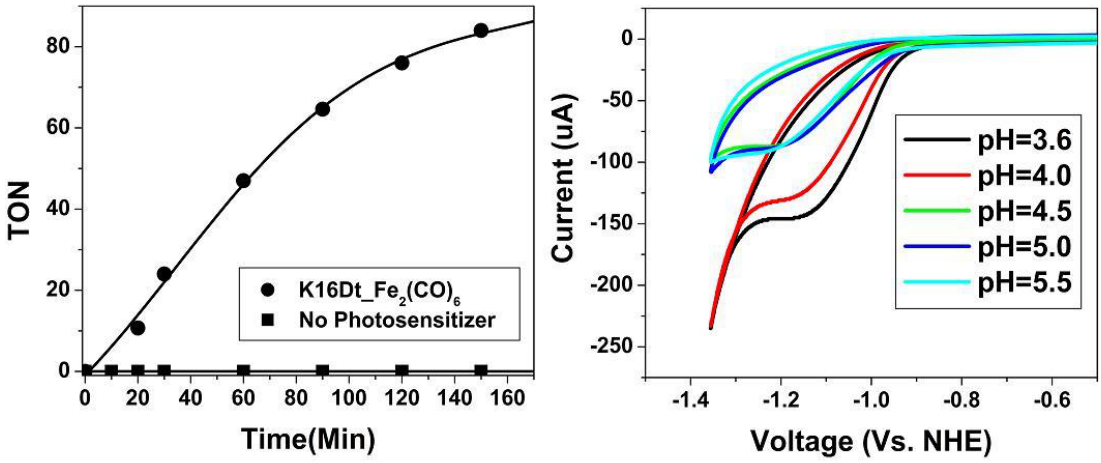

Figure 4.5: Visible light-driven hydrogen production (410–770 nm) by **K16Dt-[$Fe_2(CO)_6$]** (9.33 μM) in the presence (circles) and absence (squares) of 150 mM $Ru(bpy)_3$, in citrate buffer (50 mM) pH 4.5 (left panel); Cyclic voltammetry of 1-[Fe2(CO)6] in 100 mM citrate buffer, 25 mM NaCl, at pH in the 3.6 to 5.5 range.

Conclusions:

In summary, we have demonstrated here the synthesis of a functional (μ-S-R-S)[$Fe_2(CO)_6$] cluster anchored to an unnatural amino acid, Dt, suitable for Fmoc-based solid phase synthesis, and its successful incorporation into an alpha helical model peptide scaffold. The design allowed measurement of the effect of Dt on helix formation and the introduction of simple second sphere interactions to the cluster, which stabilize the helix. We found that the complex, **K16Dt-[$Fe_2(CO)_6$]**, catalyses photo-induced hydrogen production in the presence of a photosensitizer and a sacrificial reducing agent in water

with remarkable efficiency. Our approach allows for the directed incorporation of hydrogenase mimics into any peptide scaffold and opens the way for the design of more elaborate peptide-based architectures that could be used to test specific hypotheses on the optimal environment and on the secondary sphere of interaction of the [2Fe-2S] cluster, incorporating lessons learned from the study of natural hydrogenases as well as through the rich literature on organometallic analogues, and to include in the design properties such as compatibility with conductive materials and electrodes.

Current Work and Future Outlook:

The work presented above describes a general method to introduce [Fe-Fe] hydrogenase mimics in peptide motifs via incorporation of an artificial amino acid as an anchoring group. This method bypasses the challenges of designing specific non-covalent interactions (hydrogen bonding, electrostatic) between protein and the organometallic cofactor, which are not completely understood by covalently securing the cofactor to the

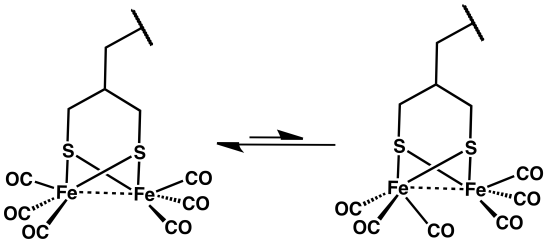

Figure 4.6: Thermodynamically favourable structure of biomimetic catalyst as compared to the catalytically and biologically relevant rotated structure, wiggly bond represents peptidic linkage.

protein matrix. Our first design, though, resulted in a solvent exposed active site, and did not provide the hydrophobic environment and second sphere interactions observed in the natural enzyme. Lacking these interactions, the model peptide **K16Dt_$Fe_2(CO)_6$** is thought to contain a thermodynamically favoured structure of the diiron hexacarbonyl

active site as compared to the catalytically relevant rotated structure seen in natural hydrogenases (Figure 4.6).

To maximize activity, second generation de novo designed hydrogenases should incorporate the structural constraints observed in the natural enzyme. We have undertaken the design of a more elaborate protein scaffold around the biomimetic cofactor: a four-helix bindle provides ideal to position side chains within the core in close proximity with the active site. The four-helix bundle integrates a synthetic single helix component containing the organometallic complex, anchored by an unnatural amino acid, and a genetically encoded component comprising the remaining three helices. Current work, described below, aims to develop semisynthetic methodology for artificial hydrogenases.

Protein Design:

We chose a de novo designed di-zinc binding 4-helix bundle protein [44,45] (PDB Code 2HZ8) as a scaffold protein for introducing an artificial hydrogenase active site unnatural amino acids to provide the central bridging dithiolate ligand. The NMR structure reveals two Zn atoms in the core of the helical bundle coordinated by tetra-glutamic acid and bis-histidine (E11, E44, E74, E104, H77, H107) as primary ligands, as shown in Figure 4.6. The design incorporated a secondary interaction shell that stabilizes these buried polar residues, comprised by, two tyrosine residues (Y18, Y51) and two aspartic acid residues (D73, D103), which hydrogen bond to (E11, E44, E74, E104, H77, H107) as shown in Figure 4.7.

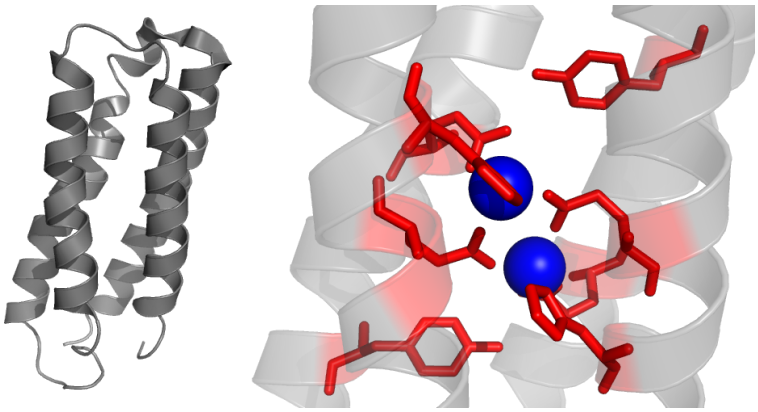

Figure 4.7: NMR structure of de novo designed di-zinc binding protein (PDB ID 2HZ8, left panel); A close up view of the primary and secondary coordination sphere of the bimetallic centers (right panel), two blue spheres represent two zinc atoms.

We set out to replace the di-zinc site with the di-iron site of the hydrogenase mimic. To accomplish this, we built a model of the artificial hydrogenase *in silico* using on the steps described below.

1) **Deletion the primary coordination sphere to the di-zinc active site:** First, we mutated the polar residues that coordinate directly the zinc atoms as follows: E11A, E44A, E74A, E104A, H77A, H107L (Figure 4.8). These mutations replace the polar active site of the parent protein with a nonpolar one.
2) **Deletion of secondary coordination sphere:** Second, we inserted the following mutations: Y18F, Y51F and D102K/D102H (Figure 4.8). The rationale behind D103K/D103H mutations is described later on.

3) **Introduction of hydrogenase mimic inside the helical bundle:** We docked the di-iron active site in such a manner that the two iron atoms overlapped with the two zinc atoms in the structure of the wild type protein. We then searched for positions inside the core of the helical bundle that would be compatible with the dithiol amino acid used to anchor the organometallic active site without affecting the backbone conformation. We found position I100 to be the most favorable for introduction of the biomimetic active site. We built a model containing I100Dt mutation and attached it to the di-iron cluster within the core of the bundle. Any steric clashes between the di-ironhexacarbonyl moiety and other amino acid side chains inside the helical bundle, were relaxed by choosing suitable side chain rotamers.

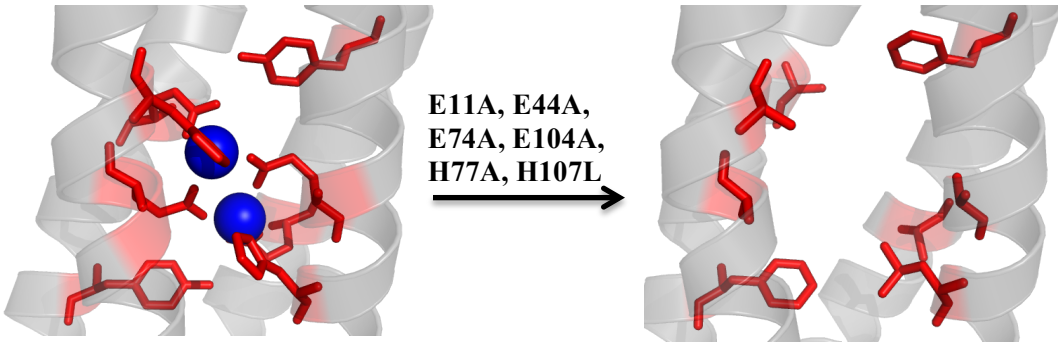

Figure 4.8: Design strategy for deletion of di-zinc active site: primary and secondary coordination sphere were deleted by mutations listed above and described in the text. D103K/D103H mutation was omitted in the picture for clarity.

To optimize the shuttling of protons to the active site, which is necessary for activity, we introduced lysine or histidine at position D102, located on the surface of the protein but close to the active site. In the natural hydrogenase this function is carried out by the central nitrogen in the azadithiolate bridging ligand; however, a

neighboring side chain located at appropriate distance from the active site could recapitulate such function.

Semisynthetic strategy towards an artificial hydrogenase; Expressed protein ligation strategy:

The proposed artificial hydrogenase described above includes an artificial amino acid, supporting a synthetic organometallic active site, within a biological protein matrix. To exploit the advantages of solid phase synthesis as well as of recombinant protein expression, we envisioned a synthetic strategy in which the 4-helix bundle (**4H**) is obtained via a [3+1] coupling [Figure 4.8]: the 3-helix (**3H**) is expressed in E. coli and contains a bio-orthogonal tag, while the 1-helix (**1H**) is synthesized in solid phase with

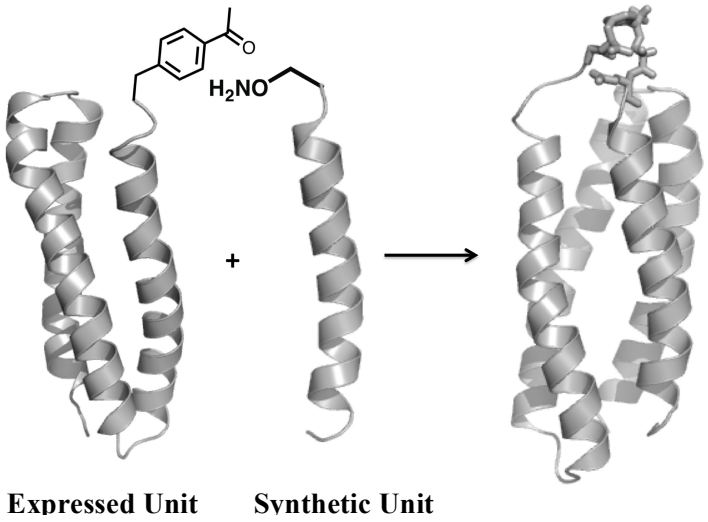

Figure 4.9: Semisynthetic strategy of artificial hydrogenase: Utilization of expressed protein ligation strategy.

the dithiol amino at a predetermined position as previously described. To incorporate the bioorthogonal tag into the 3H fragment we used a method pioneered by the Schultz laboratory that uses an engineered t-RNA/tRNA-synthase pair for site specific incorporation of artificial amino acids in expressed –protein.[46,47]

Expression and purification of 3H:

We used site-specific incorporation of para-acetylphenylalanine (pAcF) in protein using an orthogonal amber suppressor tRNA/aaRS pair, derived from the corresponding tyrosyl-Methanococcus jannaschii pair subcloned in a pVOL vector (pAcF-pVol). A TAG codon was introduced in the gene encoding **3H** corresponding to the C-terminus of the protein. A His_6 tag and a TEV cleavage site were introduced at the N-terminus of the protein to facilitate purification. The resulting gene encoding **3H** was subcloned into a pET-30c Vector (3H-pET30c). *E. coli* BL-21 competent cells were transformed using pAcF-pVol and 3H-pET30c (Figure 4.10). 3H was expressed in LB medium supplemented with 1 mM of p-AcF after IPTG induction with a yield of approximately ~45mg/liter. Cells were harvested after 18 hours by centrifugation; the periplasmic fraction was further purified by Ni-column, and TEV protease was directly added to the eluted fractions containing the desired protein. SDS-PAGE monitoring of the reaction revealed incomplete cleavage (approximately 30% as confirmed by HPLC analysis).

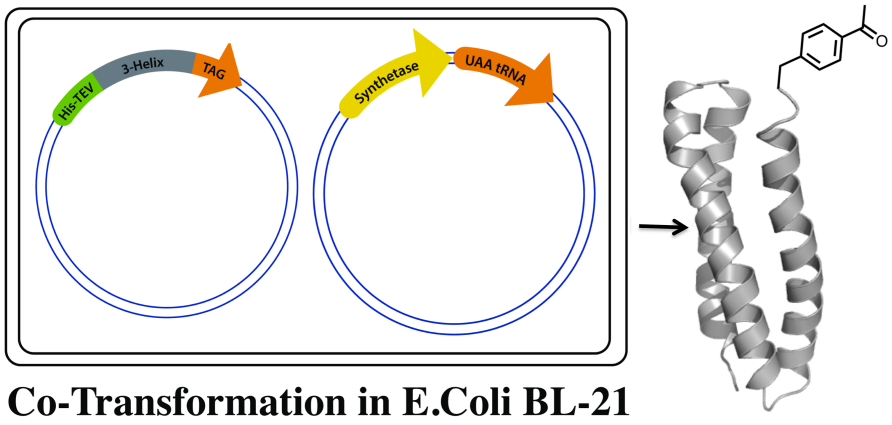

Figure 4.10: Site-specific incorporation of p-AcF in **3H** using genetic tools. E coli BL21 competent cells were co-transformed using 3H-pET30c and pAcF-pVol vectors using chloramphenicol and kanamycin double selection.

The propensity of **3H** to aggregation, caused by its solvent exposed hydrophobic core, is the most likely reason for incomplete reaction. To increase the solubility of the protein during cleavage, we added 1 (M) urea to the cleavage mixture. Under these conditions, TEV protease activity is reported to be minimally perturbed. In those conditions **3H** is well solubilized, resulting in over 90% cleavage after overnight reaction at 4°C. The reaction mixture was purified by preparative reverse phase HPLC using a C-18 column.

Synthesis of 1H:

1H containing dithiol amino acid was synthesized by standard Fmoc/tBu solid phase peptide synthesis protocol following a similar method described at the beginning of this chapter. Amino acids at all positions were double coupled except for the artificial amino acid. The amino-oxy functionality needed for conjugation to 3H was inserted by coupling ^{t}Bu-aminooxy acetic acid at the N-terminus of the peptide on-resin using a ten-fold molar excess and DIC as a coupling agent in DMF for 1.30 hours. Resin was washed with DMF and DCM and vacuum dried. Acetamidomethyl protecting groups on the thiol side chain were removed using oxidative cleavage mediated by iodine. Resin was swelled in a (1:1) DCM and methanol solution. Swelled resin was treated with the iodine solution in DMF in 10-fold molar excess and resulting solution was stirred for 1.30 hours under strict anaerobic condition. Following cleavage and repeated wash with DMF and DCM, resin was dried under vacuum. The resin was washed with DMF and DCM. The crude peptide was released from the resin using standard cleavage solutions and purified as described previously.

Synthesis of 4H:

Initial attempts at coupling **3H** and **1H** were unsuccessful in aqueous, organic and mixed aqueous: organic solvents. Some of the conditions explored included: a) 100% water, 0.1 % TFA; b) 50% water 50% acetonitrile, 0.1% TFA and c) 100% acetonitrile, 0.1% TFA. No coupling was observed under any of the above conditions. In contrast, the coupling reaction proceeds to completion in denaturing conditions (6 M urea in 0.1% TFA, water);

we observed a new peak in HPLC corresponding to the **4H** after 3 hours of reaction, verified by MALDI-TOF spectroscopy and SDS-PAGE gel [Figure 4.11]. The initial failure can be attributed to the secondary structure of the **3H**, which adversely affects

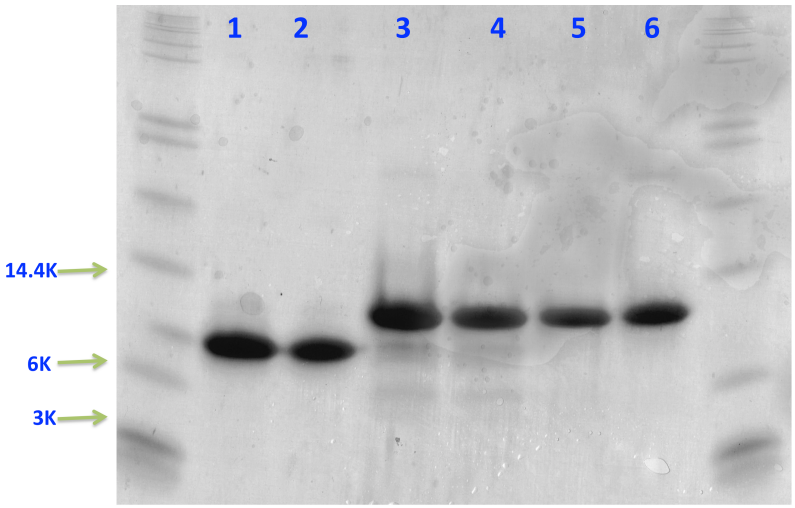

Figure 4.11: SDS-PAGE Gel of **3H** (lane 1, 2), **4H** (Lane 3, 4), **4H-$Fe_2(CO)_6$** (Lane 5, 6).

the reactivity of the ketone group, but can be reinstated in presence of a denaturing agent. The reaction rate depends on concentration of the reactants. The reaction proceeds to completion in 8-12 hrs at micromolar concentration of the reagents i.e. **3H** and **1H**, at micromolar concentration of the reagents i.e. **3H** and **1H,** it took 8-12 hours for the reaction to go to completion; at millmolar concentration, the reaction was complete in 3-4 hours, in agreement with reported oxime bond formation reaction kinetics.[49]

Cluster Incorporation reaction and UV-Vis, FTIR and ESI-MS spectra:

The Di-iron cluster was introduced at the core of the helical bundle by refluxing a solution contaning **4H** and $Fe_3(CO)_{12}$ in (3:1) MeOH:water under an argon environment. During the course of the reaction (approximately after 2-3 hours) a color change from green to red was observed. The resulting solution was lyophilized and purified using

reverse phase HPLC on a C-18 column. For comparison, we also incorporated the di-iron cluster in 1-helix too, using similar protocol. Incorporation of **4H-$Fe_2(CO)_6$** as compared

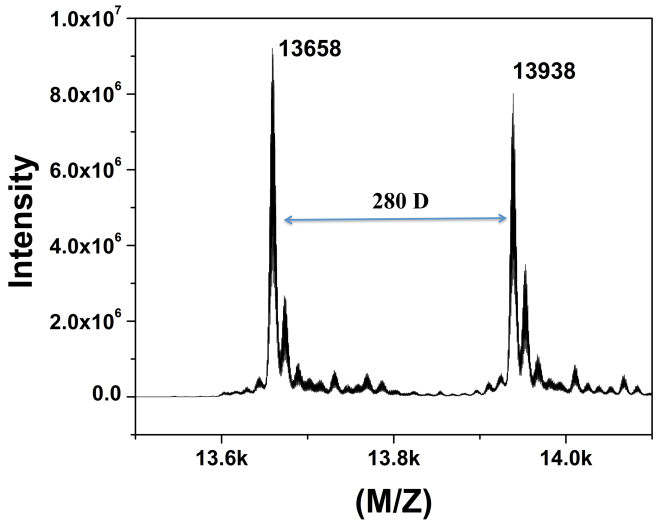

Figure 4.12: ESI-MS Spectra of **4H-$Fe_2(CO)_6$**, A mass two peaks centered around 13658D and 13938 D was observed which are attributed to the apo and holo **4H** mass respectively.

to **4H** and **3H** was confirmed using SDS-PAGE gel (Figure 4.11) and ESI-MS spectroscopy (Figure 4.12) . **4H** and **4H-$Fe_2(CO)_6$** migrates the same distance on a SDS PAGE gel. A mass difference of 280 D was observed in ESI-MS spectra between 4H and **4H-$Fe_2(CO)_6$** (Figure 4.12), which can be attributed to the attached $Fe_2S_2(CO)_6$.

Both **4H-$Fe_2(CO)_6$** and **1H-$Fe_2(CO)_6$** shows new absorption peaks in UV-Vis as compared to apo peptides, corresponding to the Fe_2S_2 complex. **1H-$Fe_2(CO)_6$** shows an absorption around 328 nm, whereas **4H- $Fe_2(CO)_6$** shows an absorption at 330 nm. This small red shift can also be observed at higher wavelength (λ= 478 nm, Figure 4.13). We attribute this shift to the change in cluster environment from 1-helix where it's more

solvent exposed to a less polar, solvent excluded environment in **4H-$Fe_2(CO)_6$.** The electronic environment around the –CO ligands can also be probed by FTIR. **1H-$Fe_2(CO)_6$** showed three major band centered around 1995, 2033 and 2074 cm^{-1} where as **4H-$Fe_2(CO)_6$** showed stretching frequency centered around 1994, 2033, 2073 cm^{-1}. Solvent dependence of CO stretching frequencies in FTIR is well studied; in the case of 1,3 propanedithiolatediironhexacarbonyl complexes, total five stretching frequencies are observed in nonpolar solvents, confirming a pseudo C_{2v} symmetry. [50,51] In polar solvent, three of these low frequency bands collapse to give rise to one broad absorption band. We observed a similar phenomenon in our system, where the low frequency broad absorption band in **1H-$Fe_2(CO)_6$** gets split into three bands in **4H-$Fe_2(CO)_6$** confirming change in polarity of the environment around the di-iron cluster.[51] In **1H-$Fe_2(CO)_6$** , all three absorption bands are broad and reminiscent of a solvent exposed di-iron site, while in **4H-$Fe_2(CO)_6$** , total five absorption bands were observed, which are much more sharper as compared to **1H-$Fe_2(CO)_6$** . These data support encapsulation of the di-iron cluster in the hydrophobic core of the 4-helix bundle as per design.

As an extension of our previous work [52], we have shown that biomimetic [Fe-Fe] hydrogenase mimic can be introduced in more complex peptide scaffolds using a chemical biology approach. This straightforward method is amenable to optimization with respect to the protein and the organometallic counterpart. For example, the biomimetic diironhexacarbonyl complex used in this study and in most of the reported molecules

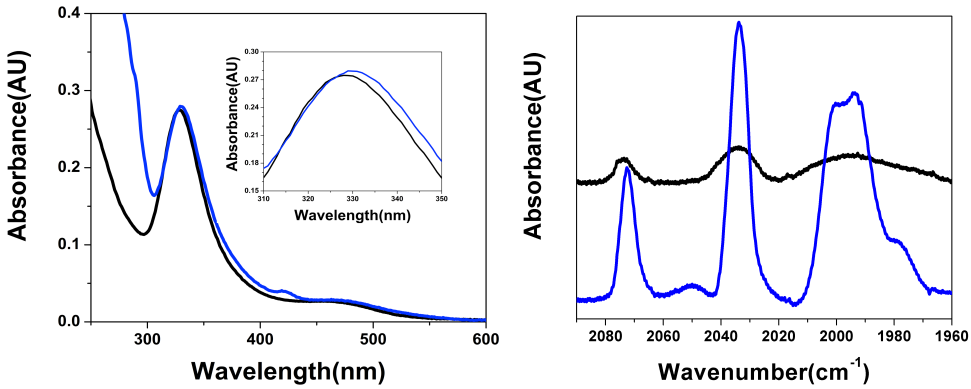

Figure 4.13: UV-Vis spectra of **1H-$Fe_2(CO)_6$** (b lack line) and **4H_$Fe_2(CO)_6$** (blue line) in 100 mM Tris.HCl, pH=7.5 (left panel) ; FTIR spectra of **1H-$Fe_2(CO)_6$** (black line) and **4H_$Fe_2(CO)_6$** (blue line, right panel) as a thin film on a CaF_2 window.

have 6-CO ligands, where as the more biologically relevant complexes comprises two-CN ligands. The –CO ligands are easily replaceable with –CN, but these solvent exposed model complexes are extremely unstable and prone to polymerization under catalytic condition. In the present system, the active site remains shielded from bulk solvent in the protein matrix, thus will not amenable towards polymerization. Such problems may be avoided in the four-helix bundle construct, in which the active site is shielded from bulk solvent. A more complex architecture allows for the design of specific hydrogen bonds with side chains and backbone polar atoms to the -CN, enforcing a rotated structure similar to the one observed in nature. Further, complex protein scaffolds can be used to connect the catalytic site with electron transfer modules, akin to what observed in natural hydrogenases. The H-cluster in [Fe-Fe] hydrogenases is composed by an azadithiol-bridged diiron site, which is attached via a shared cysteine side chain to a [4Fe-4S] cluster that acts as electron sink during the active catalytic process. We have experience engineering [4Fe4S]-cluster binding sites in proteins, and we plan to add this capacitant

to the anchored diiron hexacarbonyl site. Current work is aimed to investigate the effect of protein environment on electro/photocatalytic activity of the diiron subsite via rational mutation. Such efforts will be greatly aided by a more detailed structural elucidation of **4H- $Fe_2(CO)_6$**. Using the structure of **4H-$Fe_2(CO)_6$** , we will select positions on the protein sequence that are within 10-12 Å of the complex, and subject them to mutagenesis using directed evolution technique.

REFERENCES:

(1) Peters, J., Peters, J., Lanzilotta, W., Lanzilotta, W., Lemon, B., Lemon, B., Seefeldt, L., and Seefeldt, L. (1998) X-ray crystal structure of the Fe-only hydrogenase (Cpl) from Clostridium pasteurianum to 1.8 angstrom resolution. *Science 282*, 1853–1858.

(2) Nicolet, Y., Piras, C., Legrand, P., Hatchikian, C. E., and Fontecilla-Camps, J. C. (1999) Desulfovibrio desulfuricans iron hydrogenase: the structure shows unusual coordination to an active site Fe binuclear center. *Structure 7*, 13–23.

(3) Singleton, M. L., Crouthers, D. J., Duttweiler, R. P. 3., Reibenspies, J. H., and Darensbourg, M. Y. (2011) Sulfonated diiron complexes as water-soluble models of the [Fe-Fe]-hydrogenase enzyme active site. *Inorganic chemistry 50*, 5015–5026.

(4) Barton, B. E., Olsen, M. T., and Rauchfuss, T. B. (2010) Artificial hydrogenases. *Curr. Opin. Biotechnol. 21*, 292–297.

(5) Tard, C., and Pickett, C. J. (2009) Structural and Functional Analogues of the Active Sites of the [Fe]-, [NiFe]-, and [FeFe]-Hydrogenases. *Chem. Rev. 109*, 2245–2274.

(6) Erdem, Ö. F., Schwartz, L., Stein, M., Silakov, A., Kaur-Ghumaan, S., Huang, P., Ott, S., Reijerse, E. J., and Lubitz, W. (2011) A Model of the [FeFe] Hydrogenase Active Site with a Biologically Relevant Azadithiolate Bridge: A Spectroscopic and Theoretical Investigation. *Angew. Chem. Int. Ed. 50*, 1439–1443.

(7) Ezzaher, S., Gogoll, A., Bruhn, C., and Ott, S. (2010) Directing protonation in [FeFe] hydrogenase active site models by modifications in their second coordination sphere. *Chem. Commun. 46*, 5775–5777.

(8) Surawatanawong, P., Tye, J. W., Darensbourg, M. Y., and Hall, M. B. (2010) Mechanism of electrocatalytic hydrogen production by a di-iron model of iron-iron hydrogenase: a density functional theory study of proton dissociation constants and electrode reduction potentials. *Dalton Trans. 39*, 3093–3104.

(9) Wang, F., Wang, W.-G., Wang, X.-J., Wang, H.-Y., Tung, C.-H., and Wu, L.-Z. (2011) A Highly Efficient Photocatalytic System for Hydrogen Production by a Robust Hydrogenase Mimic in an Aqueous Solution - Wang - 2011 - Angewandte Chemie International Edition - Wiley Online Library. *Angew. Chem. Int. Ed. 50*, 3193–3197.

(10) Wang, W.-G., Wang, F., Wang, H.-Y., Tung, C.-H., and Wu, L.-Z. (2012) Electron transfer and hydrogen generation from a molecular dyad: platinum(ii) alkynyl complex anchored to [FeFe] hydrogenase subsite mimic. *Dalton Trans. 41*, 2420–2426.

(11) Quentel, F., Passard, G., and Gloaguen, F. (2012) Electrochemical hydrogen production in aqueous micellar solution by a diiron benzenedithiolate complex relevant to [FeFe] hydrogenases. *Phys Chem Chem Phys 5*.7757-7761.

(12) Sano, Y., Onoda, A., and Hayashi, T. (2011) A hydrogenase model system based on the sequence of cytochrome c: photochemical hydrogen evolution in aqueous media. *Chem. Commun. (Camb.) 47*, 8229–8231.

(13) Mulder, D. W., Shepard, E. M., Meuser, J. E., Joshi, N., King, P. W., Posewitz, M. C., Broderick, J. B., and Peters, J. W. (2011) Insights into [FeFe]-hydrogenase structure, mechanism, and maturation. *Structure 19*, 1038–1052.

(14) Singleton, M. L., Reibenspies, J. H., and Darensbourg, M. Y. (2010) A cyclodextrin host/guest approach to a hydrogenase active site biomimetic cavity. *J. Am. Chem. Soc. 132*, 8870–8871.

(15) Knorzer, P., Silakov, A., Foster, C. E., Armstrong, F. A., Lubitz, W., and Happe, T. (2012) Importance of the Protein Framework for Catalytic Activity of [FeFe]-Hydrogenases. *J. Biol. Chem. 287*, 1489–1499.

(16) Darensbourg, M. Y., and Bethel, R. D. (2012) Biomimetic chemistry: Merging the old with the new. *Nat. Chem. 4*, 11–13.

(17) Camara, J. M., and Rauchfuss, T. B. (2011) Combining acid-base, redox and substrate binding functionalities to give a complete model for the [FeFe]-hydrogenase. *Nat. Chem. 4*, 26–30.

(18) Lu, Y., Yeung, N., Sieracki, N., and Marshall, N. M. (2009) Design of functional metalloproteins. *Nature 460*, 855–862.

(19) Nanda, V., and Koder, R. L. (2010) Designing artificial enzymes by intuition and computation. *Nat. Chem. 2*, 15–24.

(20) Grzyb, J., Xu, F., Weiner, L., Reijerse, E. J., Lubitz, W., Nanda, V., and Noy, D. (2010) De novo design of a non-natural fold for an iron-sulfur protein: alpha-helical coiled-coil with a four-iron four-sulfur cluster binding site in its central core. *Biochim. Biophys. Acta 1797*, 406–413.

(21) Zastrow, M. L., PeacockAnna, F. A., Stuckey, J. A., and Pecoraro, V. L. (2012) Hydrolytic catalysis and structural stabilization in a designed metalloprotein. *Nat. Chem. 4*, 118–123.

(22) Faiella, M., Andreozzi, C., de Rosales, R. T. M., Pavone, V., Maglio, O., Nastri, F., DeGrado, W. F., and Lombardi, A. (2009) An artificial di-iron oxo-protein with phenol oxidase activity. *Nat. Chem. Biol. 5*, 882–884.

(23) Miner, K. D., Mukherjee, A., Gao, Y.-G., Null, E. L., Petrik, I. D., Zhao, X., Yeung, N., Robinson, H., and Lu, Y. (2012) A Designed Functional Metalloenzyme that Reduces O2 to H2O with Over One Thousand Turnovers. *Angew. Chem. Int. Ed.* n/a–n/a.

(24) Cordova, J. M., Noack, P. L., Hilcove, S. A., Lear, J. D., and Ghirlanda, G. (2007)

Design of a functional membrane protein by engineering a heme-binding site in glycophorin A. *J. Am. Chem. Soc. 129*, 512–518.

(25) Shinde, S., Cordova, J., Woodrum, B., and Ghirlanda, G. (2012) Modulation of function in a minimalist heme-binding membrane protein. *J Biol Inorg Chem 17*, 557–564.

(26) Koder, R. L., Anderson, J. L. R., Solomon, L. A., Reddy, K. S., Moser, C. C., and Dutton, P. L. (2009) Design and engineering of an O2 transport protein. *Nature 458*, 305–309.

(27) Sambasivan, R., and Ball, Z. T. (2010) Metallopeptides for Asymmetric Dirhodium Catalysis. *J. Am. Chem. Soc. 132*, 9289–9291.

(28) Chen, Z., Popp, B. V., Bovet, C. L., and Ball, Z. T. (2011) Site-Specific Protein Modification with a Dirhodium Metallopeptide Catalyst. *ACS Chem. Biol. 6*, 920–925.

(29) Sano, Y., Onoda, A., and Hayashi, T. (2011) Photocatalytic hydrogen evolution by a diiron hydrogenase model based on a peptide fragment of cytochrome c556 with an attached diiron carbonyl cluster and an attached ruthenium photosensitizer. *J. Inorg. Biochem. 108*, 159–162.

(30) Jones, A. K., Lichtenstein, B. R., Dutta, A., Gordon, G., and Dutton, P. L. (2007) Synthetic Hydrogenases: Incorporation of an Iron Carbonyl Thiolate into a Designed Peptide. *J. Am. Chem. Soc. 129*, 14844–14845.

(31) Morera, E., Pinnen, F., and Lucente, G. (2002) Synthesis of 1,2-dithiolane analogues of leucine for potential use in peptide chemistry. *Org. Lett. 4*, 1139–1142.

(32) Silvennoinen, G., Polborn, K., Mayer, P., and Pfaendler, H. R. (2009) *Thieme Chemistry*

(33) Kortemme, T., and Baldwin, R. (1994) Helix propensities of the amino acids measured in alanine‐based peptides without helix‐stabilizing side‐chain interactions. *Protein Sci.*

(34) Marqusee, S., Robbins, V. H., and Baldwin, R. L. (1989) Unusually stable helix formation in short alanine-based peptides. *Proceedings of the National Academy of Sciences of the United States of America 86*, 5286–5290.

(35) Cheng, R. P., Girinath, P., Suzuki, Y., Kuo, H.-T., Hsu, H.-C., Wang, W.-R., Yang, P.-A., Gullickson, D., Wu, C.-H., Koyack, M. J., Chiu, H.-P., Weng, Y.-J., Hart, P., Kokona, B., Fairman, R., Lin, T.-E., and Barrett, O. (2010) Positional Effects on Helical Ala-Based Peptides. *Biochemistry 49*, 9372–9384.

(36) Apfel, U.-P., Kowol, C. R., Halpin, Y., Kloss, F., Kuebel, J., Goerls, H., Vos, J. G., Keppler, B. K., Morera, E., Lucente, G., and Weigand, W. (2009) Investigation of amino

acid containing [FeFe] hydrogenase models concerning pendant base effects *103*, 1236–1244.

(37) Apfel, U.-P., Rudolph, M., Apfel, C., Robl, C., Langenegger, D., Hoyer, D., Jaun, B., Ebert, M.-O., Alpermann, T., Seebach, D., and Weigand, W. (2010) Reaction of Fe3(CO)12 with octreotide-chemical, electrochemical and biological investigations. *Dalton Trans. 39*, 3065–3071.

(38) Lyon, E. J., Georgakaki, I. P., Reibenspies, J. H., and Darensbourg, M. Y. (1999) Carbon Monoxide and Cyanide Ligands in a Classical Organometallic Complex Model for Fe-Only Hydrogenase. *Angew. Chem. Int. Ed. 38*, 3178–3180.

(39) Ellgen, P., Gerlach, J. (1973) Kinetics and Mechanism of Substitution-Reactions of Bis(Mercaptotricarbonyliron) Complexes. *Inorganic chemistry 12*, 2526–2532.

(40) Greenfield, N. J. (2006) Using circular dichroism spectra to estimate protein secondary structure. *Nature protocols 1*, 2876–2890.

(41) Wang, H.-Y., Wang, H.-Y., Si, G., Si, G., Cao, W.-N., Cao, W.-N., Wang, W.-G., Wang, W.-G., Li, Z.-J., Li, Z.-J., Wang, F., Wang, F., Tung, C.-H., Tung, C.-H., Wu, L.-Z., and Wu, L.-Z. (2011) A triad [FeFe] hydrogenase system for light-driven hydrogen evolution. *Chem. Commun. 47*, 8406–8408.

(42) Wang, W.-G., Wang, W.-G., Wang, F., Wang, F., Wang, H.-Y., Wang, H.-Y., Si, G., Si, G., Tung, C.-H., Tung, C.-H., Wu, L.-Z., and Wu, L.-Z. (2010) Photocatalytic Hydrogen Evolution by [FeFe] Hydrogenase Mimics in Homogeneous Solution. *Chem-Asian J 5*, 1796–1803.

(43) Felton, G. A. N., Mebi, C. A., Petro, B. J., Vannucci, A. K., Evans, D. H., Glass, R. S., and Lichtenberger, D. L. (2009) Review of electrochemical studies of complexes containing the Fe2S2 core characteristic of [FeFe]-hydrogenases including catalysis by these complexes of the reduction of acids to form dihydrogen. *J. Organomet. Chem. 694*, 2681–2699.

(44) Calhoun, J. R., Kono, H., Lahr, S., Wang, W., DeGrado, W. F., and Saven, J. G. (2003) Computational design and characterization of a monomeric helical dinuclear metalloprotein. *J Mol Biol 334*, 1101–1115.

(45) Solution NMR Structure of a Designed Metalloprotein and Complementary Molecular Dynamics Refinement. Calhoun J. R., Liu W., Spiegel K., Peraro M. D., Klein M. L., Valentine K. G., Wand A. J., Degrado W. F. (2008). *Structure 16*, 2, 210-215

(46) Liu, C. C., and Schultz, P. G. (2010) Adding New Chemistries to the Genetic Code. *Annu. Rev. Biochem. 79*, 413–444.

(47) Wang, L., Brock, A., Herberich B., Schultz P.G. (2001) Expanding the Genetic Code of Escherichia coli, *Science 292,*498.

(48) Waugh, D. S. (2011) An overview of enzymatic reagents for the removal of affinity tags. *Protein Expression and Purification 80*, 283–293.

(49) Dirksen, A., and Dawson, P. E. (2008) Rapid Oxime and Hydrazone Ligations with Aromatic Aldehydes for Biomolecular Labeling. *Bioconjugate Chem. 19*, 2543–2548.

(50) Galinato, M. G. I., Whaley, C. M., and Lehnert, N. (2010) Vibrational Analysis of the Model Complex (μ-edt)[Fe(CO) 3] 2and Comparison to Iron-Only Hydrogenase: The Activation Scale of Hydrogenase Model Systems. *Inorganic chemistry 49*, 3201–3215.

(51) Photochemical studies of iron-only hydrogenase model compounds.Mcdonald, J. c., Berg, S.,Peralto, M., Works, C.(2009). *Inorg. Chim. Acta.362*, 2, 318-324

(52) Roy, A., Madden, C., and Ghirlanda, G. (2012) Photo-induced hydrogen production in a helical peptide incorporating a [FeFe] hydrogenase active site mimic. *Chem. Commun. 48*, 9816–9818.

CHAPTER 5

PHOTOINDUCED HYDROGEN PRODUCTION FROM AN ARTIFICIAL HYDROGENASE BASED ON STREPTAVIDIN-BIOTIN TECHNOLOGY

Anindya Roy, Michael Vaughn, Giovanna Ghirlanda*

Department of Chemistry and Biochemistry, Arizona State University, Tempe, Az

Introduction

Nature has come up with extremely efficient ways to catalyze chemical reactions that appears to be otherwise herculean on a bench-top, exploring intricate protein structural features. Very often, enzymes behave as an intelligent reaction vessel, that can actively restrain the stereochemical fluxionality of the active site as well as the reaction accomplice, in such a way that might appear to be entropically grievous (ΔS), but very often turns out to be energetically (ΔG) beneficial. One such example is the [Fe-Fe] hydrogenases that reversibly catalyze proton to hydrogen conversion reaction in microorganisms. The active site of the enzyme consists of a cuboidal [4Fe-4S] cluster connected to a diiron catalytic site ligated by a non-proteinogenic 1,3 azadithiolate unit through a single cysteine side chain (Figure 5.1).[1] The diiron catalytic site is ligated by nonproteinogenic exotic organometallic ligands such as –CO and CN.[2] The –CN remains hydrogen bonded with the protein backbone as well as with side chain to clasp the active site in 'rotated structure' for effective catalysis; this enthalpic structure of the diiron site exposes a vacant site for substrate binding in both oxidized (Fe[II]-Fe[I]) and reduced form (Fe[I]-Fe[I]).[3]

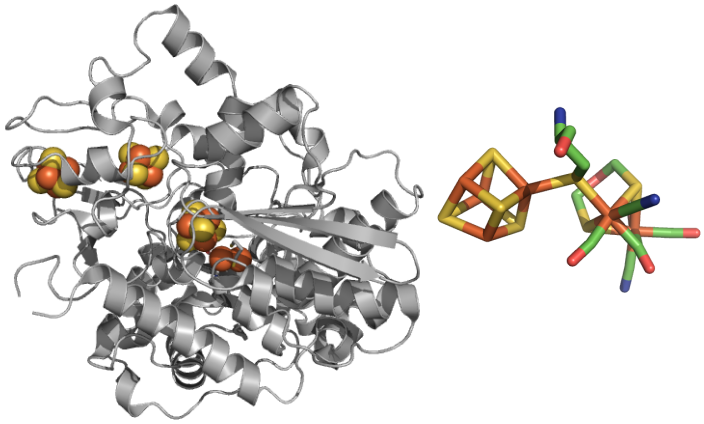

Figure 5.1: Structure of [FeFe] hydrogenase from *Desulfovibrio desulfuricans* (PDB 1HFE) (adapted from ref.). The ferredoxin-like domain and the H-cluster are highlighted on the left and on the right, respectively. All molecular figures were created with PyMOL (DeLano, W.L. (2002). The PyMOL Molecular Graphics System. (http://www.pymol.org))

Since the discovery of hydrogenases and their implication in development of a clean alternative energy, efforts towards development of artificial systems have been reverberated in handful of research endeavors, both structurally and functionally, based on the natural enzyme. One of the main goals of these biomimetic endeavors is to actualize organometallic active sites in proteins or supramolecular cavities and thus imposing the stereochemical confinement as seen in the natural enzyme, otherwise unavailable in organometallic compounds. A very few supramolecular assembly of the biomimetic [Fe-Fe] hydrogenase models have been reported so far, although a myriad of organometallic complexes have been dominant in the literature. Pickett et al reported that incorporation of a well studied diiron complex containing 1,3 propanedithiolate as

bridging ligand, in a Fmoc-Leu based hydrogel dramatically increases its stability towards UV-irradiation.[4] In an elegant study, Darensbourg and colleagues incorporated a simple organometallic complex based on 1,3 propanedithiolatodiironhexacarbonyl into a cyclodextrin.[5] This supramolecular assemby is more efficient towards photocatalytic hydrogen production as compared to the catalyst by itself, indicating advantage of suparmolecular confinement of these kind of catalysts.[6] Further, more recent studies showed that incorporation of such parent diironhexacarbonyl complexes in supramolecular arena, dramatically increases water solubility and robustness towards photocatalytic hydrogen production.[7-9] Taken together, these results point to supramolecular confinement as a promising avenue to ameliorate the catalytic properties of simple organometallic mimics of diiron hydrogenases.

Despite these premises, however, the approaches presented thus far do not lead easily to optimization of the host system. To overcome this limitation, we choose as host, a well characterized, protein based system that can be easily modified by altering its amino acid sequence. Our platform utilizes the streptavidin-biotin system, which has long been exploited in biotechnology and biomaterials applications because of its unique properties. First, the system comprises one of the strongest noncovalent interaction reported in biology, with dissociation constants in the femtomolar range. Second, streptavidin is very stable: it is resistant to denaturation within a wide range of pH, temperature, and organic solvents, including high concentrations of chemical denaturants such as urea and guanidinium hydrochloride.[10] Third, the valeric chain of biotin can be modified as needed without affecting the binding constant significantly.[11-15] Based on this reports, we hypothesized that a biomimetic proton reduction catalyst could be chemically conjugated

to a biotin molecule and sequestered within streptavidin to generate a stable supramolecular species (Figure 5.2). As a proof of concept, we biotinylated a simple diiron hexacarbonyl complex containing a propanedithiolate bridging ligand; the adduct was incubated with commercial streptavidin, and the complex characterized for its ability to generate hydrogen

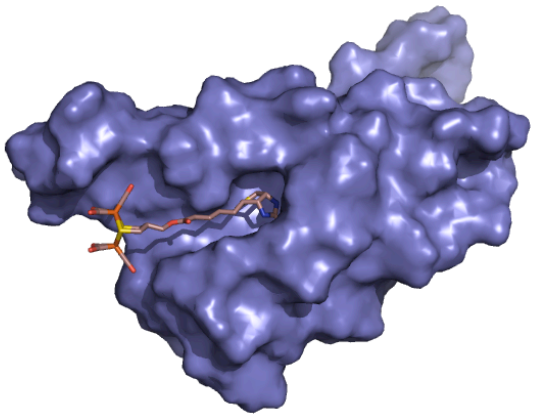

Figure 5.2: Model of streptavidin in complex with a (biotinylated (μ-S-$(CH_2)_3$-S)$[Fe_2(CO)_6]$) complex

Experimental Section:

All the chemicals were purchased from commercial sources of the highest quality available unless otherwise specified. All the reactions were performed under an argon environment. Solvents were dried when necessary following conventional literature protocol. D-Biotin was purchased from alfa aesar, Streptavidin was purchased from prozyme. All other chemicals were purchased from Sigma-Aldrich.

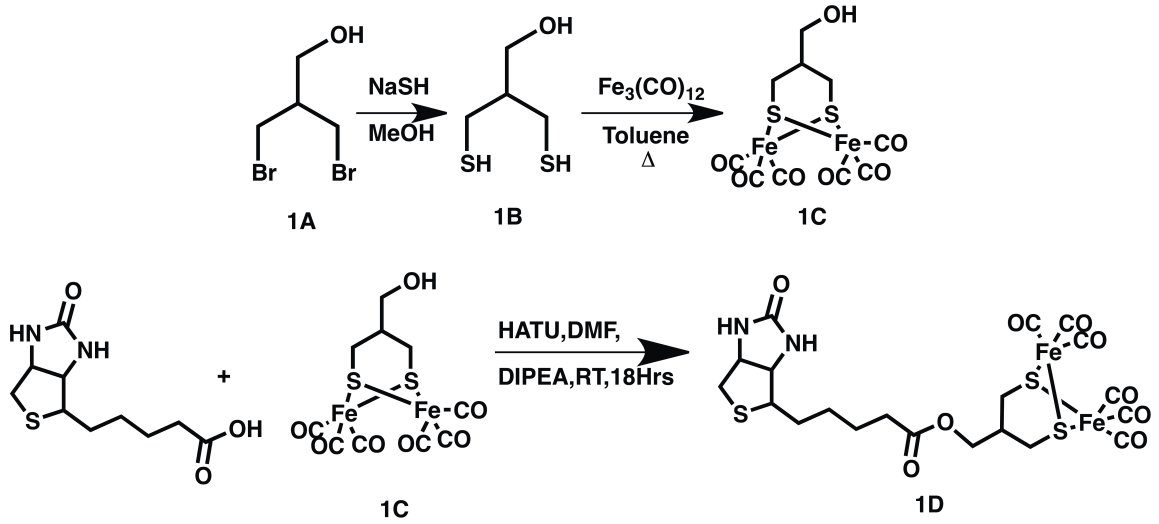

Scheme 5.1: Schematic description of Biotin-HM from a commercially available starting material

Compound 1A was synthesized using reported protocol without any modification.[16]

Synthesis of 1B:

950 mg (4.11mmol) of compound **1A** and 1.5 gm of NaSH, xH_2O (26.78 mmol, dry weight) were dissolved in 21 ml of ice-cold methanol: the solution was stirred in an ice bath for 2 hours and left stirring for overnight at room temperature. Finally, excess NaSH was quenched with equivalent amount of TFA and the resulting mixture was evaporated to dryness under reduced pressure to yield a **1B** as a yellowish liquid. The Yellow liquid was dissolved in dichloromethane and washed with (50x3) times water and dried over anhydrous Na_2SO_4 and evaporated to dryness under reduced pressure. Resulting yellowish liquid was used for the next step without any purification.

Synthesis of 1C:

To the crude dithiolate **1B** obtained from previous step in 20 ml toluene, 3.14 g (6.24 mmol) of $Fe_3(CO)_{12}$ was added under an inert atmosphere and the resulting solution was refluxed for overnight. A change in color from green to red was observed. The solvent was evaporated to dryness under reduced pressure. Resulting deep brown solution was treated with excess ethyl acetate to yield a deep red solution and a deep brown precipitate. The solution was transferred to a centrifuge tube and centrifuged @10000 g for 30 minutes to separate the insoluble iron oxide particles. The deep red solution was carefully decanted off and evaporated under reduced pressure. Resulting red compound (**1C**) was purified on a silica gel column using (2:3) ethyl acetate:hexane as an eluent. Isolated yield=850 mg (49% over two step). ^{1}H NMR (DMSO, δ [ppm]): 1.23 (m, 1H), 1.52 (dd, 2H), 2.73(dd, 2H), 3.18 (t, 2H), 4.74 (t, 1H); ^{13}C NMR (DMSO, δ [ppm]): 25.00, 46.27, 64.53, 208.09

Synthesis of 1D:

Compound **1D** was synthesized by coupling D-Biotin and **1C** in DMF using HATU as coupling agent. 180.56 mg (0.74 mmol) of Biotin and 308 mg (0.74 mmol) of compound **1C** and 281.37 mg (0.74 mmol) of HATU was dissolved in 6 ml of anhydrous DMF and 185.22 mg of dry DIPEA was added to the mixture. Resulting mixture was stirred under an inert atmosphere overnight. Next day, DMF was evaporated under reduced pressure and resulting yellowish red crude oil was purified on a silica gel column using 10% MeOH in DCM. ^{1}H NMR (DMSO, δ [ppm]): 1.19-1.67 (m, 9H), 2.28-2.34 (m, 2H), 2.59 (d, 1H), 2.77 (dd, 2H), 3.09 (m, 1H), 3.62 (m, 2H), 3.81 (d, 1H), 4.11 (m, 1H), 4.30 (t,

1H), 6.35 (s, 1H), 6.41 (s, 1H). ^{13}C NMR (DMSO, δ [ppm]): 24.82, 28.42, 33.61, 33.92, 41.29, 43.20, 55.78, 59.62, 61.48, 63.43, 66.75, 163.14, 172.96, 208.41

Incorporation of 1D in Streptavidin and purification:

Due to very low solubility in water, Biotin-HM was dissolved in DMSO as a stock and used for subsequent reactions and experiments. For the incorporation of Biotin-HM in streptavidin, a stock solution of 2 mg/ml of streptavidin in 100 mM Tris, pH 7.5 was incubated with 2/3-fold excess of Biotin-HM from a stock DMSO solution. After 15 minutes, resulting solution was passed through a PD10-desalting column (GE healthcare) previously equilibrated with the same buffer. Yellow fractions from the column were collected in 1 ml fractions and analyzed by UV-Vis spectroscopy.

Determination of binding property of Biotin-HM with Streptavidin:

Binding stoichiometry for Biotin-HM with streptavidin was analyzed using well-established 4'-hydroxyazobenzene-2-carboxylic acid or HABA displacement assay [17] HABA binds to streptavidin with low micromolar dissociation constant and HABA-SA complex gives rise to absorbance near 500 nm. In a typical HABA displacement assay, 10 μM of Streptavidin in 20 mM phosphate, 150 mM NaCl, pH 7.5 was saturated with 500 uM HABA. After incubation at room temperature for 30 minutes, resulting solution was used for spectrophotometric titration. From a stock DMSO solution of Biotin-HM, incremental amount of ligand were added to the HABA saturated Streptavidin, and decrease of absorbance at 500nm was monitored.

Results and Discussion:

Synthesis and Incorporation of Biotin-HM in Streptavidin:

As mentioned above, we wanted to start with a simplistic model of the [Fe-Fe] hydrogenase mimic. We used 3-bromo-2-(bromomethyl)propan-1-ol (1A, Scheme 5.1), which was obtained from 3-bromo-2-(bromomethyl)propanoic acid by diborane reduction following reported protocol with high yiled.[16] We replaced dibromo unit, with a dithiol unit using NaSH._Refluxing the crude dithiol compound (**1B**) with $Fe_3(CO)_{12}$ in Toluene resulted formation of alcohol functionalized diironhexacarbonyl compound **1C**. Initial coupling trial with **1C** and Biotin under normal coupling conditions, for example EDC coupling at both room and elevated temperature remained unsuccessful. Finally, in presence of a stronger coupling agent. HATU, **1D** was synthesized in high yield and homogeneity. The biotinylated complex was characterized using 1-H/13-C NMR, FTIR and also ESI-MS. Biotin-HM is highly insoluble in water, where as solubility dramatically increases upon addition of streptavidin (SA) indicating binding of the

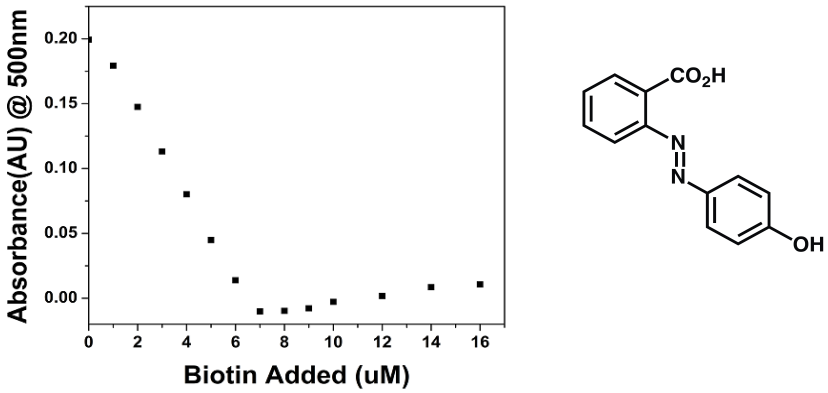

Figure 5.3: HABA displacement assay of streptavidin by Biotin-HM. Absorbance at 500 nm of a HABA saturated was monitored as a function of Biotin-HM concentration (left panel); Chemical Structure of HABA (right panel)

organometallic moiety in protein environment. The binding stoichiometry of Biotin-HM was determined by HABA displacement assay.[17] 2-(4- Hydroxyphenylazo)benzoic acid , or HABA binds to streptavidin in a (1:1) stoichiometric ratio as D-Biotin but with much lower affinityand thus it can be stoichiometrically replaced by biotin in titration experiment. HABA-streptavidin complex absorbs in the visible range, with maximum around 500 nm; and displacement with biotin causes loss of absorbance. In this assay, streptavidin is saturated with HABA using 50 molar excess of HABA and incubated for 30 minutes at room temperature. Biotin-HM was titrated in and absorbance at 500 nm was plotted as a function of biotin-HM concentration. We found that the stoichiometry of binding for biotin-HM to streptavidin is approximately 1:0.7, which is consistent with the activity of the commercial streptavidin. Thus, introduction of the diiron-hexacarbonyl moiety at the valeric chain of biotin does not affect binding stoichiometry.

UV-Vis and FTIR Spectroscopy :

Because of the extremely high affinity of biotin towards streptavidin, streptavidin-incorporated Biotin-HM can be purified away from unbound Biotin-HM using a desalting P10 column. The structural integrity of the diiron complex was verified by UV-vis and by FTIR spectroscopy. Purified Streptavidin: Biotin-HM assembly shows two distinct band in UV-Vis centered around 329 nm and 474 nm which is characteristic of Fe_2S_2 butterfly complexes and consistent with reported literature (Figure 5.4). [18,19] This also proves capture of Biotin-HM in streptavidin matrix. The electronic environment of the diiron

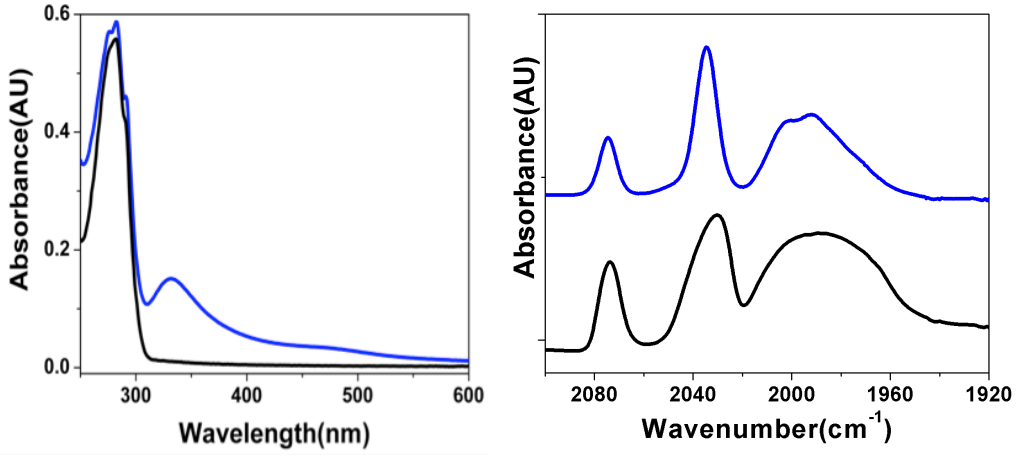

Figure 5.4: UV-Vis Spectra of Streptavidin (black trace) and Biotin-HM in complex with streptavidin after desalting (left panel). FTIR spectra of Biotin-HM in presence (blue trace) and absence (black trace) of streptavidin in the coupled –CO stretching frequency region.

cluster can be probed by FTIR by analyzing the coupled -CO stretching frequencies. Due to low solubility of Biotin-HM in water, a direct comparison of the complex in presence and absence of streptavidin in identical experimental conditions turned out to be more difficult. Instead, we compared a thin films of Biotin-HM from a solution of 20% methanol in water on a FTIR CaF_2 window in presence and absence of streptavidin. FTIR spectra of Biotin-HM show 3 major peaks at 1992, 2030, 2073.5 cm^{-1}, which are assigned to the coupled stretching frequency of –CO, consistent with related organometallic analogues.[18-20] In the presence of two molar excess of SA, all three peaks gets shifted to 1990, 2034, 2074 cm^{-1} implying a change in environment of the –CO which is attributed to the binding of Biotin-HM to SA. Taken together, the spectroscopic information collected support the presence of a structurally intact biotinylated diiron hexacarbonyl center, which is incorporated within the desired streptavidin scaffold. Incorporation

results in confinement within the protein scaffold, and more importantly, results in interaction of the cluster with the surrounding protein matrix.

Photo and Electrocatalytic Hydrogen Production:

Next we investigated how the hydrogen production efficiency of the catalyst is affected in the presence and absence of streptavidin. Catalysts of this type are known to generate hydrogen when reduced, both when irradiated in the presence of a suitable photosensitizer, and when the reducing equivalents are provided electrochemically. First we adopted a well established protocol, in which $Ru(Bpy)_3$ is photo excited by visible light: this excited species then generates the active redox state, Fe(I)Fe(0), from the resting Fe(I)Fe(I) either by oxidative or reductive quenching. Fe(I)Fe(0) center then reduces proton through formation of an intermediate Fe(I)Fe(II)H entity.[9,21-27]

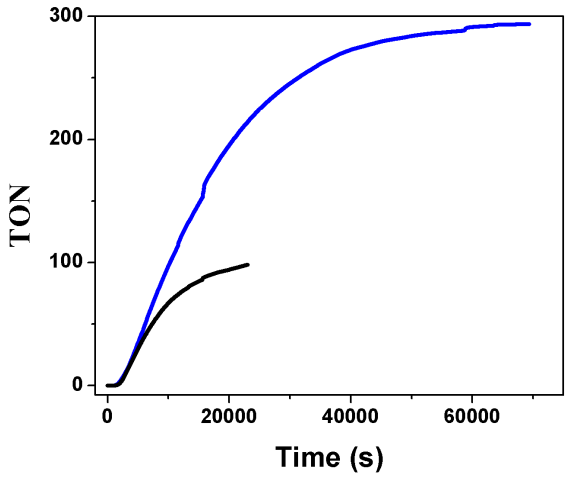

Figure 5.5: Photocatalytic hydrogen production from Biotin-HM in presence (blue trace) and absence (black trace) of streptavidin in 100 mM citrate, pH=4.5 in presence of 100 mM sodium ascorbate as sacrificial electron donor and 150 μM $Ru(bpy)_3$ as photosensitizer.

In this assay, 2.05 nmols Biotin-HM gives rise to 205.76 nmols of hydrogen resulting in a TON of 100; the conditions used were 5.14 μM Biotin-HM in 100 mM citrate buffer, pH 4.5 in presence of 100 mM ascorbate as a sacrificial electron donor and 150 μM of $Ru(Bpy)_3$ as photosensitizer. When Biotin-HM is bound within streptavidin, TON increases by 3 fold along with the lifetime of the catalyst as shown in Figure 5.5. This result supports the use of protein-based hybrid materials to augment the intrinsic catalytic activity of organometallic complexes. In general, simple [Fe-Fe] hydrogenase mimics containing diiron-hexacarbonyl are extremely inefficient as hydrogen production catalysts because of their instability towards long irradiation times: they are degraded to intermediates that are not catalytically viable.[28] We hypothesize that streptavidin insulate the catalyst from unwanted side reactions and degradation, resulting in increased overall stability and lifetime.

We also investigated electrochemical proton reduction property of Biotin-HM in

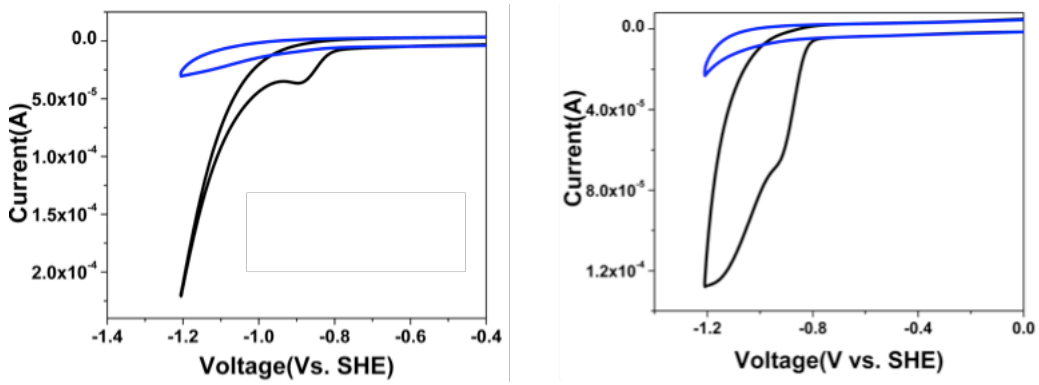

Figure 5.6: Cyclic Voltamogram of Biotin-HM in absence (black line) and presence of Streptavidin (blue line) in solution using 100 mM citrate, 100 mM Sodium Chloride, pH 4.5 (Left Panel). Cyclic Volatamogram of Streptavidin-Biotin-HM complex thin film on the surface of a pyrolytic graphite electrode (black trace, right panel), CV scan for bare

electrode under the same condition is shown in blue trace. CV conditions pyrolytic graphite working electrode, saturated calomel reference electrode, and platinum mesh counter electrode.

presence and absence of streptavidin. In 100 mM Citrate, 100 mM NaCl, pH 4.5, a catalytic current on the reductive scan was observed corresponding to proton reduction as shown in Figure 5.6. It's worth mentioning that without any catalyst, some proton reduction on bare electrode was also observed; however, the amount of hydrogen generated through this process is insignificant when compared to the catalyzed reaction. When streptavidin was added to the solution, magnitude of the catalytic current was diminished in a significant fashion. This phenomenon can be explained considering the insulation of the catalyst from active electrode surface upon binding to the protein. Streptavidin has a PI of 5.0, so we hypothesized that at pH 4.5, positively charged streptavidin can be electrostatically adsorbed on the negatively charged glassy carbon-working electrode. Indeed, when a thin film of the streptavidin-Biotin-HM complex is dried on a glassy carbon electrode surface, it gives rise to a

significant amount of catalytic wave corresponding to proton reduction (Figure 5.6). Considering the ease and robustness of covalent attachment of streptavidin to solid surface, the catalytic enhancement observed opens up the possibility of designing streptavidin-functionalized electrode surfaces for electrocatalytic hydrogen production.

Conclusions and Future Aspect:

Since the first report of streptavidin as a platform for bio-hybrid catalysts [29], there have been a tremendous amount of progress in the field of protein based hybrid organometallic

catalysts. Until now, most of these catalysts are focused on synthetic organic chemistry transformation, more specifically using protein scaffolds as a source for stereo-selection in hydrogenation and sulfoxidation of organic molecules.[17,30-32] Here, we applied the same approach to a reaction- the reduction of protons to hydrogen- that is not stereo-specific. However, we hypothesized that shielding the catatlyst from the aqueous environment would increase its efficiency by preventing unwanted side reactions. Further, the protein scaffold could potentially provide second sphere and long range interactions to augment the intrinsic reactivity of the center. In addition, the mechanism of action of these catalysts is thought to involve a thermodynamically unstable but cataltically active form of the diiron site. The natural hydrogenase utilizes specific interactions to the inorganic ligands to stabilize this enthalpic conformation. In future studies, we aim to exploit an unique advantage of the bio-hybrid systems over other supramolecular mimics of hydrogenases, as protein-based system such as the streptavidin based one, present the unique opportunity to optimize activity through a so-called chemigenetic approach. Both the protein scaffold and the ligand component can be exchanged and optimized independently, by mutating the catalytic center as well as by introducing specific mutations in the protein scaffold. Exploiting the tolerance of biotin-streptavidin binding to modifications of the valeric acid chain, these complexes can be biotinylated and introduced into streptavidin with little loss in binding affinit. Native-like secondary shell interactions can also be introduced with much ease as compared to purely organometallic complexes. For example, its worth mentioning that the bridgehead atom of the biomimetic complex used in this study is a carbon; where as its reported to be a nitrogen atom in the natural enzyme. This bridge-head nitrogen atom is believed to be

involved in proton shuttling during proton reduction.[33] Synthesizing the corresponding N-containing organometallic complex turns out to be much harder, but similar kind of proton shuttling groups, for example histidine residues, can be introduced using site directed mutagenesis in close proximity of the biomimetic active site to rescue the offset of replacing bridgehead nitrogen by carbon. To facilitate photocatalysis, photosensitizers can be introduced to the close proximity of the active site using covalent attachment. Further facilitating the development of applications and its use in devices, streptavidin-based catalysts are unique for their robustness, unparalleled in a biological/proteinogenic environment.

REFERENCES:

(1) Fontecilla-Camps, J. C., Volbeda, A., Cavazza, C., and Nicolet, Y. (2007) Structure/function relationships of [NiFe]- and [FeFe]-hydrogenases. *107*, 4273–4303.

(2) Peters, J., Peters, J., Lanzilotta, W., Lanzilotta, W., Lemon, B., Lemon, B., Seefeldt, L., and Seefeldt, L. (1998) X-ray crystal structure of the Fe-only hydrogenase (Cpl) from Clostridium pasteurianum to 1.8 angstrom resolution. *Science 282*, 1853–1858.

(3) Darensbourg, M. Y., Lyon, E. J., Zhao, X., and Georgakaki, I. P. (2003) The organometallic active site of [Fe]hydrogenase: Models and entatic states. *Proc. Natl. Acad. Sci. USA 100*, 3683–3688.

(4) Frederix, P. W. J. M., Kania, R., Wright, J. A., Lamprou, D. A., Ulijn, R. V., Pickett, C. J., and Hunt, N. T. (2012) Encapsulating [FeFe]-hydrogenase model compounds in peptide hydrogels dramatically modifies stability and photochemistry. *Dalton Trans. 41*, 13112–13119.

(5) Singleton, M. L., Reibenspies, J. H., and Darensbourg, M. Y. (2010) A cyclodextrin host/guest approach to a hydrogenase active site biomimetic cavity. *J. Am. Chem. Soc. 132*, 8870–8871.

(6) Li, X., Wang, M., Zheng, D., Han, K., and Dong, J. (2012) Photocatalytic H 2 production in aqueous solution with host-guest inclusions formed by insertion of an FeFe-hydrogenase mimic and an organic dye into cyclodextrins, *Energy & Environmental Science 5,*8220-8224

(7) Wang, F., Liang, W.-J., Jian, J.-X., Li, C.-B., Chen, B., Tung, C.-H., and Wu, L.-Z. (2013) Exceptional Poly(acrylic acid)-Based Artificial [FeFe]-Hydrogenases for Photocatalytic H 2Production in Water. *Angew. Chem. Int. Ed. 52*, 8134–8138.

(8) Jian, J.-X., Liu, Q., Li, Z.-J., Wang, F., Li, X.-B., Li, C.-B., Bin Liu, Meng, Q.-Y., Bin Chen, Feng, K., Tung, C.-H., and Wu, L.-Z. (2013) Chitosan confinement enhances hydrogenphotogeneration from a mimic of the diironsubsite of [FeFe]-hydrogenase. *Nature Communications 4*, 1–9.

(9) Wang, F., Wang, W.-G., Wang, X.-J., Wang, H.-Y., Tung, C.-H., and Wu, L.-Z. (2011) A Highly Efficient Photocatalytic System for Hydrogen Production by a Robust Hydrogenase Mimic in an Aqueous Solution - Wang - 2011 - Angewandte Chemie International Edition - Wiley Online Library. *Angew. Chem. Int. Ed. 50*, 3193–3197.

(10) GREEN, N. M. (1965) A Spectrophotometric assay for avidin and biotin based on binding of dyes by avidin. *Biochem. J. 94*, 23C–24C.

(11) Lo, K. K.-W., and Hui, W.-K. (2005) Design of Rhenium(I) Polypyridine Biotin Complexes as a New Class of Luminescent Probes for Avidin. *Inorganic chemistry 44*, 1992–2002.

(12) Lo, K. K.-W., and Lee, T. K.-M. (2004) Luminescent Ruthenium(II) Polypyridine Biotin Complexes: Synthesis, Characterization, Photophysical and Electrochemical Properties, and Avidin-Binding Studies. *Inorganic chemistry 43*, 5275–5282.

(13) Lo, K., Chan, J., Lui, L. H., and Chung, C. K. (2004) Novel Luminescent Cyclometalated Iridium(III) Diimine Complexes That Contain a Biotin Moiety - Organometallics (ACS Publications). *Organometallics*.

(14)Lin, C. C., Lin, C. W., and Chan, A. S. C., Catalytic hydrogenation of itaconic acid in a biotinylated Pyrphos–rhodium(I) system in a protein cavity.*Tetrahedron-Assymetry 10,* 1887-1893

(15) Heinisch, T., and Ward, T. R. (2010) Design strategies for the creation of artificial metalloenzymes. *Curr Opin Chem Biol 14*. 184-199.

(16) Hicks, M. R., Rullay, A. K., Pedrido, R., Crout, D. H., and Pinheiro, T. J. T. (2008) Efficient Synthesis of Methanesulphonate-Derived Lipid Chains for Attachment of Proteins to Lipid Membranes. *Synthetic Communications 38*, 3726–3750.

(17) Sauser, J., Zocchi, A., Gilardoni, F., and Ward, T. R. (2004) Artificial Metalloenzymes: (Strept)avidin as Host for Enantioselective Hydrogenation by Achiral Biotinylated Rhodium−Diphosphine Complexes. *Journal of the American Chemical Society 126.*14411-14418.

(18) Jones, A. K., Lichtenstein, B. R., Dutta, A., Gordon, G., and Dutton, P. L. (2007) Synthetic Hydrogenases: Incorporation of an Iron Carbonyl Thiolate into a Designed Peptide. *J. Am. Chem. Soc. 129*, 14844–14845.

(19) Roy, A., Madden, C., and Ghirlanda, G. (2012) Photo-induced hydrogen production in a helical peptide incorporating a [FeFe] hydrogenase active site mimic. *Chem. Commun 48,* 9816-9818.

(20) Sano, Y., Onoda, A., and Hayashi, T. (2011) A hydrogenase model system based on the sequence of cytochrome c: photochemical hydrogen evolution in aqueous media. *Chem. Commun. (Camb.) 47*, 8229–8231.

(21) Na, Y., Wang, M., Pan, J., Zhang, P., Åkermark, B., and Sun, L. (2008) Visible Light-Driven Electron Transfer and Hydrogen Generation Catalyzed by Bioinspired [2Fe2S] Complexes. *Inorganic chemistry 47*, 2805–2810.

(22) Zhang, P., Wang, M., Na, Y., Li, X., Jiang, Y., and Sun, L. (2010) Homogeneous photocatalytic production of hydrogen from water by a bioinspired [Fe2S2] catalyst with high turnover numbers. *Dalton Trans. 39*, 1204–1206.

(23) Streich, D., Streich, D., Astuti, Y., Astuti, Y., Orlandi, M., Orlandi, M., Schwartz, L., Schwartz, L., Lomoth, R., Lomoth, R., Hammarström, L., Hammarström, L., Ott, S., and Ott, S. (2010) High-Turnover Photochemical Hydrogen Production Catalyzed by a

Model Complex of the [FeFe]-Hydrogenase Active Site. *Chem. Eur. J. 16*, 60–63.

(24) Wang, H.-Y., Wang, W.-G., Si, G., Wang, F., Tung, C.-H., and Wu, L.-Z. (2010) Photocatalytic Hydrogen Evolution from Rhenium(I) Complexes to [FeFe] Hydrogenase Mimics in Aqueous SDS Micellar Systems: A Biomimetic Pathway. *Langmuir 26*, 9766–9771.

(25) Li, X., Wang, M., Zhang, S., Pan, J., Na, Y., Liu, J., Åkermark, B., and Sun, L. (2008) Noncovalent Assembly of a Metalloporphyrin and an Iron Hydrogenase Active-Site Model: Photo-Induced Electron Transfer and Hydrogen Generation. *J. Phys. Chem. B 112*, 8198–8202.

(26) Song, L.-C., Wang, L.-X., Tang, M.-Y., Li, C.-G., Song, H.-B., and Hu, Q.-M. (2009) Synthesis, Structure, and Photoinduced Catalysis of [FeFe]-Hydrogenase Active Site Models Covalently Linked to a Porphyrin or Metalloporphyrin Moiety †. *Organometallics 28*, 3834–3841.

(27) Kluwer, A. M., Kapre, R., Hartl, F., Lutz, M., Spek, A. L., Brouwer, A. M., van Leeuwen, P. W. N. M., and Reek, J. N. H. (2009) Self-assembled biomimetic [2Fe2S]-hydrogenase-based photocatalyst for molecular hydrogen evolution. *Proc. Natl. Acad. Sci. USA 106*, 10460–10465.

(28) Wang, M., Chen, L., Li, X., and Sun, L. (2011) Approaches to efficient molecular catalyst systems for photochemical H2 production using [FeFe]-hydrogenase active site mimics. *Dalton Trans. 40*, 12793–12800.

(29) Wilson, M. E., and Whitesides, G. M. (1978) Conversion of a protein to a homogeneous asymmetric hydrogenation catalyst by site-specific modification with a diphosphinerhodium(I) moiety. *J. Am. Chem. Soc. 100*, 306–307.

(30) Creus, M., Pordea, A., Rossel, T., and Sardo, A. (2008) X-Ray Structure and Designed Evolution of an Artificial Transfer Hydrogenase. *Angew. Chem.47,*1400-1404.

(31) Dürrenberger, M., Heinisch, T., Wilson, Y. M., Rossel, T., Nogueira, E., Knörr, L., Mutschler, A., Kersten, K., Zimbron, M. J., Pierron, J., Schirmer, T., and Ward, T. R. (2011) Artificial Transfer Hydrogenases for the Enantioselective Reduction of Cyclic Imines. *Angew. Chem. 123*, 3082–3085.

(32) Artificial Metalloenzyme for Enantioselective Sulfoxidation Based on Vanadyl-Loaded Streptavidin, *Journal of the American Chemical Society 130,* 8085-8088.

(33) Mulder, D. W., Shepard, E. M., Meuser, J. E., Joshi, N., King, P. W., Posewitz, M. C., Broderick, J. B., and Peters, J. W. (2011) Insights into [FeFe]-hydrogenase structure, mechanism, and maturation. *Structure 19*, 1038–1052.

CHAPTER 1 REFERENCES:

(1) Cammack, R., Frey, M., and Robson, R. (2001) Hydrogen As a Fuel: Learning From Nature. Taylor and Francis, London.

(2) Amao, Y. (2011) Solar Fuel Production Based on the Artificial Photosynthesis System. ChemCatChem 3, 458–474.

(3) Gust, D., Moore, T. A., and Moore, A. L. (2012) Realizing artificial photosynthesis. Faraday Discuss. 155, 9–26.

(4) Gust, D., Moore, T. A., and Moore, A. L. (2009) Solar Fuels via Artificial Photosynthesis. Acc. Chem. Res. 42, 1890–1898.

(5) Wydrzynski, T. J., and Hillier, W. (2009) Molecular Solar Fuels. RCS, Cambridge, UK.

(6) Vignais, P. M., Billoud, B., and Meyer, J. (2001) Classification and phylogeny of hydrogenases. FEMS Microbiol. Rev. 25, 455–501.

(7) Vignais, P. M., and Billoud, B. (2007) Occurrence, Classification, and Biological Function of Hydrogenases: An Overview. Chem. Rev. 107, 4206–4272.

(8) Meyer, J. (2007) [FeFe] hydrogenases and their evolution: a genomic perspective. Cell. Mol. Life Sci. 64, 1063–1084.

(9) Shima, S., and Ermler, U. (2011) Structure and Function of [Fe]-Hydrogenase and its Iron–Guanylylpyridinol (FeGP) Cofactor. Eur. J. Inorg. Chem. 2011, 963–972.

(10) Shima, S., and Thauer, R. K. (2007) A third type of hydrogenase catalyzing H2 activation. Chem. Rec. 7, 37–46.

(11) Fontecilla-Camps, J. C., Volbeda, A., Cavazza, C., and Nicolet, Y. (2007) Structure/function relationships of [NiFe]- and [FeFe]-hydrogenases. 107, 4273–4303.

(12) Vincent, K. A., Parkin, A., and Armstrong, F. A. (2007) Investigating and Exploiting the Electrocatalytic Properties of Hydrogenases. Chem. Rev. 107, 4366–4413.

(13) Frey, M. (2002) Hydrogenases: Hydrogen-Activating Enzymes. ChemBioChem 3, 153–160.

(14) de Lacey, A. L., Fernandez, V. M., Rousset, M., and Cammack, R. (2007) Activation and Inactivation of Hydrogenase Function and the Catalytic Cycle: Spectroelectrochemical Studies. Chem. Rev. 107, 4304–4330.

(15) Volbeda, A., Charon, M.-H., Piras, C., Hatchikian, E. C., Frey, M., and Fontecilla-Camps, J. C. (1995) Crystal structure of the nickel-iron hydrogenase from Desulfovibrio

gigas. Nature 373, 580–587.

(16) Peters, J. W., Lanzilotta, W. N., Lemon, B. J., and Seefeldt, L. C. (1998) X-ray Crystal Structure of the Fe-Only Hydrogenase (CpI) from Clostridium pasteurianum to 1.8 Angstrom Resolution. Science 282, 1853–1858.

(17) Nicolet, Y., Piras, C., Legrand, P., Hatchikian, C. E., and Fontecilla-Camps, J. C. (1999) Desulfovibrio desulfuricans iron hydrogenase: the structure shows unusual coordination to an active site Fe binuclear center. Structure 7, 13–23.

(18) Nicolet, Y., de Lacey, A. L., Vernède, X., Fernandez, V. M., Hatchikian, E. C., and Fontecilla-Camps, J. C. (2001) Crystallographic and FTIR Spectroscopic Evidence of Changes in Fe Coordination Upon Reduction of the Active Site of the Fe-Only Hydrogenase from Desulfovibrio desulfuricans. J. Am. Chem. Soc. 123, 1596–1601.

(19) Happe, R. P., Roseboom, W., Pierik, A. J., Albracht, S. P. J., and Bagley, K. A. (1997) Biological activition of hydrogen. Nature 385, 126–126.

(20) Bagley, K. A., Duin, E. C., Roseboom, W., Albracht, S. P. J., and Woodruff, W. H. (1995) Infrared-Detectable Group Senses Changes in Charge Density on the Nickel Center in Hydrogenase from Chromatium vinosum. Biochemistry 34, 5527–5535.

(21) Pierik, A. J., Hulstein, M., Hagen, W. R., and Albracht, S. P. J. (1998) A low-spin iron with CN and CO as intrinsic ligands forms the core of the active site in [Fe]-hydrogenases. Eur J Biochem 258, 572–578.

(22) Hoffmann, P. (2012) Tomorrow's Energy: Hydrogen, Fuel Cells, and Prospects for a Cleaner Planet. MIT Press, Cambridge, MA.

(23) Bingham, A. S., Smith, P. R., and Swartz, J. R. (2012) Evolution of an [FeFe] hydrogenase with decreased oxygen sensitivity. Int. J. Hydrogen Energy 37, 2965–2976.

(24) Stapleton, J. A., and Swartz, J. R. (2010) Development of an In Vitro Compartmentalization Screen for High-Throughput Directed Evolution of [FeFe] Hydrogenases. PLoS ONE 5, 1–8.

(25) Liu, T., DuBois, D. L., and Bullock, R. M. (2013) An iron complex with pendent amines as a molecular electrocatalyst for oxidation of hydrogen. Nat. Chem. 5, 228–233.

(26) Camara, J. M., and Rauchfuss, T. B. (2011) Combining acid-base, redox and substrate binding functionalities to give a complete model for the [FeFe]-hydrogenase. Nat. Chem. 4, 26–30.

(27) Ogo, S., Ichikawa, K., Kishima, T., Matsumoto, T., Nakai, H., Kusaka, K., and Ohhara, T. (2013) A Functional [NiFe]Hydrogenase Mimic That Catalyzes Electron and Hydride Transfer from H2. Science 339, 682–684.

(28) Wilson, A. D., Newell, R. H., McNevin, M. J., Muckerman, J. T., Rakowski DuBois, M., and DuBois, D. L. (2005) Hydrogen Oxidation and Production Using Nickel-Based Molecular Catalysts with Positioned Proton Relays. J. Am. Chem. Soc. 128, 358–366.

(29) Smith, S. E., Yang, J. Y., DuBois, D. L., and Bullock, R. M. (2012) Reversible Electrocatalytic Production and Oxidation of Hydrogen at Low Overpotentials by a Functional Hydrogenase Mimic. Angew. Chem. 124, 3206–3209.

(30) Le Goff, A., Artero, V., Jousselme, B., Tran, P. D., Guillet, N., Métayé, R., Fihri, A., Palacin, S., and Fontecave, M. (2009) From Hydrogenases to Noble Metal–Free Catalytic Nanomaterials for H2 Production and Uptake. Science 326, 1384–1387.

(31) Cammack, R. (1999) Bioinorganic chemistry: Hydrogenase sophistication. Nature 397, 214–215.

(32) Mulder, D. W., Shepard, E. M., Meuser, J. E., Joshi, N., King, P. W., Posewitz, M. C., Broderick, J. B., and Peters, J. W. (2011) Insights into [FeFe]-hydrogenase structure, mechanism, and maturation. Structure 19, 1038–1052.

(33) Peters, J. W., and Broderick, J. B. (2012) Emerging Paradigms for Complex Iron-Sulfur Cofactor Assembly and Insertion. Annu. Rev. Biochem. 81, 429–450.

(34) Böck, A., King, P. W., Blokesch, M., and Posewitz, M. C. (2006) Advances in Microbial Physiology, in Advances in Microbial Physiology (Robert, K. P., Ed.), pp 1–225. Academic Press.

(35) Nicolet, Y., Lemon, B. J., Fontecilla-Camps, J. C., and Peters, J. W. (2000) A novel FeS cluster in Fe-only hydrogenases. Trends Biochem. Sci 25, 138–143.

(36) Lemon, B. J., and Peters, J. W. (1999) Binding of Exogenously Added Carbon Monoxide at the Active Site of the Iron-Only Hydrogenase (CpI) from Clostridium pasteurianum. Biochemistry 38, 12969–12973.

(37) Lespinat, P. A., Berlier, Y., Fauque, G., Czechowski, M., Dimon, B., and Le Gall, J. (1986) The pH dependence of proton-deuterium exchange, hydrogen production and uptake catalyzed by hydrogenases from sulfate-reducing bacteria. Biochimie 68, 55–61.

(38) Darensbourg, M. Y., Lyon, E. J., Zhao, X., and Georgakaki, I. P. (2003) The organometallic active site of [Fe]hydrogenase: Models and entatic states. Proc. Natl. Acad. Sci. USA 100, 3683–3688.

(39) Winkler, M., Esselborn, J., and Happe, T. (2013) Molecular basis of [FeFe]-hydrogenase function: An insight into the complex interplay between protein and catalytic cofactor. Biochim. Biophys. Act - Bioenerg. in press.

(40) Kubas, G. J. (2007) Fundamentals of H2 Binding and Reactivity on Transition Metals Underlying Hydrogenase Function and H2 Production and Storage. Chem. Rev.

107, 4152–4205.

(41) Bruschi, M., Greco, C., Bertini, L., Fantucci, P., Ryde, U., and Gioia, L. D. (2010) Functionally Relevant Interplay between the Fe4S4 Cluster and CN− Ligands in the Active Site of [FeFe]-Hydrogenases. J. Am. Chem. Soc. 132, 4992–4993.

(42) Liu, Z.-P., and Hu, P. (2002) A Density Functional Theory Study on the Active Center of Fe-Only Hydrogenase: Characterization and Electronic Structure of the Redox States. J. Am. Chem. Soc. 124, 5175–5182.

(43) Darensbourg, M. Y., and Bethel, R. D. (2012) Biomimetic chemistry: Merging the old with the new. Nat. Chem. 4, 11–13.

(44) Knorzer, P., Silakov, A., Foster, C. E., Armstrong, F. A., Lubitz, W., and Happe, T. (2012) Importance of the Protein Framework for Catalytic Activity of [FeFe]-Hydrogenases. J. Biol. Chem. 287, 1489–1499.

(45) Pandey, A. S., Harris, T. V., Giles, L. J., Peters, J. W., and Szilagyi, R. K. (2008) Dithiomethylether as a Ligand in the Hydrogenase H-Cluster. J. Am. Chem. Soc. 130, 4533–4540.

(46) Lyon, E. J., Georgakaki, I. P., Reibenspies, J. H., and Darensbourg, M. Y. (1999) Carbon Monoxide and Cyanide Ligands in a Classical Organometallic Complex Model for Fe-Only Hydrogenase. Angew. Chem. Int. Ed. 38, 3178–3180.

(47) Schmidt, M., Contakes, S. M., and Rauchfuss, T. B. (1999) First Generation Analogues of the Binuclear Site in the Fe-Only Hydrogenases: Fe2(μ-SR)2(CO)4(CN)22. J. Am. Chem. Soc. 121, 9736–9737.

(48) Le Cloirec, A., C Davies, S., J Evans, D., L Hughes, D., J Pickett, C., P Best, S., and Borg, S. (1999) A di-iron dithiolate possessing structural elements of the carbonyl/cyanide sub-site of the H-centre of Fe-only hydrogenase. Chem. Commun. 0, 2285–2286.

(49) Erdem, Ö. F., Schwartz, L., Stein, M., Silakov, A., Kaur-Ghumaan, S., Huang, P., Ott, S., Reijerse, E. J., and Lubitz, W. (2011) A Model of the [FeFe] Hydrogenase Active Site with a Biologically Relevant Azadithiolate Bridge: A Spectroscopic and Theoretical Investigation. Angew. Chem. Int. Ed. 50, 1439–1443.

(50) Singleton, M. L., Crouthers, D. J., Duttweiler, R. P. 3., Reibenspies, J. H., and Darensbourg, M. Y. (2011) Sulfonated diiron complexes as water-soluble models of the [Fe-Fe]-hydrogenase enzyme active site. Inorganic chemistry 50, 5015–5026.

(51) Barton, B. E., Olsen, M. T., and Rauchfuss, T. B. (2010) Artificial hydrogenases. Curr. Opin. Biotechnol. 21, 292–297.

(52) Tard, C., and Pickett, C. J. (2009) Structural and Functional Analogues of the Active

Sites of the [Fe]-, [NiFe]-, and [FeFe]-Hydrogenases. Chem. Rev. 109, 2245–2274.

(53) Ezzaher, S., Gogoll, A., Bruhn, C., and Ott, S. (2010) Directing protonation in [FeFe] hydrogenase active site models by modifications in their second coordination sphere. Chem. Commun. 46, 5775–5777.

(54) Surawatanawong, P., Tye, J. W., Darensbourg, M. Y., and Hall, M. B. (2010) Mechanism of electrocatalytic hydrogen production by a di-iron model of iron-iron hydrogenase: a density functional theory study of proton dissociation constants and electrode reduction potentials. Dalton Trans. 39, 3093–3104.

(55) Wang, F., Wang, W.-G., Wang, X.-J., Wang, H.-Y., Tung, C.-H., and Wu, L.-Z. (2011) A Highly Efficient Photocatalytic System for Hydrogen Production by a Robust Hydrogenase Mimic in an Aqueous Solution - Wang - 2011 - Angewandte Chemie International Edition - Wiley Online Library. Angew. Chem. Int. Ed. 50, 3193–3197.

(56) Wang, W.-G., Wang, F., Wang, H.-Y., Tung, C.-H., and Wu, L.-Z. (2012) Electron transfer and hydrogen generation from a molecular dyad: platinum(II) alkynyl complex anchored to [FeFe] hydrogenase subsite mimic. Dalton Trans. 41, 2420–2426.

(57) Singleton, M. L., Reibenspies, J. H., and Darensbourg, M. Y. (2010) A cyclodextrin host/guest approach to a hydrogenase active site biomimetic cavity. J. Am. Chem. Soc. 132, 8870–8871.

(58) Hsieh, C.-H., Erdem, Ö. F., Harman, S. D., Singleton, M. L., Reijerse, E., Lubitz, W., Popescu, C. V., Reibenspies, J. H., Brothers, S. M., Hall, M. B., and Darensbourg, M. Y. (2012) Structural and Spectroscopic Features of Mixed Valent FeIIFeI Complexes and Factors Related to the Rotated Configuration of Diiron Hydrogenase. J. Am. Chem. Soc. 134, 13089–13102.

(59) DeGrado, W. F., Summa, C. M., Pavone, V., Nastri, F., and Lombardi, A. (1999) De novo design and structural characterization of metalloproteins. Annu. Rev. Biochem. 68, 779–819.

(60) He, C., Wang, M., Zhang, X., Wang, Z., Chen, C., Liu, J., Åkermark, B., and Sun, L. (2004) An Unusual Cyclization in a Bis(cysteinyl-S) Diiron Complex Related to the Active Site of Fe-Only Hydrogenases. Angew. Chem. 116, 3655–3658.

(61) de Hatten, X., Bothe, E., Merz, K., Huc, I., and Metzler-Nolte, N. (2008) A Ferrocene–Peptide Conjugate as a Hydrogenase Model System. Eur. J. Inorg. Chem. 2008, 4530–4537.

(62) de Hatten, X., Cournia, Z., Huc, I., Smith, J. C., and Metzler-Nolte, N. (2007) Force-Field Development and Molecular Dynamics Simulations of Ferrocene–Peptide Conjugates as a Scaffold for Hydrogenase Mimics. Chem. Eur. J. 13, 8139–8152.

(63) de Hatten, X., Weyhermüller, T., and Metzler-Nolte, N. (2004) Ferrocenoyl peptides

with sulfur-containing side chains: synthesis, solid state and solution structures. J. Organomet. Chem. 689, 4856–4867.

(64) Jones, A. K., Lichtenstein, B. R., Dutta, A., Gordon, G., and Dutton, P. L. (2007) Synthetic Hydrogenases: Incorporation of an Iron Carbonyl Thiolate into a Designed Peptide. J. Am. Chem. Soc. 129, 14844–14845.

(65) Sano, Y., Onoda, A., and Hayashi, T. (2011) A hydrogenase model system based on the sequence of cytochrome c: photochemical hydrogen evolution in aqueous media. Chem. Commun. (Camb.) 47, 8229–8231.

(66) Sano, Y., Onoda, A., and Hayashi, T. (2011) Photocatalytic hydrogen evolution by a diiron hydrogenase model based on a peptide fragment of cytochrome c556 with an attached diiron carbonyl cluster and an attached ruthenium photosensitizer. J. Inorg. Biochem. 108, 159–162.

(67) Apfel, U.-P., Volkers, P., Tard, C., Kowol, C. R., Rauchfuss, T. B., Pickett, C. J., Halpin, Y., Kloss, F., Kuebel, J., Goerls, H., Vos, J. G., Keppler, B. K., Morera, E., Lucente, G., and Weigand, W. (2007) Extending the motif of the [FeFe]-hydrogenase active site models: Protonation of Fe-2(NR)(2)(CO)(6-x)L-x species. J. Inorg. Biochem. 101, 1748–1751.

(68) Roy, S., Shinde, S., Hamilton, G. A., Hartnett, H. E., and Jones, A. K. (2011) Artificial [FeFe]-Hydrogenase: On Resin Modification of an Amino Acid to Anchor a Hexacarbonyldiiron Cluster in a Peptide Framework. Eur. J. Inorg. Chem. (Darensbourg, M. Y., and Weigand, W., Eds.) 2011, 1050–1055.

(69) Helm, M. L., Stewart, M. P., Bullock, R. M., DuBois, M. R., and DuBois, D. L. (2011) A Synthetic Nickel Electrocatalyst with a Turnover Frequency Above 100,000 s-1 for H2 Production. Science 333, 863–866.

(70) Jain, A., Lense, S., Linehan, J. C., Raugei, S., Cho, H., DuBois, D. L., and Shaw, W. J. (2011) Incorporating peptides in the outer-coordination sphere of bioinspired electrocatalysts for hydrogen production. Inorganic chemistry 50, 4073–4085.

(71) O'Hagan, M., Ho, M. H., Yang, J. Y., Appel, A. M., Rakowski DuBois, M., Raugei, S., Shaw, W. J., DuBois, D. L., and Bullock, R. M. (2012) Proton delivery and removal in [Ni(P(R)2N(R')2)2]2+ hydrogen production and oxidation catalysts. J. Am. Chem. Soc. 134, 19409–19424.

(72) O'Hagan, M., Shaw, W. J., Raugei, S., Chen, S., Yang, J. Y., Kilgore, U. J., DuBois, D. L., and Bullock, R. M. (2011) Moving protons with pendant amines: proton mobility in a nickel catalyst for oxidation of hydrogen. J. Am. Chem. Soc. 133, 14301–14312.

(73) Pool, D. H., Stewart, M. P., O'Hagan, M., Shaw, W. J., Roberts, J. A., Bullock, R. M., and DuBois, D. L. (2012) Acidic ionic liquid/water solution as both medium and proton source for electrocatalytic H2 evolution by [Ni(P2N2)2]2+ complexes. Proc. Natl.

Acad. Sci. USA 109, 15634–15639.

(74) Shaw, W. J., Helm, M. L., and DuBois, D. L. (2013) A modular, energy-based approach to the development of nickel containing molecular electrocatalysts for hydrogen production and oxidation. Biochim. Biophys. Acta.1827, 1123-1139.

(75) Jacques, P.-A., Artero, V., Pecaut, J., and Fontecave, M. (2009) Cobalt and nickel diimine-dioxime complexes as molecular electrocatalysts for hydrogen evolution with low overvoltages. Proc. Natl. Acad. Sci. USA 106, 20627–20632.

(76) Zhang, P., Jacques, P.-A., Chavarot-Kerlidou, M., Wang, M., Sun, L., Fontecave, M., and Artero, V. (2012) Phosphine Coordination to a Cobalt Diimine–Dioxime Catalyst Increases Stability during Light-Driven H2 Production. Inorganic chemistry 51, 2115–2120.

(77) Fourmond, V., Canaguier, S., Golly, B., Field, M. J., Fontecave, M., and Artero, V. (2011) A nickel-manganese catalyst as a biomimic of the active site of NiFe hydrogenases: a combined electrocatalytical and DFT mechanistic study. Energy Environ. Sci. 4, 2417–2427.

(78) Canaguier, S., Fourmond, V., Perotto, C. U., Fize, J., Pecaut, J., Fontecave, M., Field, M. J., and Artero, V. (2013) Catalytic hydrogen production by a Ni-Ru mimic of NiFe hydrogenases involves a proton-coupled electron transfer step. Chem. Commun. 49, 5004–5006.

(79) McCormick, T. M., Han, Z., Weinberg, D. J., Brennessel, W. W., Holland, P. L., and Eisenberg, R. (2011) Impact of Ligand Exchange in Hydrogen Production from Cobaloxime-Containing Photocatalytic Systems. Inorganic chemistry 50, 10660–10666.

(80) McNamara, W. R., Han, Z., Yin, C. J., Brennessel, W. W., Holland, P. L., and Eisenberg, R. (2012) Cobalt-dithiolene complexes for the photocatalytic and electrocatalytic reduction of protons in aqueous solutions. Proc. Natl. Acad. Sci. USA 109, 15594–15599.

(81) McNamara, W. R., Han, Z., Alperin, P. J., Brennessel, W. W., Holland, P. L., and Eisenberg, R. (2011) A Cobalt–Dithiolene Complex for the Photocatalytic and Electrocatalytic Reduction of Protons. J. Am. Chem. Soc. 133, 15368–15371.

(82) Du, P., Schneider, J., Luo, G., Brennessel, W. W., and Eisenberg, R. (2009) Visible light-driven hydrogen production from aqueous protons catalyzed by molecular cobaloxime catalysts. Inorganic chemistry 48, 4952–4962.

(83) Eckenhoff, W. T., McNamara, W. R., Du, P., and Eisenberg, R. (2013) Cobalt complexes as artificial hydrogenases for the reductive side of water splitting. Biochim. Biophys. Act - Bioenerg. 1827, 958–973.

(84) Shaw, W. J. (2012) The Outer-Coordination Sphere: Incorporating Amino Acids and

Peptides as Ligands for Homogeneous Catalysts to Mimic Enzyme Function. Cat. Rev. - Sci. Eng. 54, 489–550.

(85) Reback, M. L., Ginovska-Pangovska, B., Ho, M.-H., Jain, A., Squier, T. C., Raugei, S., Roberts, J. A. S., and Shaw, W. J. (2013) The Role of a Dipeptide Outer-Coordination Sphere on H2-Production Catalysts: Influence on Catalytic Rates and Electron Transfer. Chem. Eur. J. 19, 1928–1941.

(86) Jain, A., Reback, M. L., Lindstrom, M. L., Thogerson, C. E., Helm, M. L., Appel, A. M., and Shaw, W. J. (2012) Investigating the Role of the Outer-Coordination Sphere in [Ni(PPh2NPh-R2)2]2+ Hydrogenase Mimics. Inorganic chemistry 51, 6592–6602.

(87) Fontecave, M. (2006) Iron-sulfur clusters: ever-expanding roles. Nat. Chem. Biol. 2, 171–174.

(88) Beinert, H. (1997) Iron-Sulfur clusters: Nature's modular, multipurpose structures. Science 277, 653–659.

(89) Klausner, R. D., and Rouault, T. A. (1993) A double life: cytosolic aconitase as a regulatory RNA binding protein. Molecular biology of the cell 4, 1–5.

(90) Koay, M. S., Antonkine, M. L., Gartner, W., and Lubitz, W. (2008) Modelling low-potential [Fe4S4] clusters in proteins. Chem. Biodivers. 5, 1571–1587.

(91) Brereton, P. S., Verhagen, M. F., Zhou, Z. H., and Adams, M. W. (1998) Effect of iron-sulfur cluster environment in modulating the thermodynamic properties and biological function of ferredoxin from Pyrococcus furiosus. Biochemistry 37, 7351–7362.

(92) Hoppe, A., Pandelia, M. E., Gartner, W., and Lubitz, W. (2011) [Fe(4)S(4)]- and [Fe(3)S(4)]-cluster formation in synthetic peptides. Biochim. Biophys. Acta 1807, 1414–1422.

(93) Klingen, A. R., and Ullmann, G. M. (2004) Negatively charged residues and hydrogen bonds tune the ligand histidine pKa values of Rieske iron-sulfur proteins. Biochemistry 43, 12383–12389.

(94) Beck, B. W., Xie, Q., and Ichiye, T. (2001) Sequence determination of reduction potentials by cysteinyl hydrogen bonds and peptide pipoles in [4Fe-4S] ferredoxins. Biophysical journal 81, 601–613.

(95) Kolling, D. J., Brunzelle, J. S., Lhee, S., Crofts, A. R., and Nair, S. K. (2007) Atomic resolution structures of rieske iron-sulfur protein: role of hydrogen bonds in tuning the redox potential of iron-sulfur clusters. Structure 15, 29–38.

(96) Backes, G., Mino, Y., Loehr, T., Meyer, T., Cusanovich, M. A., Sweeney, W. V., Adman, E. T., and Sanders-Loehr, J. (1991) The enviornment of Fe4S4 clusters in ferredoxins and high-potential iron proteins. New information from x-ray crystallography

and resoance raman spectroscopy. J. Am. Chem. Soc. 113, 2055–2064.

(97) Coldren, C. D., Hellinga, H. W., and Caradonna, J. P. (1997) The rational design and construction of a cuboidal iron–sulfur protein. Proc. Natl. Acad. Sci. USA 94, 6635–6640.

(98) Mulholland, S. E., Gibney, B. R., Rabanal, F., and Dutton, P. L. (1998) Characterization of the fundamental protein ligand requirements of [4Fe-4S](2+/+) clusters with sixteen amino acid maquettes. J. Am. Chem. Soc. 120, 10296–10302.

(99) Mulholland, S. E., Gibney, B. R., Rabanal, F., and Dutton, P. L. (1999) Determination of nonligand amino acids critical to [4Fe-4S]2+/+ assembly in ferredoxin maquettes. Biochemistry 38, 10442–10448.

(100) Gibney, B. R., Mulholland, S. E., Rabanal, F., and Dutton, P. L. (1996) Ferredoxin and ferredoxin-heme maquettes. Proceedings of the National Academy of Sciences of the United States of America 93, 15041–15046.

(101) Laplaza, C. E., and Holm, R. H. (2001) Helix-loop-helix peptides as scaffolds for the construction of bridged metal assemblies in proteins: the spectroscopic A-cluster structure in carbon monoxide dehydrogenase. J. Am. Chem. Soc. 123, 10255–10264.

(102) Scott, M. P., and Biggins, J. (1997) Introduction of a [4Fe-4S (S-cys)4]+1,+2 iron-sulfur center into a four-alpha helix protein using design parameters from the domain of the Fx cluster in the Photosystem I reaction center. Protein Sci. 6, 340–346.

(103) Antonkine, M. L., Breitenstein, C., Epel, B., Bill, E., Gärtner, W., and Lubitz, W. (2008) De novo Peptides Modeling the Binding Sites of [4Fe-4S] Clusters in Photosystem I. Photosynthesis. Energy from the Sun; 14th International Congress on Photosynthesis 1257–1260.

(104) Grzyb, J., Xu, F., Nanda, V., Luczkowska, R., Reijerse, E., Lubitz, W., and Noy, D. (2012) Empirical and computational design of iron-sulfur cluster proteins. Biochim. Biophys. Acta 1817, 1256–1262.

(105) Grzyb, J., Xu, F., Weiner, L., Reijerse, E. J., Lubitz, W., Nanda, V., and Noy, D. (2010) De novo design of a non-natural fold for an iron-sulfur protein: alpha-helical coiled-coil with a four-iron four-sulfur cluster binding site in its central core. Biochim. Biophys. Acta 1797, 406–413.

(106) Koga, N., Tatsumi-Koga, R., Liu, G., Xiao, R., Acton, T. B., Montelione, G. T., and Baker, D. (2012) Principles for designing ideal protein structures. Nature 491, 222–227.

(107) Guntas, G., Purbeck, C., and Kuhlman, B. (2010) Engineering a protein–protein interface using a computationally designed library. Proc. Natl. Acad. Sci. USA.

(108) Samish, I., MacDermaid, C. M., Perez-Aguilar, J. M., and Saven, J. G. (2011) Theoretical and Computational Protein Design. Annu. Rev. Phys. Chem. 62, 129–149.

(109) Nanda, V., and Koder, R. L. (2010) Designing artificial enzymes by intuition and computation. Nat. Chem. 2, 15–24.

(110) Suárez, M., and Jaramillo, A. (2009) Challenges in the computational design of proteins. J. R. Soc. Interface.

(111) Peacock, A. F. A., Iranzo, O., and Pecoraro, V. L. (2009) Harnessing natures ability to control metal ion coordination geometry using de novo designed peptides. Dalton Trans. 0, 2271–2280.

(112) Ghosh, D., and Pecoraro, V. L. (2005) Probing metal–protein interactions using a de novo design approach. Curr Opin Chem Biol 9, 97–103.

(113) Senes, A. (2011) Computational design of membrane proteins. Curr. Opin. Struct. Biol. 21, 460–466.

(114) Ghirlanda, G. (2009) Design of membrane proteins: toward functional systems. Curr Opin Chem Biol 13, 643–651.

(115) Shinde, S., Cordova, J., Woodrum, B., and Ghirlanda, G. (2012) Modulation of function in a minimalist heme-binding membrane protein. J Biol Inorg Chem 17, 557–564.

(116) Yin, H., Slusky, J. S., Berger, B. W., Walters, R. S., Vilaire, G., Litvinov, R. I., Lear, J. D., Caputo, G. A., Bennett, J. S., and DeGrado, W. F. (2007) Computational Design of Peptides That Target Transmembrane Helices. Science 315, 1817–1822.

(117) Koder, R. L., Anderson, J. L. R., Solomon, L. A., Reddy, K. S., Moser, C. C., and Dutton, P. L. (2009) Design and engineering of an O2 transport protein. Nature 458, 305–309.

(118) Reig, A. J., Pires, M. M., Snyder, R. A., Wu, Y., Jo, H., Kulp, D. W., Butch, S. E., Calhoun, J. R., Szyperski, T. G., Solomon, E. I., and DeGrado, W. F. (2012) Alteration of the oxygen-dependent reactivity of de novo Due Ferri proteins. Nat. Chem. 4, 900–906.

(119) Wilcoxen, K. M., Leman, L. J., Weinberger, D. A., Huang, Z.-Z., and Ghadiri, M. R. (2007) Biomimetic Catalysis of Intermodular Aminoacyl Transfer. J. Am. Chem. Soc. 129, 748–749.

(120) Khare, S. D., Kipnis, Y., Greisen, P. J., Takeuchi, R., Ashani, Y., Goldsmith, M., Song, Y., Gallaher, J. L., Silman, I., Leader, H., Sussman, J. L., Stoddard, B. L., Tawfik, D. S., and Baker, D. (2012) Computational redesign of a mononuclear zinc metalloenzyme for organophosphate hydrolysis. Nat. Chem. Biol. 8, 294–300.

(121) Der, B. S., Edwards, D. R., and Kuhlman, B. (2012) Catalysis by a De Novo Zinc-Mediated Protein Interface: Implications for Natural Enzyme Evolution and Rational Enzyme Engineering. Biochemistry 51, 3933–3940.

(122) Zastrow, M. L., PeacockAnna, F. A., Stuckey, J. A., and Pecoraro, V. L. (2012) Hydrolytic catalysis and structural stabilization in a designed metalloprotein. Nat. Chem. 4, 118–123.

(123) Faiella, M., Andreozzi, C., de Rosales, R. T. M., Pavone, V., Maglio, O., Nastri, F., DeGrado, W. F., and Lombardi, A. (2009) An artificial di-iron oxo-protein with phenol oxidase activity. Nat. Chem. Biol. 5, 882–884.

(124) Faiella, M., Maglio, O., Nastri, F., Lombardi, A., Lista, L., Hagen, W. R., and Pavone, V. (2012) Inside Cover: De Novo Design, Synthesis and Characterisation of MP3, A New Catalytic Four-Helix Bundle Hemeprotein (Chem. Eur. J. 50/2012). Chem. Eur. J. 18, 15890–15890.

(125) Lichtenstein, B. R., Farid, T. A., Kodali, G., Solomon, L. A., Anderson, J. L., Sheehan, M. M., Ennist, N. M., Fry, B. A., Chobot, S. E., Bialas, C., Mancini, J. A., Armstrong, C. T., Zhao, Z., Esipova, T. V., Snell, D., Vinogradov, S. A., Discher, B. M., Moser, C. C., and Dutton, P. L. (2012) Engineering oxidoreductases: maquette proteins designed from scratch. Biochem. Soc. Trans. 40, 561–566.

CHAPTER 2 REFERENCES:

(1) Woolfson, D. N., Bartlett, G. J., Bruning, M., and Thomson, A. R. (2012) New currency for old rope: from coiled-coil assemblies to α-helical barrels. *Curr. Opin. Struct. Biol.*22, 432-441.

(2) Lill, R. (2009) Function and biogenesis of iron-sulphur proteins. *Nature 460*, 831–838.

(3) Crick, F. H. C. (1953) The packing of α-helices: simple coiled-coils. *Acta crystallographica 6*, 689–697.

(4) Beinert, H. (1997) Iron-Sulfur clusters: Nature's modular, multipurpose structures. *Science 277*, 653–659.

(5) Grzyb, J., Xu, F., Weiner, L., Reijerse, E. J., Lubitz, W., Nanda, V., and Noy, D. (2010) De novo design of a non-natural fold for an iron-sulfur protein: alpha-helical coiled-coil with a four-iron four-sulfur cluster binding site in its central core. *Biochim. Biophys. Acta 1797*, 406–413.

(6) Delano, W. L. (2005) MacPymol: a PyMol-based Molecular Graphics Application for MacOS X. Delano Scientific, LLC, South San Francisco, CA, USA.

(7) Meyer, J. (2008) Iron-sulfur protein folds, iron-sulfur chemistry, and evolution. *J Biol*

Inorg Chem 13, 157–170.

(8) Eck, R. V., and Dayhoff, M. O. (1966) Evolution of the structure of ferredoxin based on living relics of primitive amino Acid sequences. *Science 152*, 363–366.

(9) Laurie, A. T. R., and Jackson, R. M. (2005) Q-SiteFinder: an energy-based method for the prediction of protein-ligand binding sites. *Bioinformatics (Oxford, England) 21*, 1908–1916.

(10) Hinchliffe, P., and Sazanov, L. A. (2005) Organization of iron-sulfur clusters in respiratory complex I. *Science 309*, 771–774.

(11) Sazanov, L. A., and Hinchliffe, P. (2006) Structure of the hydrophilic domain of respiratory complex I from Thermus thermophilus. *Science 311*, 1430–1436.

(12) Jordan, P., Fromme, P., Witt, H. T., Klukas, O., Saenger, W., and Krauss, N. (2001) Three-dimensional structure of cyanobacterial photosystem I at 2.5 A resolution. *Nature 411*, 909–917.

(13) Peters, J., Peters, J., Lanzilotta, W., Lanzilotta, W., Lemon, B., Lemon, B., Seefeldt, L., and Seefeldt, L. (1998) X-ray crystal structure of the Fe-only hydrogenase (Cpl) from Clostridium pasteurianum to 1.8 angstrom resolution. *Science 282*, 1853–1858.

(14) Fontecilla-Camps, J. C., Volbeda, A., Cavazza, C., and Nicolet, Y. (2007) Structure/function relationships of [NiFe]- and [FeFe]-hydrogenases. *107*, 4273–4303.

(15) Antonkine, M. L., Maes, E. M., Czernuszewicz, R. S., Breitenstein, C., Bill, E., Falzone, C. J., Balasubramanian, R., Lubner, C., Bryant, D. A., and Golbeck, J. H. (2007) Chemical rescue of a site-modified ligand to a [4Fe-4S] cluster in PsaC, a bacterial-like dicluster ferredoxin bound to Photosystem I. *Biochim. Biophys. Acta 1767*, 712–724.

(16) Astashkin, A. V., Enemark, J. H., and Raitsimring, A. (2006) 26.5–40 GHz Ka-band pulsed EPR spectrometer. *Concepts in Magnetic Resonance Part B: Magnetic Resonance Engineering 29B*, 125–136.

(17) Krishna, S. S., Sadreyev, R. I., and Grishin, N. V. (2006) A tale of two ferredoxins: sequence similarity and structural differences. *BMC Struct. Biol. 6*, 8.

(18) Hoppe, A., Pandelia, M. E., Gartner, W., and Lubitz, W. (2011) [Fe(4)S(4)]- and [Fe(3)S(4)]-cluster formation in synthetic peptides. *Biochim. Biophys. Acta 1807*, 1414–1422.

(19) Antonkine, M. L., and Golbeck, J. H. (2006) Abstract - SpringerLink. *Photosystem I*.

(20) Carter, P. (1971) Spectrophotometric determination of serum iron at the submicrogram level with a new reagent (ferrozine). *Anal Biochem 40*, 450–458.

(21) Mulder, D. W., Shepard, E. M., Meuser, J. E., Joshi, N., King, P. W., Posewitz, M. C., Broderick, J. B., and Peters, J. W. (2011) Insights into [FeFe]-hydrogenase structure, mechanism, and maturation. *Structure 19*, 1038–1052.

(22) Nicolet, Y., Piras, C., Legrand, P., Hatchikian, C. E., and Fontecilla-Camps, J. C. (1999) Desulfovibrio desulfuricans iron hydrogenase: the structure shows unusual coordination to an active site Fe binuclear center. *Structure 7*, 13–23.

(23) Dubini, A., Mus, F., Seibert, M., Grossman, A. R., and Posewitz, M. C. (2009) Flexibility in anaerobic metabolism as revealed in a mutant of Chlamydomonas reinhardtii lacking hydrogenase activity. *J. Biol. Chem. 284*, 7201–7213.

(24) Scott, M. P., and Biggins, J. (1997) Introduction of a [4Fe-4S (S-cys)4]+1,+2 iron-sulfur center into a four-alpha helix protein using design parameters from the domain of the Fx cluster in the Photosystem I reaction center. *Protein Sci. 6*, 340–346.

(25) Antonkine, M. L., Koay, M. S., Epel, B., Breitenstein, C., Gopta, O., Gärtner, W., Bill, E., and Lubitz, W. (2009) Synthesis and characterization of de novo designed peptides modelling the binding sites of [4Fe-4S] clusters in photosystem I. *Biochim. Biophys. Acta 1787*, 995–1008.

(26) Kennedy, M. L., and Gibney, B. R. (2002) Proton coupling to [4Fe-4S](2+/+) and [4Fe-4Se](2+/+) oxidation and reduction in a designed protein. *J. Am. Chem. Soc. 124*, 6826–6827.

(27) Coldren, C. D., Hellinga, H. W., and Caradonna, J. P. (1997) The rational design and construction of a cuboidal iron–sulfur protein. *Proc. Natl. Acad. Sci. USA 94*, 6635–6640.

(28) Grzyb, J., Xu, F., Nanda, V., Luczkowska, R., Reijerse, E., Lubitz, W., and Noy, D. (2012) Empirical and computational design of iron-sulfur cluster proteins. *Biochim. Biophys. Acta 1817*, 1256–1262.

(29) Han, G. W., Yang, X. L., McMullan, D., Chong, Y. E., Krishna, S. S., Rife, C. L., Weekes, D., Brittain, S. M., Abdubek, P., Ambing, E., Astakhova, T., Axelrod, H. L., Carlton, D., Caruthers, J., Chiu, H. J., Clayton, T., Duan, L., Feuerhelm, J., Grant, J. C., Grzechnik, S. K., Jaroszewski, L., Jin, K. K., Klock, H. E., Knuth, M. W., Kumar, A., Marciano, D., Miller, M. D., Morse, A. T., Nigoghossian, E., Okach, L., Paulsen, J., Reyes, R., van den Bedem, H., White, A., Wolf, G., Xu, Q., Hodgson, K. O., Wooley, J., Deacon, A. M., Godzik, A., Lesley, S. A., Elsliger, M. A., Schimmel, P., and Wilson, I. A. (2010) Structure of a tryptophanyl-tRNA synthetase containing an iron-sulfur cluster. *Acta crystallographica. Section F, Structural biology and crystallization communications 66*, 1326–1334.

(30) Laplaza, C. E., and Holm, R. H. (2001) Helix-loop-helix peptides as scaffolds for the construction of bridged metal assemblies in proteins: the spectroscopic A-cluster structure in carbon monoxide dehydrogenase. *J. Am. Chem. Soc. 123*, 10255–10264.

(31) Gibney, B. R., Mulholland, S. E., Rabanal, F., and Dutton, P. L. (1996) Ferredoxin and ferredoxin-heme maquettes. *Proceedings of the National Academy of Sciences of the United States of America 93*, 15041–15046.

(32) Roy, A., Madden, C., and Ghirlanda, G. (2012) Photo-induced hydrogen production in a helical peptide incorporating a [FeFe] hydrogenase active site mimic. *Chem. Commun. (Camb.)* 48, 9816-9818.

(33) Faiella, M., Roy, A., Sommer, D. J., and Ghirlanda, G. Design of functional proteins: towards artificial hydrogenases. *Biopolymers-peptide science*.100, 558-571.

(34) Beinert, H. (2000) Iron-sulfur proteins: ancient structures, still full of surprises. *J Biol Inorg Chem 5*, 2–15.

(35) Koay, M. S., Antonkine, M. L., Gartner, W., and Lubitz, W. (2008) Modelling low-potential [Fe4S4] clusters in proteins. *Chem. Biodivers. 5*, 1571–1587.

(36) Sweeney, W. V., and Rabinowitz, J. C. (1980) Proteins containing 4Fe-4S clusters: an overview. *Annu. Rev. Biochem. 49*, 139–161.

(37) Jin, Z., Heinnickel, M., Krebs, C., Shen, G., Golbeck, J. H., and Bryant, D. A. (2008) Biogenesis of Iron-Sulfur Clusters in Photosystem I: Holo-NfuA from the Cyanobacterium Synochococcus Sp. PCC 7002 rapidly and efficiently transfers [4Fe-4S] clusters to apo-PSac in vitro. *J. Biol. Chem. 283*, 28426–28435.

(38) Bertini, I., Gray, H. B., Lippard, S. J., and Valentine, J. S. (1994) Bioinorganic chemistry.

(39) Ogihara, N. L., Ghirlanda, G., Bryson, J. W., Gingery, M., DeGrado, W. F., and Eisenberg, D. (2001) Design of three-dimensional domain-swapped dimers and fibrous oligomers. *Proceedings of the National Academy of Sciences of the United States of America 98*, 1404–1409.

(40) Papaefthymiou, G. C., Frankel, R. B., and Foner, S. (1980) Magnetic Properties of [Fe 4 S 4(SR) 4] 3- Clusters. *J. Phys. Colloques.*41, 493-494.

(41) Milov, A. D., Maryasov, A. G., and Tsvetkov, Y. D. (1998) Pulsed electron double resonance (PELDOR) and its applications in free-radicals research. *Applied Magnetic Resonance*. 15, 107-143.

(42) Schiemann, O., and Prisner, T. F. (2007) Long-range distance determinations in biomacromolecules by EPR spectroscopy. *Quarterly Reviews of Biophysics 40*, 1–53.

(43) Astashkin, A. V., Seravalli, J., Mansoorabadi, S. O., Reed, G. H., and Ragsdale, S. W. (2006) Pulsed electron paramagnetic resonance experiments identify the paramagnetic intermediates in the pyruvate ferredoxin oxidoreductase catalytic cycle. *J. Am. Chem. Soc. 128*, 3888–3889.

(44) Jeschke, G. (2012) DEER Distance Measurements on Proteins, in *Annual Review of Physical Chemistry, Vol 63* (Johnson, M. A., and Martinez, T. J., Eds.), 419–446.

(45) Swanson, M. A., Kathirvelu, V., Majtan, T., Frerman, F. E., Eaton, G. R., and Eaton, S. S. (2009) DEER Distance Measurement Between a Spin Label and a Native FAD Semiquinone in Electron Transfer Flavoprotein. *J. Am. Chem. Soc. 131*, 15978.

(46) Sen, K. I., Wu, H., Backer, J. M., and Gerfen, G. J. (2010) The Structure of p85ni in Class IA Phosphoinositide 3-Kinase Exhibits Interdomain Disorder. *Biochemistry 49*, 2159–2166.

(47) Astashkin, A. V., Rajapakshe, A., Cornelison, M. J., Johnson-Winters, K., and Enemark, J. H. (2012) Determination of the Distance between the Mo(V) and Fe(III) Heme Centers of Wild Type Human Sulfite Oxidase by Pulsed EPR Spectroscopy. *Journal of Physical Chemistry 116*, 1942–1950.

(48) Gordon-Grossman, M., Kaminker, I., Gofman, Y., Shai, Y., and Goldfarb, D. (2011) W-Band pulse EPR distance measurements in peptides using Gd3+-dipicolinic acid derivatives as spin labels. *Physical Chemistry Chemical Physics 13*, 10771–10780.

(49) Lovett, J. E., Bowen, A. M., Timmel, C. R., Jones, M. W., Dilworth, J. R., Caprotti, D., Bell, S. G., Wong, L. L., and Harmer, J. (2009) Structural information from orientationally selective DEER spectroscopy. *Physical Chemistry Chemical Physics 11*, 6840–6848.

(50) Elsasser, C., Brecht, M., and Bittl, R. (2002) Pulsed electron-electron double resonance on multinuclear metal clusters: Assignment of spin projection factors based on the dipolar interaction. *J. Am. Chem. Soc. 124*, 12606–12611.

(51) Elsaesser, C., Brecht, M., and Bittl, R. (2005) Treatment of spin-coupled metal-centres in pulsed electron-electron double-resonance experiments. *Biochem. Soc. Trans. 33*, 15–19.

(52) Martin, R. E., Pannier, M., Diederich, F., Gramlich, V., Hubrich, M., and Spiess, H. W. (1998) Determination of end-to-end distances in a series of TEMPO diradicals of up to 2.8 nm length with a new four-pulse double electron electron resonance experiment. *Angew. Chem. Int. Ed. 37*, 2834–2837.

(53) Torres, R. A., Lovell, T., Noodleman, L., and Case, D. A. (2003) Density functional and reduction potential calculations of Fe4S4 clusters. *J. Am. Chem. Soc. 125*, 1923–1936.

(54) Zastrow, M. L., PeacockAnna, F. A., Stuckey, J. A., and Pecoraro, V. L. (2012) Hydrolytic catalysis and structural stabilization in a designed metalloprotein. *Nat. Chem. 4*, 118–123.

(55) Salgado, E. N., Radford, R. J., and Tezcan, F. A. (2010) Metal-directed protein self-

assembly. *Acc. Chem. Res. 43*, 661–672.

(56) Cordova, J. M., Noack, P. L., Hilcove, S. A., Lear, J. D., and Ghirlanda, G. (2007) Design of a functional membrane protein by engineering a heme-binding site in glycophorin A. *J. Am. Chem. Soc. 129*, 512–518.

(57) Shinde, S., Cordova, J., Woodrum, B., and Ghirlanda, G. (2012) Modulation of function in a minimalist heme-binding membrane protein. *J Biol Inorg Chem 17*, 557–564.

(58) Calhoun, J. R., Nastri, F., Maglio, O., Pavone, V., Lombardi, A., and DeGrado, W. F. (2005) Artificial diiron proteins: from structure to function. *Biopolymers 80*, 264–278.

(59) Shiga, D., Funahashi, Y., Masuda, H., Kikuchi, A., Noda, M., Uchiyama, S., Fukui, K., Kanaori, K., Tajima, K., Takano, Y., Nakamura, H., Kamei, M., and Tanaka, T. (2012) Creation of a binuclear purple copper site within a de novo coiled-coil protein. *Biochemistry 51*, 7901–7907.

(60) Chakraborty, S., Iranzo, O., Zuiderweg, E. R. P., and Pecoraro, V. L. (2012) Experimental and theoretical evaluation of multisite cadmium(II) exchange in designed three-stranded coiled-coil peptides. *J. Am. Chem. Soc. 134*, 6191–6203.

(61) Der, B. S., Machius, M., Miley, M. J., Mills, J. L., Szyperski, T. A., and Kuhlman, B. (2011) Metal-mediated affinity and orientation specificity in a computationally designed protein homodimer. *J. Am. Chem. Soc 134,* 375-385

(62) Ghirlanda, G. (2009) Design of membrane proteins: toward functional systems. *Curr Opin Chem Biol 13*, 643–651.

(63) Ghirlanda, G., Osyczka, A., Liu, W., Antolovich, M., Smith, K. M., Dutton, P. L., Wand, A. J., and DeGrado, W. F. (2004) De novo design of a D2-symmetrical protein that reproduces the diheme four-helix bundle in cytochrome bc1. *J. Am. Chem. Soc. 126*, 8141–8147.

CHAPTER 3 REFERENCES:

(1) Fontecilla-Camps, J. C., Volbeda, A., Cavazza, C., and Nicolet, Y. (2007) Structure/function relationships of [NiFe]- and [FeFe]-hydrogenases. *107*, 4273–4303.

(2) Meyer, J. (2008) Iron-sulfur protein folds, iron-sulfur chemistry, and evolution. *J Biol Inorg Chem 13*, 157–170.

(3) Orengo, C. A., and Thornton, J. M. Protein Families and their Evolution- A structural Perspective. *Annual Reviews 74,*867-900.

(4) Scott, M. P., and Biggins, J. (1997) Introduction of a [4Fe-4S (S-cys)4]+1,+2 iron-sulfur center into a four-alpha helix protein using design parameters from the domain of

the Fx cluster in the Photosystem I reaction center. *Protein Sci. 6*, 340–346.

(5) Antonkine, M. L., Maes, E. M., Czernuszewicz, R. S., Breitenstein, C., Bill, E., Falzone, C. J., Balasubramanian, R., Lubner, C., Bryant, D. A., and Golbeck, J. H. (2007) Chemical rescue of a site-modified ligand to a [4Fe-4S] cluster in PsaC, a bacterial-like dicluster ferredoxin bound to Photosystem I. *Biochim. Biophys. Acta 1767*, 712–724.

(6) Antonkine, M. L., Koay, M. S., Epel, B., Breitenstein, C., Gopta, O., Gärtner, W., Bill, E., and Lubitz, W. (2009) Synthesis and characterization of de novo designed peptides modelling the binding sites of [4Fe-4S] clusters in photosystem I. *Biochim. Biophys. Acta 1787*, 995–1008.

(7) Kennedy, M. C., Kent, T. A., Emptage, M., Merkle, H., Beinert, H., and Münck, E. (1984) Evidence for the formation of a linear [3Fe-4S] cluster in partially unfolded aconitase. *J. Biol. Chem. 259*, 14463–14471.

(8) Grzyb, J., Xu, F., Weiner, L., Reijerse, E. J., Lubitz, W., Nanda, V., and Noy, D. (2010) De novo design of a non-natural fold for an iron-sulfur protein: alpha-helical coiled-coil with a four-iron four-sulfur cluster binding site in its central core. *Biochim. Biophys. Acta 1797*, 406–413.

(9) Coldren, C. D., Hellinga, H. W., and Caradonna, J. P. (1997) The rational design and construction of a cuboidal iron–sulfur protein. *Proc. Natl. Acad. Sci. USA 94*, 6635–6640.

(10) Gibney, B. R., Mulholland, S. E., Rabanal, F., and Dutton, P. L. (1996) Ferredoxin and ferredoxin-heme maquettes. *Proceedings of the National Academy of Sciences of the United States of America 93*, 15041–15046.

(11) Roy, A., Sarrou, I., Astashkin, A., and Ghirlanda, G. (2013) De novo Design of an Artificial bis-[4Fe-4S] Binding Protein. *Biochemistry 53*,43, 7586-7594.

(12) Sherman, B. D., Pillai, S., Kodis, G., Bergkamp, J., Mallouk, T. E., Gust, D., Moore, T. A., and Moore, A. L. (2011) A porphyrin-stabilized iridium oxide water oxidation catalyst. *Can. J. Chem. 89*, 152–157.

(13) Loewe, R. S., Ambroise, A., Muthukumaran, K., Padmaja, K., Lysenko, A. B., Mathur, G., Li, Q., Bocian, D. F., Misra, V., and Lindsey, J. S. (2004) Porphyrins Bearing Mono or Tripodal Benzylphosphonic Acid Tethers for Attachment to Oxide Surfaces. *J. Org. Chem. 69*, 1453–1460.

(14) Guldi, D. M., Zilbermann, I., Anderson, G., Li, A., Balbinot, D., Jux, N., Hatzimarinaki, M., Hirsch, A., and Prato, M. (2004) Multicomponent redox gradients on photoactive electrode surfaces. *Chem. Commun. (Camb.)* 726–727.

(15) Ogihara, N. L., Ghirlanda, G., Bryson, J. W., Gingery, M., DeGrado, W. F., and Eisenberg, D. (2001) Design of three-dimensional domain-swapped dimers and fibrous oligomers. *Proceedings of the National Academy of Sciences of the United States of*

America 98, 1404–1409.

(16) Han, G. W., Yang, X. L., McMullan, D., Chong, Y. E., Krishna, S. S., Rife, C. L., Weekes, D., Brittain, S. M., Abdubek, P., Ambing, E., Astakhova, T., Axelrod, H. L., Carlton, D., Caruthers, J., Chiu, H. J., Clayton, T., Duan, L., Feuerhelm, J., Grant, J. C., Grzechnik, S. K., Jaroszewski, L., Jin, K. K., Klock, H. E., Knuth, M. W., Kumar, A., Marciano, D., Miller, M. D., Morse, A. T., Nigoghossian, E., Okach, L., Paulsen, J., Reyes, R., van den Bedem, H., White, A., Wolf, G., Xu, Q., Hodgson, K. O., Wooley, J., Deacon, A. M., Godzik, A., Lesley, S. A., Elsliger, M. A., Schimmel, P., and Wilson, I. A. (2010) Structure of a tryptophanyl-tRNA synthetase containing an iron-sulfur cluster. *Acta crystallographica. Section F, Structural biology and crystallization communications 66*, 1326–1334.

(17) Sweeney, W. V., and Rabinowitz, J. C. (1980) Proteins containing 4Fe-4S clusters: an overview. *Annu. Rev. Biochem. 49*, 139–161.

(18) Jin, Z., Heinnickel, M., Krebs, C., Shen, G., Golbeck, J. H., and Bryant, D. A. (2008) Biogenesis of Iron-Sulfur Clusters in Photosystem I:Holo-NfuA from the Cyanobacterium Synchococcus Sp. PCC 70002 rapidly and efficiently transfers [4Fe-4S] clusters to apo PSac in vitro. *J. Biol. Chem. 283*, 28426–28435.

(19) Koay, M. S., Antonkine, M. L., Gartner, W., and Lubitz, W. (2008) Modelling low-potential [Fe4S4] clusters in proteins. *Chem. Biodivers. 5*, 1571–1587.

(20) Eck, R. V., and Dayhoff, M. O. (1966) Evolution of the structure of ferredoxin based on living relics of primitive amino Acid sequences. *Science 152*, 363–366.

(21) Duff, J. L. C., Breton, J. L. J., Butt, J. N., Armstrong, F. A., and Thomson, A. J. (1996) Novel redox chemistry of [3Fe-4S] clusters : Electrochemical characterization of the all-Fe (II) form of the [3Fe-4S] cluster generated reversibly in various proteins and its spectroscopic investigation in Sulfolobus acidocaldarius ferredoxin. *J. Am. Chem. Soc. 118*, 8593–8603.

(22) Armstrong, F. A., George, S. J., Thomson, A. J., Yates, M. G., (1988)Direct electrochemistry in the characterisation of redox proteins: Novel properties of Azotobacter 7Fe ferredoxin. *FEBS lett. 234,*1, 107-110

(23) Tagawa, K., and Arnon, D. I. (1968) Oxidation-reduction potentials and stoichiometry of electron transfer in ferredoxins. *Biochim. Biophys. Act - Bioenerg. 153*, 602–613.

(24) Mulder, D. W., Shepard, E. M., Meuser, J. E., Joshi, N., King, P. W., Posewitz, M. C., Broderick, J. B., and Peters, J. W. (2011) Insights into [FeFe]-hydrogenase structure, mechanism, and maturation. *Structure 19*, 1038–1052.

(25) Kurisu, G., Kusunoki, M., Katoh, E., Yamazaki, T., Teshima, K., Onda, Y., Kimata-Ariga, Y., and Hase, T. (2001) Structure of the electron transfer complex between

ferredoxin and ferredoxin-NADP+ reductase. *Nat. Struct Biol. 8*, 117–121.

(26) Hanke, G. T., Satomi, Y., Shinmura, K., Takao, T., and Hase, T. (2011) A screen for potential ferredoxin electron transfer partners uncovers new, redox dependent interactions. *Biochimica et Biophysica Acta (BBA) - Proteins and Proteomics 1814*, 366–374.

(27) Zastrow, M. L., PeacockAnna, F. A., Stuckey, J. A., and Pecoraro, V. L. (2012) Hydrolytic catalysis and structural stabilization in a designed metalloprotein. *Nat. Chem. 4*, 118–123.

CHAPTER 4 References:

(1) Peters, J., Peters, J., Lanzilotta, W., Lanzilotta, W., Lemon, B., Lemon, B., Seefeldt, L., and Seefeldt, L. (1998) X-ray crystal structure of the Fe-only hydrogenase (Cpl) from Clostridium pasteurianum to 1.8 angstrom resolution. *Science 282*, 1853–1858.

(2) Nicolet, Y., Piras, C., Legrand, P., Hatchikian, C. E., and Fontecilla-Camps, J. C. (1999) Desulfovibrio desulfuricans iron hydrogenase: the structure shows unusual coordination to an active site Fe binuclear center. *Structure 7*, 13–23.

(3) Singleton, M. L., Crouthers, D. J., Duttweiler, R. P. 3., Reibenspies, J. H., and Darensbourg, M. Y. (2011) Sulfonated diiron complexes as water-soluble models of the [Fe-Fe]-hydrogenase enzyme active site. *Inorganic chemistry 50*, 5015–5026.

(4) Barton, B. E., Olsen, M. T., and Rauchfuss, T. B. (2010) Artificial hydrogenases. *Curr. Opin. Biotechnol. 21*, 292–297.

(5) Tard, C., and Pickett, C. J. (2009) Structural and Functional Analogues of the Active Sites of the [Fe]-, [NiFe]-, and [FeFe]-Hydrogenases. *Chem. Rev. 109*, 2245–2274.

(6) Erdem, Ö. F., Schwartz, L., Stein, M., Silakov, A., Kaur-Ghumaan, S., Huang, P., Ott, S., Reijerse, E. J., and Lubitz, W. (2011) A Model of the [FeFe] Hydrogenase Active Site with a Biologically Relevant Azadithiolate Bridge: A Spectroscopic and Theoretical Investigation. *Angew. Chem. Int. Ed. 50*, 1439–1443.

(7) Ezzaher, S., Gogoll, A., Bruhn, C., and Ott, S. (2010) Directing protonation in [FeFe] hydrogenase active site models by modifications in their second coordination sphere. *Chem. Commun. 46*, 5775–5777.

(8) Surawatanawong, P., Tye, J. W., Darensbourg, M. Y., and Hall, M. B. (2010) Mechanism of electrocatalytic hydrogen production by a di-iron model of iron-iron hydrogenase: a density functional theory study of proton dissociation constants and electrode reduction potentials. *Dalton Trans. 39*, 3093–3104.

(9) Wang, F., Wang, W.-G., Wang, X.-J., Wang, H.-Y., Tung, C.-H., and Wu, L.-Z. (2011) A Highly Efficient Photocatalytic System for Hydrogen Production by a Robust

Hydrogenase Mimic in an Aqueous Solution - Wang - 2011 - Angewandte Chemie International Edition - Wiley Online Library. *Angew. Chem. Int. Ed. 50*, 3193–3197.

(10) Wang, W.-G., Wang, F., Wang, H.-Y., Tung, C.-H., and Wu, L.-Z. (2012) Electron transfer and hydrogen generation from a molecular dyad: platinum(ii) alkynyl complex anchored to [FeFe] hydrogenase subsite mimic. *Dalton Trans. 41*, 2420–2426.

(11) Quentel, F., Passard, G., and Gloaguen, F. (2012) Electrochemical hydrogen production in aqueous micellar solution by a diiron benzenedithiolate complex relevant to [FeFe] hydrogenases. *Phys Chem Chem Phys 5*.7757-7761.

(12) Sano, Y., Onoda, A., and Hayashi, T. (2011) A hydrogenase model system based on the sequence of cytochrome c: photochemical hydrogen evolution in aqueous media. *Chem. Commun. (Camb.) 47*, 8229–8231.

(13) Mulder, D. W., Shepard, E. M., Meuser, J. E., Joshi, N., King, P. W., Posewitz, M. C., Broderick, J. B., and Peters, J. W. (2011) Insights into [FeFe]-hydrogenase structure, mechanism, and maturation. *Structure 19*, 1038–1052.

(14) Singleton, M. L., Reibenspies, J. H., and Darensbourg, M. Y. (2010) A cyclodextrin host/guest approach to a hydrogenase active site biomimetic cavity. *J. Am. Chem. Soc. 132*, 8870–8871.

(15) Knorzer, P., Silakov, A., Foster, C. E., Armstrong, F. A., Lubitz, W., and Happe, T. (2012) Importance of the Protein Framework for Catalytic Activity of [FeFe]-Hydrogenases. *J. Biol. Chem. 287*, 1489–1499.

(16) Darensbourg, M. Y., and Bethel, R. D. (2012) Biomimetic chemistry: Merging the old with the new. *Nat. Chem. 4*, 11–13.

(17) Camara, J. M., and Rauchfuss, T. B. (2011) Combining acid-base, redox and substrate binding functionalities to give a complete model for the [FeFe]-hydrogenase. *Nat. Chem. 4*, 26–30.

(18) Lu, Y., Yeung, N., Sieracki, N., and Marshall, N. M. (2009) Design of functional metalloproteins. *Nature 460*, 855–862.

(19) Nanda, V., and Koder, R. L. (2010) Designing artificial enzymes by intuition and computation. *Nat. Chem. 2*, 15–24.

(20) Grzyb, J., Xu, F., Weiner, L., Reijerse, E. J., Lubitz, W., Nanda, V., and Noy, D. (2010) De novo design of a non-natural fold for an iron-sulfur protein: alpha-helical coiled-coil with a four-iron four-sulfur cluster binding site in its central core. *Biochim. Biophys. Acta 1797*, 406–413.

(21) Zastrow, M. L., PeacockAnna, F. A., Stuckey, J. A., and Pecoraro, V. L. (2012) Hydrolytic catalysis and structural stabilization in a designed metalloprotein. *Nat. Chem.*

4, 118–123.

(22) Faiella, M., Andreozzi, C., de Rosales, R. T. M., Pavone, V., Maglio, O., Nastri, F., DeGrado, W. F., and Lombardi, A. (2009) An artificial di-iron oxo-protein with phenol oxidase activity. *Nat. Chem. Biol. 5*, 882–884.

(23) Miner, K. D., Mukherjee, A., Gao, Y.-G., Null, E. L., Petrik, I. D., Zhao, X., Yeung, N., Robinson, H., and Lu, Y. (2012) A Designed Functional Metalloenzyme that Reduces O2 to H2O with Over One Thousand Turnovers. *Angew. Chem. Int. Ed.* n/a–n/a.

(24) Cordova, J. M., Noack, P. L., Hilcove, S. A., Lear, J. D., and Ghirlanda, G. (2007) Design of a functional membrane protein by engineering a heme-binding site in glycophorin A. *J. Am. Chem. Soc. 129*, 512–518.

(25) Shinde, S., Cordova, J., Woodrum, B., and Ghirlanda, G. (2012) Modulation of function in a minimalist heme-binding membrane protein. *J Biol Inorg Chem 17*, 557–564.

(26) Koder, R. L., Anderson, J. L. R., Solomon, L. A., Reddy, K. S., Moser, C. C., and Dutton, P. L. (2009) Design and engineering of an O2 transport protein. *Nature 458*, 305–309.

(27) Sambasivan, R., and Ball, Z. T. (2010) Metallopeptides for Asymmetric Dirhodium Catalysis. *J. Am. Chem. Soc. 132*, 9289–9291.

(28) Chen, Z., Popp, B. V., Bovet, C. L., and Ball, Z. T. (2011) Site-Specific Protein Modification with a Dirhodium Metallopeptide Catalyst. *ACS Chem. Biol. 6*, 920–925.

(29) Sano, Y., Onoda, A., and Hayashi, T. (2011) Photocatalytic hydrogen evolution by a diiron hydrogenase model based on a peptide fragment of cytochrome c556 with an attached diiron carbonyl cluster and an attached ruthenium photosensitizer. *J. Inorg. Biochem. 108*, 159–162.

(30) Jones, A. K., Lichtenstein, B. R., Dutta, A., Gordon, G., and Dutton, P. L. (2007) Synthetic Hydrogenases: Incorporation of an Iron Carbonyl Thiolate into a Designed Peptide. *J. Am. Chem. Soc. 129*, 14844–14845.

(31) Morera, E., Pinnen, F., and Lucente, G. (2002) Synthesis of 1,2-dithiolane analogues of leucine for potential use in peptide chemistry. *Org. Lett. 4*, 1139–1142.

(32) Silvennoinen, G., Polborn, K., Mayer, P., and Pfaendler, H. R. (2009) *Thieme Chemistry*

(33) Kortemme, T., and Baldwin, R. (1994) Helix propensities of the amino acids measured in alanine‐based peptides without helix‐stabilizing side‐chain interactions. *Protein Sci.*

(34) Marqusee, S., Robbins, V. H., and Baldwin, R. L. (1989) Unusually stable helix formation in short alanine-based peptides. *Proceedings of the National Academy of Sciences of the United States of America 86*, 5286–5290.

(35) Cheng, R. P., Girinath, P., Suzuki, Y., Kuo, H.-T., Hsu, H.-C., Wang, W.-R., Yang, P.-A., Gullickson, D., Wu, C.-H., Koyack, M. J., Chiu, H.-P., Weng, Y.-J., Hart, P., Kokona, B., Fairman, R., Lin, T.-E., and Barrett, O. (2010) Positional Effects on Helical Ala-Based Peptides. *Biochemistry 49*, 9372–9384.

(36) Apfel, U.-P., Kowol, C. R., Halpin, Y., Kloss, F., Kuebel, J., Goerls, H., Vos, J. G., Keppler, B. K., Morera, E., Lucente, G., and Weigand, W. (2009) Investigation of amino acid containing [FeFe] hydrogenase models concerning pendant base effects *103*, 1236–1244.

(37) Apfel, U.-P., Rudolph, M., Apfel, C., Robl, C., Langenegger, D., Hoyer, D., Jaun, B., Ebert, M.-O., Alpermann, T., Seebach, D., and Weigand, W. (2010) Reaction of Fe3(CO)12 with octreotide-chemical, electrochemical and biological investigations. *Dalton Trans. 39*, 3065–3071.

(38) Lyon, E. J., Georgakaki, I. P., Reibenspies, J. H., and Darensbourg, M. Y. (1999) Carbon Monoxide and Cyanide Ligands in a Classical Organometallic Complex Model for Fe-Only Hydrogenase. *Angew. Chem. Int. Ed. 38*, 3178–3180.

(39) Ellgen, P., Gerlach, J. (1973) Kinetics and Mechanism of Substitution-Reactions of Bis(Mercaptotricarbonyliron) Complexes. *Inorganic chemistry 12*, 2526–2532.

(40) Greenfield, N. J. (2006) Using circular dichroism spectra to estimate protein secondary structure. *Nature protocols 1*, 2876–2890.

(41) Wang, H.-Y., Wang, H.-Y., Si, G., Si, G., Cao, W.-N., Cao, W.-N., Wang, W.-G., Wang, W.-G., Li, Z.-J., Li, Z.-J., Wang, F., Wang, F., Tung, C.-H., Tung, C.-H., Wu, L.-Z., and Wu, L.-Z. (2011) A triad [FeFe] hydrogenase system for light-driven hydrogen evolution. *Chem. Commun. 47*, 8406–8408.

(42) Wang, W.-G., Wang, W.-G., Wang, F., Wang, F., Wang, H.-Y., Wang, H.-Y., Si, G., Si, G., Tung, C.-H., Tung, C.-H., Wu, L.-Z., and Wu, L.-Z. (2010) Photocatalytic Hydrogen Evolution by [FeFe] Hydrogenase Mimics in Homogeneous Solution. *Chem-Asian J 5*, 1796–1803.

(43) Felton, G. A. N., Mebi, C. A., Petro, B. J., Vannucci, A. K., Evans, D. H., Glass, R. S., and Lichtenberger, D. L. (2009) Review of electrochemical studies of complexes containing the Fe2S2 core characteristic of [FeFe]-hydrogenases including catalysis by these complexes of the reduction of acids to form dihydrogen. *J. Organomet. Chem. 694*, 2681–2699.

(44) Calhoun, J. R., Kono, H., Lahr, S., Wang, W., DeGrado, W. F., and Saven, J. G. (2003) Computational design and characterization of a monomeric helical dinuclear

metalloprotein. *J Mol Biol 334*, 1101–1115.

(45) Solution NMR Structure of a Designed Metalloprotein and Complementary Molecular Dynamics Refinement. Calhoun J. R., Liu W., Spiegel K., Peraro M. D., Klein M. L., Valentine K. G., Wand A. J., Degrado W. F. (2008). *Structure 16*, 2, 210-215

(46) Liu, C. C., and Schultz, P. G. (2010) Adding New Chemistries to the Genetic Code. *Annu. Rev. Biochem. 79*, 413–444.

(47) Wang, L., Brock, A., Herberich B., Schultz P.G. (2001) Expanding the Genetic Code of Escherichia coli, *Science 292,*498.

(48) Waugh, D. S. (2011) An overview of enzymatic reagents for the removal of affinity tags. *Protein Expression and Purification 80*, 283–293.

(49) Dirksen, A., and Dawson, P. E. (2008) Rapid Oxime and Hydrazone Ligations with Aromatic Aldehydes for Biomolecular Labeling. *Bioconjugate Chem. 19*, 2543–2548.

(50) Galinato, M. G. I., Whaley, C. M., and Lehnert, N. (2010) Vibrational Analysis of the Model Complex (μ-edt)[Fe(CO) 3] 2and Comparison to Iron-Only Hydrogenase: The Activation Scale of Hydrogenase Model Systems. *Inorganic chemistry 49*, 3201–3215.

(51) Photochemical studies of iron-only hydrogenase model compounds.Mcdonald, J. c., Berg, S.,Peralto, M., Works, C.(2009). *Inorg. Chim. Acta.362*, 2, 318-324

(52) Roy, A., Madden, C., and Ghirlanda, G. (2012) Photo-induced hydrogen production in a helical peptide incorporating a [FeFe] hydrogenase active site mimic. *Chem. Commun. 48*, 9816–9818.

CHAPTER 5 REFERENCES:

(1) Fontecilla-Camps, J. C., Volbeda, A., Cavazza, C., and Nicolet, Y. (2007) Structure/function relationships of [NiFe]- and [FeFe]-hydrogenases. *107*, 4273–4303.

(2) Peters, J., Peters, J., Lanzilotta, W., Lanzilotta, W., Lemon, B., Lemon, B., Seefeldt, L., and Seefeldt, L. (1998) X-ray crystal structure of the Fe-only hydrogenase (Cpl) from Clostridium pasteurianum to 1.8 angstrom resolution. *Science 282*, 1853–1858.

(3) Darensbourg, M. Y., Lyon, E. J., Zhao, X., and Georgakaki, I. P. (2003) The organometallic active site of [Fe]hydrogenase: Models and entatic states. *Proc. Natl. Acad. Sci. USA 100*, 3683–3688.

(4) Frederix, P. W. J. M., Kania, R., Wright, J. A., Lamprou, D. A., Ulijn, R. V., Pickett, C. J., and Hunt, N. T. (2012) Encapsulating [FeFe]-hydrogenase model compounds in peptide hydrogels dramatically modifies stability and photochemistry. *Dalton Trans. 41*, 13112–13119.

(5) Singleton, M. L., Reibenspies, J. H., and Darensbourg, M. Y. (2010) A cyclodextrin host/guest approach to a hydrogenase active site biomimetic cavity. *J. Am. Chem. Soc. 132*, 8870–8871.

(6) Li, X., Wang, M., Zheng, D., Han, K., and Dong, J. (2012) Photocatalytic H 2 production in aqueous solution with host-guest inclusions formed by insertion of an FeFe-hydrogenase mimic and an organic dye into cyclodextrins, *Energy & Environmental Science 5,*8220-8224

(7) Wang, F., Liang, W.-J., Jian, J.-X., Li, C.-B., Chen, B., Tung, C.-H., and Wu, L.-Z. (2013) Exceptional Poly(acrylic acid)-Based Artificial [FeFe]-Hydrogenases for Photocatalytic H 2Production in Water. *Angew. Chem. Int. Ed. 52*, 8134–8138.

(8) Jian, J.-X., Liu, Q., Li, Z.-J., Wang, F., Li, X.-B., Li, C.-B., Bin Liu, Meng, Q.-Y., Bin Chen, Feng, K., Tung, C.-H., and Wu, L.-Z. (2013) Chitosan confinement enhances hydrogenphotogeneration from a mimic of the diironsubsite of [FeFe]-hydrogenase. *Nature Communications 4*, 1–9.

(9) Wang, F., Wang, W.-G., Wang, X.-J., Wang, H.-Y., Tung, C.-H., and Wu, L.-Z. (2011) A Highly Efficient Photocatalytic System for Hydrogen Production by a Robust Hydrogenase Mimic in an Aqueous Solution - Wang - 2011 - Angewandte Chemie International Edition - Wiley Online Library. *Angew. Chem. Int. Ed. 50*, 3193–3197.

(10) GREEN, N. M. (1965) A Spectrophotometric assay for avidin and biotin based on binding of dyes by avidin. *Biochem. J. 94*, 23C–24C.

(11) Lo, K. K.-W., and Hui, W.-K. (2005) Design of Rhenium(I) Polypyridine Biotin Complexes as a New Class of Luminescent Probes for Avidin. *Inorganic chemistry 44*, 1992–2002.

(12) Lo, K. K.-W., and Lee, T. K.-M. (2004) Luminescent Ruthenium(II) Polypyridine Biotin Complexes: Synthesis, Characterization, Photophysical and Electrochemical Properties, and Avidin-Binding Studies. *Inorganic chemistry 43*, 5275–5282.

(13) Lo, K., Chan, J., Lui, L. H., and Chung, C. K. (2004) Novel Luminescent Cyclometalated Iridium(III) Diimine Complexes That Contain a Biotin Moiety - Organometallics (ACS Publications). *Organometallics*.

(14)Lin, C. C., Lin, C. W., and Chan, A. S. C., Catalytic hydrogenation of itaconic acid in a biotinylated Pyrphos–rhodium(I) system in a protein cavity.*Tetrahedron-Assymetry 10,* 1887-1893

(15) Heinisch, T., and Ward, T. R. (2010) Design strategies for the creation of artificial metalloenzymes. *Curr Opin Chem Biol 14*. 184-199.

(16) Hicks, M. R., Rullay, A. K., Pedrido, R., Crout, D. H., and Pinheiro, T. J. T. (2008) Efficient Synthesis of Methanesulphonate-Derived Lipid Chains for Attachment of

Proteins to Lipid Membranes. *Synthetic Communications 38*, 3726–3750.

(17) Sauser, J., Zocchi, A., Gilardoni, F., and Ward, T. R. (2004) Artificial Metalloenzymes: (Strept)avidin as Host for Enantioselective Hydrogenation by Achiral Biotinylated Rhodium−Diphosphine Complexes. *Journal of the American Chemical Society 126.*14411-14418.

(18) Jones, A. K., Lichtenstein, B. R., Dutta, A., Gordon, G., and Dutton, P. L. (2007) Synthetic Hydrogenases: Incorporation of an Iron Carbonyl Thiolate into a Designed Peptide. *J. Am. Chem. Soc. 129*, 14844–14845.

(19) Roy, A., Madden, C., and Ghirlanda, G. (2012) Photo-induced hydrogen production in a helical peptide incorporating a [FeFe] hydrogenase active site mimic. *Chem. Commun 48,* 9816-9818.

(20) Sano, Y., Onoda, A., and Hayashi, T. (2011) A hydrogenase model system based on the sequence of cytochrome c: photochemical hydrogen evolution in aqueous media. *Chem. Commun. (Camb.) 47*, 8229–8231.

(21) Na, Y., Wang, M., Pan, J., Zhang, P., Åkermark, B., and Sun, L. (2008) Visible Light-Driven Electron Transfer and Hydrogen Generation Catalyzed by Bioinspired [2Fe2S] Complexes. *Inorganic chemistry 47*, 2805–2810.

(22) Zhang, P., Wang, M., Na, Y., Li, X., Jiang, Y., and Sun, L. (2010) Homogeneous photocatalytic production of hydrogen from water by a bioinspired [Fe2S2] catalyst with high turnover numbers. *Dalton Trans. 39*, 1204–1206.

(23) Streich, D., Streich, D., Astuti, Y., Astuti, Y., Orlandi, M., Orlandi, M., Schwartz, L., Schwartz, L., Lomoth, R., Lomoth, R., Hammarström, L., Hammarström, L., Ott, S., and Ott, S. (2010) High-Turnover Photochemical Hydrogen Production Catalyzed by a Model Complex of the [FeFe]-Hydrogenase Active Site. *Chem. Eur. J. 16*, 60–63.

(24) Wang, H.-Y., Wang, W.-G., Si, G., Wang, F., Tung, C.-H., and Wu, L.-Z. (2010) Photocatalytic Hydrogen Evolution from Rhenium(I) Complexes to [FeFe] Hydrogenase Mimics in Aqueous SDS Micellar Systems: A Biomimetic Pathway. *Langmuir 26*, 9766–9771.

(25) Li, X., Wang, M., Zhang, S., Pan, J., Na, Y., Liu, J., Åkermark, B., and Sun, L. (2008) Noncovalent Assembly of a Metalloporphyrin and an Iron Hydrogenase Active-Site Model: Photo-Induced Electron Transfer and Hydrogen Generation. *J. Phys. Chem. B 112*, 8198–8202.

(26) Song, L.-C., Wang, L.-X., Tang, M.-Y., Li, C.-G., Song, H.-B., and Hu, Q.-M. (2009) Synthesis, Structure, and Photoinduced Catalysis of [FeFe]-Hydrogenase Active Site Models Covalently Linked to a Porphyrin or Metalloporphyrin Moiety †. *Organometallics 28*, 3834–3841.

(27) Kluwer, A. M., Kapre, R., Hartl, F., Lutz, M., Spek, A. L., Brouwer, A. M., van Leeuwen, P. W. N. M., and Reek, J. N. H. (2009) Self-assembled biomimetic [2Fe2S]-hydrogenase-based photocatalyst for molecular hydrogen evolution. *Proc. Natl. Acad. Sci. USA 106*, 10460–10465.

(28) Wang, M., Chen, L., Li, X., and Sun, L. (2011) Approaches to efficient molecular catalyst systems for photochemical H2 production using [FeFe]-hydrogenase active site mimics. *Dalton Trans. 40*, 12793–12800.

(29) Wilson, M. E., and Whitesides, G. M. (1978) Conversion of a protein to a homogeneous asymmetric hydrogenation catalyst by site-specific modification with a diphosphinerhodium(I) moiety. *J. Am. Chem. Soc. 100*, 306–307.

(30) Creus, M., Pordea, A., Rossel, T., and Sardo, A. (2008) X-Ray Structure and Designed Evolution of an Artificial Transfer Hydrogenase. *Angew. Chem.47,*1400-1404.

(31) Dürrenberger, M., Heinisch, T., Wilson, Y. M., Rossel, T., Nogueira, E., Knörr, L., Mutschler, A., Kersten, K., Zimbron, M. J., Pierron, J., Schirmer, T., and Ward, T. R. (2011) Artificial Transfer Hydrogenases for the Enantioselective Reduction of Cyclic Imines. *Angew. Chem. 123*, 3082–3085.

(32) Artificial Metalloenzyme for Enantioselective Sulfoxidation Based on Vanadyl-Loaded Streptavidin, *Journal of the American Chemical Society 130,* 8085-8088.

(33) Mulder, D. W., Shepard, E. M., Meuser, J. E., Joshi, N., King, P. W., Posewitz, M. C., Broderick, J. B., and Peters, J. W. (2011) Insights into [FeFe]-hydrogenase structure, mechanism, and maturation. *Structure 19*, 1038–1052.

APPENDIX A

PERMISSION TO REPRODUCE CHAPTER 1 FROM *BIOPOLYMERS-PROTEIN SCIENCE*

ANINDYA ROY <aroy10@asu.edu>

Thank you for your RightsLink / John Wiley and Sons transaction

Copyright Clearance Center <rightslink@marketing.copyright.com> Mon, Feb 17, 2014 at 4:11 PM
Reply-To: Copyright Clearance Center <reply-fe5c1075726404757012-14153369_HTML-1054436414-114453-70263@info.copyright.com>
To: aroy10@asu.edu

To view this email as a web page, go here.

Do Not Reply Directly to This Email

To ensure that you continue to receive our emails,
please add rightslink@marketing.copyright.com to your address book.

RightsLink | Copyright Clearance Center

Thank You For Your Order!

Dear Anindya Roy,

Thank you for placing your order through Copyright Clearance Center's RightsLink service. John Wiley and Sons has partnered with RightsLink to license its content. This notice is a confirmation that your order was successful.

Your order details and publisher terms and conditions are available by clicking the link below:
http://s100.copyright.com/CustomerAdmin/PLF.jsp?ref=ff937025-b65f-4480-b32b-cbbd07e71f5e

Order Details
Licensee: Anindya Roy
License Date: Feb 17, 2014
License Number: 3331570829674
Publication: Biopolymers
Title: De novo design of functional proteins: Toward artificial hydrogenases
Type Of Use: Dissertation/Thesis
Total: 0.00 USD

To access your account, please visit https://myaccount.copyright.com.

Please note: Online payments are charged immediately after order confirmation; invoices are issued daily and are payable immediately upon receipt.

To ensure we are continuously improving our services, please take a moment to complete our customer satisfaction survey.

APPENDIX B

PERMISSION TO REPRODUCE CHAPTER 2 FROM *BIOCHEMISTRY*

Home | Create Account | Help

Title: De Novo Design of an Artificial Bis[4Fe-4S] Binding Protein

Author: Anindya Roy, Iosifina Sarrou, Michael D. Vaughn, Andrei V. Astashkin, and Giovanna Ghirlanda

Publication: Biochemistry

Publisher: American Chemical Society

Date: Oct 1, 2013

User ID

Password

Enable Auto Login

LOGIN

Forgot Password/User ID?

If you're a copyright.com user, you can login to RightsLink using your copyright.com credentials. Already **a RightsLink user** or want to learn more?

PERMISSION/LICENSE IS GRANTED FOR YOUR ORDER AT NO CHARGE

This type of permission/license, instead of the standard Terms & Conditions, is sent to you because no fee is being charged for your order. Please note the following:

- Permission is granted for your request in both print and electronic formats, and translations.
- If figures and/or tables were requested, they may be adapted or used in part.
- Please print this page for your records and send a copy of it to your publisher/graduate school.
- Appropriate credit for the requested material should be given as follows: "Reprinted (adapted) with permission from (COMPLETE REFERENCE CITATION). Copyright (YEAR) American Chemical Society." Insert appropriate information in place of the capitalized words.
- One-time permission is granted only for the use specified in your request. No additional uses are granted (such as derivative works or other editions). For any other uses, please submit a new request.

BACK CLOSE WINDOW

APPENDIX C

PERMISSION TO REPRODUCE CHAPTER 4 FROM *CHEMICAL COMMUNICATIONS*

Reproduced from *Chem. Commun.*, 2012,48, 9816-9818

APPENDIX D

CO-AUTHOR APPROVAL FOR USING TEXTS

Permission was taken from following authors to use texts in the thesis for chapters 1, 2, 3, 4 and 5.

1) Dayn Joseph Sommer

2) Marina Faiella

3) Josephine Sarrou

4) Andrei Astashkine

5) Michael Vaughn

6) Chris Madden